Canadian Technical Report of
Fisheries and Aquatic Sciences 2747

2007

OCEAN BOTTOM ACOUSTIC OBSERVATIONS IN THE SCOTIAN SHELF GULLY DURING AN EXPLORATION SEISMIC SURVEY – A DETAILED STUDY

by

N. A. Cochrane

Ocean Sciences Division
Bedford Institute of Oceanography
Department of Fisheries and Oceans
P.O. Box 1006
Dartmouth, NS
B2Y 4A2

Cat. No. Fs 97-6/2747E ISSN 0706-6457

Correct citation for this publication:

Cochrane, N. A. 2007. Ocean Bottom Acoustic Observations in the Scotian Shelf Gully During an Exploration Seismic Survey – A Detailed Study. Can. Tech. Rep. Fish. Aquat. Sci. 2747: viii + 73p.

TABLE OF CONTENTS

LIST OF TABLES

LIST OF FIGURES

ABSTRACT

Cochrane, N. A. 2005. Ocean bottom acoustic observations in the Scotian Shelf Gully during an exploration seismic survey – a detailed study. Can. Tech. Rep. Fish. Aquat. Sci. 2747: viii + 73p.

Data are analysed from 4 hydrophone-equipped recording packages bottom-deployed in 1000-1700 m water depths in the Scotian Shelf Gully Marine Protected Area during an exploration seismic survey. Analysis indicates that exploration seismic impulses propagated to ranges of 40 – 55 km within the water column are highly elongated in time and frequently dominate acoustic background levels over all or most of the 11 s inter-pulse interval. Frequently observed "click" type signals with significant spectral content below 2 kHz are attributed to sperm whale vocalizations. Other click signals of contrasting character logged by a single instrument equipped with a high frequency pulsed-signal detector sensitive to signals up to 20 kHz are tentatively ascribed to northern bottlenose whales. Seismic impulse levels at range are modeled in the spectral domain using a theoretical source array model in conjunction with a Parabolic Equation acoustic transmission loss model. Discrepancies between predicted and observed seismic levels are ascribed to limitations in field measurements and/or predictive modeling methodologies. The sensitivity of predicted seismic levels to selected propagation model parameters is explored. Improvements in instrumentation and methodologies are suggested.

RÉSUMÉ

Cochrane, N. A. 2005. Observations acoustiques du fond océanique dans le Goulet de la plate-forme néo-écossaise pendant un levé sismique d'exploration – une étude détaillée. Can. Tech. Rep. Fish. Aquat. Sci. 2747: viii + 73p.

On analyse les données de 4 dispositifs enregistreurs munis d'hydrophones déployés sur le fond par des profondeurs de l'eau de 1000 à 1700 m dans le Goulet de la plate-forme néo-écossaise pendant un levé d'exploration sismique. L'analyse révèle que les impulsions d'exploration sismique se propagent à des distances de 40 à 55 km dans la colonne d'eau pendant de longues durées et dominent fréquemment les niveaux acoustiques naturels pendant presque toute la durée des intervalles de 11 s entre les impulsions. Les signaux de type «click» fréquemment observés et d'une importante teneur spectrale inférieure à 2 kHz sont attribués aux vocalisations des grands cachalots. D'autres signaux de type «click» de nature contrastante enregistrés par un unique instrument muni d'un détecteur sensible aux impulsions de haute fréquence pouvant atteindre 20 kHz ont été de manière tentative attribués aux baleines à bec communes. L'intensité des impulsions sismiques à leur portée utile maximale est modélisée dans le domaine spectral au moyen d'un modèle théorique de dispositif de sources utilisé en conjonction avec un modèle de la perte de transmission acoustique basé sur l'équation parabolique. Les écarts entre les intensités sismiques prévues et observées sont attribués aux limites des mesures sur le terrain et/ou des méthodologies de modélisation prédictive. La sensibilité des intensités sismiques prévues à des paramètres choisis du modèle de propagation est explorée. Des améliorations des instruments et des méthodologies sont suggérées.

INTRODUCTION

During the summer of 2003 Marathon Canada Petroleum ULC conducted a 3-D seismic survey in Scotian Shelf/Slope exploration leases EL2410 and EL2411, designated "Cortland" & "Empire" respectively (Fig. 1). Seismic lines within EL2410, shot with a 3090 in^3 towed airgun array from Petroleum Geo-Services vessel *Ramform Viking*, approached to within 4.5 km of the Gully Marine Protected Area (MPA) boundary (Austin et al. 2004) and to within about 16 km of the Gully Whale Sanctuary within the MPA. The Whale Sanctuary is the home of the Committee on the Status of Endangered Wildlife in Canada (COSEWIC) designated "endangered" northern bottlenose whale (NBW) (Hooker & Whitehead 2002) and hosts a variety of other cetacean species. The center of the NBW concentration area lies about 35 km from the nearest seismic approach.

Prior to seismic shooting, levels of exploration-seismic-origin sound propagating into the Whale Sanctuary and adjacent areas of the outer Gully were predictively modeled in an industry-commissioned seismic environmental assessment (Moulton et al. 2003). Uncertainties in this modeling, stemming in part from the inability of specifying in advance the specific seismic source and the exact water column structures governing sound propagation, made it advisable to institute a direct field monitoring program. The resultant inter-institutional "Gully Seismic Research Program" was coordinated by the Centre for Offshore Oil and Gas Environmental Research (COOGER) out of BIO. One component undertaken by the Ocean Sciences Division (OSD), BIO, consisted of a pilot study of seismic origin near-bottom sound intensities at $\geq$ 1000 m depths within both the Gully MPA NBW concentration area and the deeper-water region of the MPA to the south. This effort utilized modified Geological Survey of Canada (GSC) Ocean Bottom Seismometer (OBS) instrument packages configured to record water column sound pressures from a single integral hydrophone. While recognizing that the instrumentation, even after adaptation, would have mission-specific limitations in regard to recording endurance, frequency bandwidth, and necessary deployment undesirably close to a major acoustic interface, i.e. the ocean bottom, the OBSs constituted the only available equipment affording deep, non-intrusive, low noise recording which could be fielded within the survey time constraints.

To complement this effort, Marathon Canada engaged JASCO research Ltd. in a field monitoring and modeling study of the seismic array's short to long-range fields (Austin et al. 2004) in the upper 200 m of the water column. The short-range portion of these studies, utilizing vessel *Strait Signet*, was conducted in the western portion of survey block EL2410, outside the Gully. An extensive series of upper water column acoustic observations were also conducted in and around the Gully MPA by the University of Quebec at Rimouski and the DFO Institut Maurice Lamontagne (IML).

The OBS portion of the Gully Seismic Research Program had the following objectives:

1) To monitor near-bottom acoustic levels originating from exploration seismics during close survey approaches to the Gully Marine Protected Area, as well as to monitor the ambient background noise field.
2) To identify cetacean vocalizations, especially those of the endangered northern bottlenose whale (NBW), and to explore any systematic time variations in these vocalizations which might correlate with periods of active seismic shooting.
3) To explore the spatial-temporal correlation of cetacean vocalizations in the Gully whale concentration area in order to assess the feasibility of future whale tracking by acoustic triangulation.
4) To compare field-observed seismic acoustic levels with those predicted by retrospectively-parameterized theoretical models. This would elucidate both the general utility and limitations of predictive modeling.

The current report largely confines itself to objectives 1) and 4). An earlier report (Cochrane 2005) covered much of the same material in a condensed form. The expanded report provides full analytical details, corrects a significant error in the shot point origin of "Profile 1", introduces modest refinements in the computation of acoustic transmission losses along the remaining Profiles, and provides additional modeling results.

METHODS

INSTRUMENTATION

Ocean Bottom Seismometers

Six advanced OBS instruments were utilized. Three instruments were newly constructed (henceforth designated "new"). Three existing units were upgraded to approximately identical status (henceforth designated "modified"). Construction and upgrades were contracted to Omnitech Electronics Inc. (Dartmouth, Nova Scotia). Detailed technical specifications and contract administration were handled by the GSC after technical consultations with Ocean Physics Section, OSD, BIO.

OBSs are designed for free-drop deployment from a vessel. Subsequent internal digital data recording begins at a pre-programmed start-up time. For recovery, an integral VEMCO Ltd. custom ballast weight release is activated by either surface acoustic command or after a pre-programmed time interval, allowing the instrument to float to the surface. For their primary design application of recording earth-borne seismic signals, the units are equipped with three mutually perpendicular geophones and a single hydrophone, the latter mounted about 0.5 m above the base. For this present study's objective of recording water-column propagated sound, only the hydrophone signal was utilized, the geophone channels being deactivated.

OBS electronics are designed around the Persistor Instruments CF2 microcomputer. In a trade-off between a broad frequency response, desirable for capturing marine mammal vocalizations, and recording endurance, constrained by available data storage capacity (a

single 20 GB mini ATA HDD furnishing 8 GB of available storage via 4 x 2 GB FAT16 partitions), the acoustic signal(s) was sampled at a 5 kHz rate to 16 bit resolution. The three "modified" OBSs recorded a single bandpass-filtered hydrophone channel. The three "new" instruments recorded 2 channels, both sampled at 5 kHz: Channel 1 consisted of the filtered hydrophone signal as in the "modified" instruments. Channel 2 consisted of the time domain output of a "click detector". The click detector was designed to furnish a distinctive output for marine mammal click vocalization signals above the 2.5 kHz Nyquist folding frequency. Data for both "new" and "modified" instruments were recorded in discrete 32 MB files with a 512 Byte data header containing timing and configuration information. Single-channel file acquisitions lasted 3355 s (just under 56 min) separated by 87 s non-acquisition, inter-file gaps while data were transferred from RAM to hard drive (hard drive mechanical noise emissions precluded effective data acquisition during transfer). Single-channel unit recording endurance was about 9.8 days. For the dual-channel units, both single file and total recording endurance were halved.

The rationale for the OBS click detector was the detection of short, nearly monochromatic acoustic bursts or "clicks" from, especially, the above mentioned endangered northern bottlenose whale. The available literature indicated that NBW clicks occur in trains, each click tending to be about 0.3 ms in duration with peak spectral components between 21 - 25 kHz for deep-diving animals, but longer, typically 0.5 – 3 ms duration, and of generally lower and more variable spectral content, 4 - 21 kHz, for animals near-surface (Hooker & Whitehead 2002). To capture such vocalizations lying well above the Nyquist and low-pass (LP) cut-off frequencies of the direct hydrophone channel, the analog hydrophone signal before LP filtering was routed to a full-wave rectifier followed by a 2 kHz LP filter to extract the millisecond-order duration modulation envelopes of individual clicks. Envelope amplitudes were subsequently high-pass (HP) filtered to block DC levels and digitized at the standard 5 kHz rate. By appropriate choice of filter time constants, short clicks of dominantly high frequency content, which were totally invisible on the direct hydrophone channel, yielded recorded waveforms distinct from those produced by lower frequency, longer duration clicks clearly visible on the direct channel and believed to originate from other cetacean species. This will be further elaborated below. While clicks of predominately high frequency content could be detected by this methodology, determination of the precise spectral content or even click amplitude – except possibly the comparative amplitudes of clicks of similar character – was precluded.

"Modified" OBSs utilized Ocean & Atmospheric Science, Inc (OAS) model E-2SD hydrophones with specified omni-directional pressure frequency responses flat to ± 1 dB from 0 to 5 kHz and nominal mid-band sensitivities of -187 dB re 1V/μPa. These hydrophones were coupled to high impedance pre-amps integral to the OBS electronics. Two OAS field-utilized hydrophones were recalibrated post-experiment at spot frequencies of 165 and 250 Hz under contract to IBK Technologies Ltd. Resultant measured sensitivities were within 0.4 dB of the nominal value which was used in subsequent calculations. "New" OBSs utilized High Tech. Inc. (HTI) model HTI-90-U series hydrophones with built-in preamps and mid-band sensitivities, including preamp,

of about -149.5 dB re 1V/μPa. The HTI hydrophone responses (for "click detector" operation) extended to about 20 kHz. The HTI hydrophones had been calibrated by the manufacturer pre-delivery and were not recalibrated.

To document stand-alone OBS recording gains and frequency responses, one randomly chosen "new" and one "modified" OBS unit were analysed in the Ocean Physics Section, Ocean Sciences Division, at BIO. OBS measured mid-band voltage amplification gains, overall system predicted pressure sensitivities at the hydrophone, and pressure sensitivities per digitizing interval for the recorded data stream are listed in Table 1. Laboratory-measured OBS electronics frequency responses from the hydrophone inputs relative to the mid-band gains listed in Table 1 are shown in Fig. 2. Voltage outputs (i.e. max +ve & -ve) of the "new" OBS click detector for 2 ms sine wave bursts of varying frequency injected at the hydrophone input are shown in Fig. 3. It is observed that burst (carrier) frequencies above about 2 kHz result in almost purely –ve going output voltage responses. For frequencies below 2 kHz the response rapidly changes to a nearly symmetric bipolar form i.e. one containing roughly equal +ve and –ve going excursions. This characteristic was found to be relatively insensitive to the input burst length.

On OBS recovery, all recorded data was transferred to a portable PC hard drive for analysis. Native format OBS files were additionally converted to the WAVE file format. This provided the option for either numeric analysis in the simple native file format or, alternatively, direct audible examination or the application of "canned" analytical software developed for traditional audio interests using the WAVE format. A custom *MS Windows*[1] program allowed visual examination of native format waveforms in either calibrated linear (μPa) or logarithmic (dB re 1μPa) forms with flexible zoom capability in amplitude and/or time base. Provision was also included for display of the signal 1st digital time derivative (DD), i.e. successive amplitude differences. The DD technique introduces a ω^2 response factor into the dominantly "red" oceanic ambient noise spectrum (Clay & Medwin 1977) de-emphasizing low frequency background "rumble" and greatly enhancing the visibility of higher frequency "click" or "squeal" type marine mammal vocalizations captured on the direct hydrophone channel.

Sound Speed Profiles

For acoustic propagation-related sound speed profile determinations, relevant oceanic data were gathered from deep Seabird SBE-9 CTD (Conductivity-Temperature-Depth) profiles from CCGS *Hudson* in the general Gully region preceding the experiment, and from Sippican X-7 XBT (Expendable Bathythermograph) Sippican XSV-02 (Expendable Sound Velocity) probe profiles from CCGS *Edward Cornwallis* during the experiment. Reference is also made to complementary CTD-based sound profiles collected by both *Ramsford Viking* and *Strait Signet*. Our CTD data were reduced to sound speed profiles using the formulas of Clay & Medwin (1977) or Mackenzie (1981). XBT temperature profiles were converted to sound speed assuming a fixed salinity of 35 ppm – except at shallow depths where a linear salinity gradient from 32 ppm at the surface to 35 ppm at 165 m was used for better general conformity to many Scotian Shelf observations. The

[1] *Microsoft* and *Windows* are trademarks or registered trademarks of Microsoft Corp.

effect of the latter adjustment is minor. Water column acoustic attenuations (less critical) were estimated using the methods of Francois & Garrison (1982a, b).

ACOUSTIC LEVEL PREDICTION

The principal objective is to explore the predictability of received acoustic levels given detailed knowledge of the seismic source, the path bathymetry, and the character of the propagation media i.e. the ocean sound speed and attenuation distributions and the geoacoustic bottom parameters.

Generally sound propagation to long ranges is more readily modeled in the frequency (spectral) domain than in the time domain. More specifically, modeling received spectral domain signal amplitudes from a given source at a given location requires both a spectral source radiation model and a compatible range-dependent transmission loss propagation model. The received spectral sound pressure level, *SPL*, (in dB re to 1 $\mu Pa^2/Hz$) at frequency *f*, receiver range *R*, and depth z, can be related to the modeled seismic spectral source *SL* measured at a reference range of 1 m from the source located at depth d, using the propagation model derived transmission loss, *TL*:

$$SPL(R,z,f) = SL(1\,\mathrm{m},d,f) + TL(R,z,d,f) \qquad (1)$$

An applicable seismic source model developed in-house as well as applicable propagation models will be discussed before proceeding to their usage in the prediction of OBS observed sound levels.

Seismic Source Array Model

Ramform Viking employed dual 3090 cu. in. airgun arrays. Individual arrays were discharged at 22 s intervals with shot times staggered to yield 1 shot every 11 s. Each array consisted of 3 parallel non-identical sub-arrays towed side-by-side at 12.5 m lateral separation (Fig. 4). Constituent SODERA G airguns of 20 to 250 cu. in. were streamed at 6 m depth. Approximately half the sources consisted of gun pairs or "clusters" at about 0.8 m lateral separation. Guns were discharged simultaneously (±1 ms) at a pressure of 2500 psi.

Seismic airgun arrays are designed to enhance the vertical downward radiation of energy at exploration frequencies (<100 Hz). This is accomplished by, first, simultaneously firing all guns so that the "first break" pressure signature of each gun adds in-phase in the far field perpendicular to the array plane (i.e. downwards) and, secondly, by suspending airguns 5 – 6 m below surface so that their inverted, pressure-release surface reflections are delayed sufficiently to enhance the array's downward spectral signature in the primary exploration frequency band. For a sound velocity of 1480 m/s and a 6 m gun depth, the spectral component at 62 Hz will be maximally enhanced. Array directivities generally decrease for lower and higher frequency components. At higher frequencies directivity is determined by the superposition of direct pulses and "Lloyd Mirror" pulse

reflections from the water surface. Array "side lobes" appear in selected frequency radiation patterns when individual airgun spacings significantly exceed ½ the relevant acoustic wavelength. For the *Viking* source, where sub arrays are spaced 12.5 m apart, side-lobe effects in the pattern perpendicular to the sub array spread should begin to appear at about 60 Hz.

To estimate the array time-domain pressure signature at an arbitrary point in space as defined by azimuth, dip-angle, and range from either the array center or its surface projection one can simply linearly add individual gun pressure pulses with appropriate propagation path delays, each gun modeled as an omni-directional point radiator. Inverted water surface reflections can be included as appropriate. The properly scaled squared Fourier transformation of the summation yields the corresponding spectral representation. This simplistic approach has the frequently serious limitation of ignoring the interactions between simultaneously discharged airguns (Vaage et al. 1984, Ziolkowski et al. 1982, Nooteboom 1978, Giles and Johnston 1973). Air bubbles ejected by individual guns do not oscillate at free ambient pressure but rather are subjected to the superimposed pressure fields generated by nearby guns thereby modifying their radiated "bubble pulses". Industry commonly overcomes this problem by measuring the time domain pressure signal at a large number of hydrophones distributed among the array elements from which the true pressure signature of each airgun can be uniquely determined by solving a system of linear equations. This approach also allows subsequent computation of the far-field signature by the appropriate summation. Alternatively, sophisticated algorithms have been developed to precisely model the basic physics of airgun interactions thereby also yielding a more accurate theoretical representation of the seismic pulse than afforded by non-interactive summation (Laws et al. 1990). Since direct measurements are largely unavailable for the *Viking* array and physical interaction models involve a complexity beyond that feasible for this preliminary study, we utilize the simple linear approach with modification only for the case of the airgun clusters where non-linear effects are strong and cannot be ignored even to first order.

Airgun interactions influence bubble pulse oscillations rather than initial pulse rise times. In general, the minimum separations at which airguns do not significantly interact are roughly proportional to $(VP_{gun}/P_{ambient})^{1/3}$ where V is the airgun volume and $P_{gun}/P_{\text{ambient}}$, the ratio of airgun to ambient pressure (Vaage et al. 1984). These investigators review three variant literature-reported formulations yielding minimum separations for negligible interaction. Using representative *Viking* array (Fig. 4) gun sizes of 20, 100, and 250 cu. in., corresponding critical separation distances are roughly 1 – 2 m, 1.5 – 3 m, and 2 – 4 m respectively. It is concluded that adjacent sub-arrays at 12.5 m separation do not significantly interact (the equivalent single airgun size of a cluster generally differs from the arithmetic sum of component capacities, but if one simply assumes 2 x 250 cu. in. = 500 cu. in. the interaction distance would be 3 – 6 m). For individual sub-arrays the largest airgun clusters are placed at the ends (14 m separations) and therefore should not significantly mutually interact. However, some interaction might be expected between adjacent guns of the sub-array. The "end" dual-gun clusters are spaced 3 m from

adjacent guns as opposed to 2 m between the remaining guns which should limit their immediately adjacent interactions.

In our formulation the peak radiated pressure P of an isolated airgun is assumed given by:

$$P = 0.708\, V^{1/3} (P_{gun} / 2000)^{0.75} \qquad (2)$$

The coefficient of proportionality has been chosen for consistency with "industry" units, P specified in bars, V in cu. in., and P_{gun} in psi, the convention followed below. The above relation follows from the volume and pressure dependencies reported by Vaage et al. (1983) and our interpretation of empirical measurements of G Gun pressure signatures reported by the manufacturer (Seismic Systems Inc. & Sodera 2004).

For clusters of N identical airguns, the modified pressure P_0 is assumed to be:

$$P_0 = P(N)^{0.75} \qquad (3)$$

Giles & Johnson (1973) suggest an exponent of 0.85 while the manufacturer's data and one example by Laws et al. (1990) suggest the slightly variant exponent of 0.75 which we have utilized.

For a **very shallow** seismic source Vaage et al (1983) find the ratio of the peak-to-peak (p-p) amplitudes, including superimposed surface reflections, of the 1st and 2nd bubble pulses to the primary pulse p-p amplitude to be directly proportional to depth.

The 0-peak (0-p) bubble pulse to primary ratios have been approximated by

$$\frac{P_1}{P_0} = 0.0962\, z \qquad (4)$$

$$\frac{P_2}{P_0} = 0.02516\, z \qquad (5)$$

where z is the airgun depth (in meters) from surface and where the proportionality constants have been obtained by modeling and comparing the experimental Sodera G-Gun signatures reported by the manufacturer (Seismic Systems Inc. & Sodera 2004) and by Oakwood Computing Associates in connection with their sophisticated GUNDALF airgun array modeling program (Oakwood Computing Associates 2004). The Sodera and Oakwood Computing experimental measures are quite consistent when air gun depth is taken into account. The Oakwood Computing results also indicate that G-Gun bubble pulse ratios do not change significantly with gun volume, contrary to the $V^{0.25}$ dependence suggested by Vaage et al. (1983). Amplitudes for gun clusters were inferred by similar methodologies.

The primary to first bubble pulse period, $T1$, is given by

$$T1 = 0.1744\ V^{1/3}\ Z_0^{-5/6}\ (P_{gun}/2000)^{1/3} \qquad (6)$$

using the functional form of Giles & Johnston (1973) and a proportionality constant derived from the reported Sodera data. $T1$ is in seconds, P_{gun} the gun pressure in psi consistent with previous usage, V in cu. in., and Z_0 the ambient hydrostatic pressure in meters of water including atmospheric, i.e. 10.1 + 6 = 16.1 m for a gun at 6 m below surface. The Sodera data indicated virtually identical periods for bubble oscillations beyond the 1st.

Rise and fall times of the positive pressure portions of the initial and immediately following successive bubble oscillation pulses are crucial in determining the seismic signature spectrum. The literature contains few reliable experimental measures of the rise time of the initial discharge which is especially critical in determining radiated power at frequencies above 100 Hz. Much reported data has been low-pass filtered at 100 – 200 Hz since the high frequency spectral "tail" is deemed of little importance to deep seismic exploration objectives. Nevertheless, some data exists. Verbeek & McGee (1995) show a high time resolution recorded signature of a 10 cu. in. airgun. Johnston (1980) reports the oscillographic pressure signature of a 100 cu. in. airgun at 1200 and 2000 psi. Wardle et al. (2001) show a high resolution signature of a 3 x 150 cu. in. Sodera cluster gun. By trial and error comparison we found that, in all cases, initial primary pulse signatures are reasonably well approximated by a linear pressure rise to maximum over a period τ_{RT} (in seconds) given by (units as previous):

$$\tau_{RT} = 2.43\times10^{-6}\ V^{1/3}\ P_{gun}^{1/2}\ N^{0.75} \qquad (7)$$

The initial exponential decay time constant for the primary pulse was similarly chosen as:

$$\tau_S = 5.46\times10^{-4}\ V^{1/3} \qquad (8)$$

The initial pressure pulse is assumed to decline exponentially over a period equal to two time constants and then linearly to zero at a predetermined zero crossing point.

Remaining (bubble pulse) exponential time constants were assumed proportional to the cube-root of airgun volume, and to the hydrostatic depth to the negative 0.6 power as suggested by analogy with explosives (Chapman 1985). Proportionality constants were determined by reference to the literature-reported signatures above.

The rise time constant of the 1st bubble pulse (following the initial impulse) radiated pressure (approaching maximum) is set to

$$\tau_R = 1\times10^{-2}\ V^{1/3}\ Z_0^{-0.6} \qquad (9)$$

and the time constant for the initial portion of the fall:

$$\tau_D = 0.64\ \tau_R \qquad (10)$$

Identical time constants were used for the 2nd bubble pulse (the initial impulse and a maximum of two following bubble pulses were modeled for any array gun). The 1st and 2nd bubble oscillations were each modeled by a linear rise from zero over 1 "rise" time constant , an exponential rise to maximum over a 2nd identical time constant period, followed by an exponential fall, then a linear fall to zero, each fall over identical periods equal to one "fall" time constant.

The negative pressure portions of the radiated wave field are inherently more diffiult to infer since they are largely obscured to direct empirical measurement by surface reflections unless the airgun source is placed quite deep – where bubble pulse behaviours differ markedly from those at shallow depths. Briefly, the negative going pressure pulse is modeled as a negative going sinusoid with known zero crossing points and with an amplitude consistent with the piece-wise preservation of total seismic moment. That is, the integral of radiated pressure over the -ve pressure pulse must balance the integral over defined portions of the bounding +ve going pulses in such a manner that the total radiated pressure pulse integral is zero (i.e. is of zero mean).

Some computed examples are shown for the *Viking* airgun array. Fig. 5 shows the far-field time domain signature directly under the array, i.e. 90º below the horizontal plane, and the corresponding spectrum for a simulated 5 kHz sampling rate, 1/3 octave spectral smoothing being applied. Also shown are similar plots at 10º off the horizontal plane but not including surface reflections. Fig. 6 shows the azimuthal radiation pattern at 10º off the horizontal for several frequency components.

Acoustic Propagation Model

Acceptable long-range acoustic propagation models for exploration seismic sources must rigorously accommodate "low" acoustic frequencies, that is frequencies with corresponding wavelengths comparable to the lesser of the water column depth or the vertical dimensions of any water column sound velocity structures constraining long range propagation (for example sound channels). Acceptable models must also have the capability of handling at least moderate range dependencies in the propagation environment and of properly describing the distribution of sound within a wavelength of the top and bottom water column boundaries. The above constraints are arguably best met by Parabolic Equation type propagation models as used in this analysis.

Parabolic Equation (PE) models, for a given source function, represent proximate far-field solutions of the governing 1-way Helmholtz equations (Jensen et al. 2000). PE formulations differ largely in the approximations employed to reduce a square-root differential operator term to a form tractable to numerical solution. Increasingly sophisticated (and complex) approximations yield better wide angle performance i.e. more accurate estimates for energy propagating further from the horizontal plane. At

continental shelf depths long-range propagated sound is generally physically constrained by successive reflections off the sea surface and the bottom. For soft sediment bottoms, sound incident at grazing angles less than 20 - 30º is totally reflected with only minor attenuation. Sound reflected at steeper angles suffers enhanced loss since a portion of the incident energy is refracted into the bottom. Such sound, subjected to multiple lossy reflections, decays rapidly with range. PE implementations employed for long range continental shelf depth path predictions should perform well at grazing angles in excess of 30º.

Three PE formulations were initially explored for this analysis. The first two were the classical "Tappert" model in the form presented in Jensen et al. (2000) and the "Wide Angle" model of Thomson & Chapman (1983) in the form described by Thomson (1990). Both utilize "split-step" Fourier solution techniques which were programmed from first principles for an interactive MS Windows[1] environment. Resultant codes enable direct sound speed data assimilation from XBT and CTD profiles and direct graphical display of results. The Tappert model is valid for waves propagating up to about 20º from the horizontal. The Thomson & Chapman PE model performs well to somewhat beyond 20º. However, neither model readily incorporates spatially variant density which can be only included by numerically approximating the spatially smoothed 1st and 2nd vertical derivatives of the density function (Jensen 2000). Our attempts to incorporate density have not met with good results for long propagation ranges using these two algorithms.

An extremely wide-angle PE formulation which utilizes a Padé series expansion of the square root operator and which more naturally incorporates spatially variant density is described by Collins (1989). A convenient split-step solution, described by Collins (1993), incorporates the Padé expansion of an exponential function of the square root operator term. Published FORTRAN code (RAM model) for the split-step Padé solution was adapted and incorporated into the Fortran-based MS Windows framework (Lahey[2] LF95 v5.6 + Winteracter[3] 4.0) developed for the earlier PE models. Use of 5 Padé terms results in good performance for energy propagating up to about 75º from the horizontal. For computational simplicity and efficiency the RAM code utilized considered only compressional waves and assumes smooth interfaces at the water surface and, locally, at the bottom. This latter model was used exclusively for the results computed below.

For *TL* estimation, an omnidirectional PE model source was assumed, specifically the "Collins self-starter" (Collins 1992). Our coding also permitted use of the wide-angle analytic "Greene's source" (Jensen et al. 2000). On testing, Greene's source yielded nearly identical results to the Collins source in our applications. Water surface reflections are not included at source but are implicitly added by the PE model. The computational grid extended to just over 4 km depth. A strong artificial absorbing layer starting at 3 km depth was used to suppress reflections from the grid lower boundary. An identical vertical grid increment of 0.5 m was used from 25 Hz (lowest computed center

[1] *Microsoft Windows* is a trademark or registered trademark of Microsoft Corp.
[2] Lahey Computer Systems, Inc., 865 Tahoe Blvd., P.O. Box 6091, Incline Village, NV 89450.
[3] Copyright Interactive Software Services, Ltd., Westwood House, Littleton Drive, Huntington, Staffs WS12 4TS, UK

frequency) to 400 Hz (highest computed center frequency). A horizontal increment of 10 m was used at all frequencies.

At a given acoustic frequency, transmission loss typically varies spatially in a rapid manner due to the constructive and destructive interference of energy arriving along differing paths. For mid-water observation points, rapid spatial *TL* variability can be reduced by spatial averaging. Since the OBS hydrophone sits near-bottom, where especially rapid vertical variability in *TL* might be expected, and since the bottom acoustic interface is frequently sloping, neither direct vertical nor horizontal spatial averaging was considered a safe procedure. Alternatively, *TL* was averaged over 10 equi-logarithmically-spaced frequencies spanning a 1/3 octave band centered on the nominal frequency. This more computation-intensive procedure yielded significant spatial smoothing of small scale interference effects while retaining full grid resolution.

Predicted OBS received levels were derived from Eq. 1, setting the source spectral SPL to that given by the far-field array model for sound emitted close to the horizontal. The source spectral SPL was averaged over a 1/3 octave bandwidth for consistency with the *TL* term computed and averaged over a similar bandwidth as described above.

FIELD EXPERIMENT

OBSs were field-deployed (Table 2, Fig. 1) on June 17th and successfully recovered on July 4th utilizing CCGS *Edward Cornwallis* via contract to Geoforce Consultants Ltd. Dual-channel OBSs (Stations #1, 2, & 3) were placed along a 10 km line transecting the known NBW congregation area (Hooker et al. 1999) within the MPA. Stations #2 & 3 were deployed 2 km apart to enable examination of the spatial correlation of whale vocalizations in order to establish the feasibility of future 3-D animal localization using a denser recording array. Single-channel OBS instruments (Stations #4, 5, & 6) were placed close to the intersection points of three track lines "A", "B", and "C" (not shown) acoustically modeled in a pre-survey Environmental Assessment (Moulton et al. 2003). Deployment depths listed in Table 2 are inferred from bathymetric charts, the standard bathymetric sounders on *Cornwallis* proving ineffective in these water depths.

The initial field plan was for *Viking* to shoot through the origins of the previously modeled track lines prior to the commencement of regular survey profiling. Execution of the original plan was precluded by the delayed on-site arrival of *Viking* combined with further delays to adjust exploration gear buoyancies to ambient conditions and due to unfavourable sea states. Instead, *Viking* commenced its regular scheduled survey, which was confined to the western half of EL2410 during the available OBS observation window, relegating data gathering to an opportunistic basis. Due to successive delays in survey initiation and external constraints on the availability of the OBSs it was decided to initiate pre-programmed recording as late as possible into the deployment consistent with the recovery of near maximum length data sets (starting 1500Z June 23rd for Stations 4, 5 & 6, and exactly 5 days later for Stations 1, 2 & 3 which acquired data at twice the rate).

XBT and XSV profiles, for sound speed control, were obtained at OBS deployments and recoveries. All XSV profiles proved sufficiently noisy (cause undetermined, possibly grounding problem) to preclude their direct usage for subsequent propagation modeling although, in general, they supported XBT derived velocity profiles when rough comparison was possible. Deep water CTD profiles from CCGS *HUDSON* in or near the Gully area in April and May 2003, prior to OBS deployments, afforded the opportunity to explore longer term seasonal variations in the sound speed profile and to document the deeper portions of the profile lying beyond the penetration depths of the expendable probes. Data used to compute sound speed are listed in Table 3.

ANALYSIS

BASIC ACOUSTIC OBSERVATIONS

General

On OBS recovery it was discovered that instruments from Stations #2 and #3 had failed almost immediately on deployment due to flooded data port connectors. Station #4 recorded only a 3-day data set due to a firmware glitch which caused the available recording media to be inefficiently utilized. Stations #1, 5, and 6 recorded essentially full data sets.

Seismics

Seismic impulses were visible on OBS recordings during most periods of active seismic shooting. Impulse amplitudes ranged from in excess of full scale (maximum recording dynamic range) to below ambient background and invisible or discernible only in the 1st derivative signal. Seismic pulse envelopes at 40 – 60 km range tended to be highly elongated in time compared to the theoretical source pulse at origin. Envelope rise times were typically ~0.5 s followed by a roughly exponential amplitude decay of time constant 1.5 - 2.5 s (Fig. 7). The impulse decay was frequently clearly visible during the first 5 – 6 s of the 11 s survey interpulse interval. In several observations spanning the sudden cessation of airgun profiling, acoustic levels continued to fall beyond 11 s from the last recorded pulse (Fig. 8) indicating that the non-seismic ambient noise background was not being reached during any point in the immediately prior seismic shooting.

To further explore relationships between observed acoustic levels and seismic shooting periods, all recorded OBS data were systematically scrutinized. Displayed in Figs. 9 to 12 are the maximum instantaneous pressure excursions from zero (i.e. peak absolute amplitude) over consecutive 300 s analysis intervals, RMS amplitudes **averaged** over the same 300 s intervals, and maximum and minimum RMS amplitudes averaged over any consecutive 1 s interval embedded within a 300 s primary analysis interval. Also marked are the periods of active seismic shooting including the initial ~30 minute ramp-up to full array power. No filtering or other forms of signal conditioning have been applied except

the removal of small instrument-specific DC level offsets. Corresponding probability density functions (PDFs) for the acoustic levels presented in Figs. 9 to 12 are reproduced in Figs. 13 to 16 respectively. Three separate groups of PDFs are shown: One PDF group encompassing all recorded station data; a second group limited to seismic shooting periods only; and a third group covering non-shooting periods only. The numerical PDFs (vertical axes) are the probability of an observed acoustic pressure level falling within a 1 dB amplitude increment centered on discrete integer amplitudes on the horizontal axis. For display, plotted probabilities have been joined.

The following general observations are made:

1) Acoustic levels at Stations #5 and 6 are consistently and significantly enhanced during seismic shooting. Seismic shooting levels at Station #6 are generally 3 – 5 dB higher than at Station #5. Signal clipping, i.e. signal levels exceeding instrument dynamic range of about 145 dB 0-p (Table 1), was very frequently observed at Station #6, but only occasionally at Station #5, and then, for short intervals only.

2) Mid-transect minimum acoustic levels (blue traces) in any 1 s window over consecutive 300 s intervals during seismic shooting at Stations #5 and 6 are frequently enhanced at least 10 dB over corresponding values for non-shooting intervals. At both ends of N-S survey transects, received seismic levels are lower but the transition from shooting to non-shooting minimum levels is still frequently 6 – 7 dB. This could be interpreted as indicating that non-seismic ambient background is not being reached at any point in the 11 s inter-shot interval. Nevertheless, an alternative mechanism is also possible: The population of low-level 1 s intervals in any 300 s stretch will be considerably higher for non-shooting than for shooting periods due to the lack of the high level seismic signal in the former. Therefore probability would dictate finding a lower RMS interval within the larger available population i.e. the non-shooting interval. This problem is likely exacerbated by the presence of low frequency rumble below the main seismic frequencies which would effect the variance (i.e. RMS level) of the 1 s samples in a somewhat erratic manner. High-pass pre-filtering OBS data at about 10 Hz or so to include only seismic origin frequencies before the computation of statistical measures might provide a more definitive test. Visual inspection of records at the cessation of shooting (one example has been shown in Fig. 8) appears to reveal cases attributable to each mechanism. The contrast between shooting and non-shooting minimum signal PDFs is very apparent in Figs. 15 and 16.

3) Acoustic levels at Stations #1 and 4 are less noticeably enhanced during seismic shooting. Shooting intervals are very limited for Station #1 but during these periods seismic signals are frequently rivalled or obscured by high background noise levels of non-exploration seismic origin. Station #1 noise levels show frequent intense outbursts of 6 – 8 hour duration and averaging about 117 dB re 1 Pa RMS having no clear simultaneous counterparts at Stations #5 and 6 (also note extended high end roll-off of 300 s RMS level PDF and 300 s maximum signal PDF for non-shooting periods in Fig. 13). On inspection of the time domain signal, a strong continuous 37 Hz sinusoidal component points to a ship origin. Similar types of noise are not observed at the other

OBS stations. Mutual comparison of levels at Stations #1 and 4 is difficult due to lack of temporal overlap.

4) At almost exactly 18:11Z 28 June (Day 178.758), source time, there occurred a sudden ~10 db drop of observed signal levels at both Stations #5 & 6 within the space of 1 seismic ping. Available seismic logs from *Viking* documented no changes in array discharge pattern such as shutting down one or more subarrays. The drop affected both source arrays (which discharge alternately). Since the "high" and "low" states maintained the same discharge cycle at both OBS stations without time shift it seems unlikely that two differing surveys were being observed, the sudden shutdown of one allowing the other to be unmasked.

5) During **quieter** non-shooting periods, ambient noise levels at all stations are fairly similar, about 100 dB RMS at Station #1 and 2-3 dB higher at Stations #4, 5, & 6 judged from successive 300 s RMS levels (also note low end PDF cut-offs for 5 min. RMS levels for non-shooting periods in Figs. 13 to 16).

For Station #1, in the NBW whale concentration area, the highest 0-peak signal level **clearly originating from seismics** was 139.4 dB occurring at 04:21:02 Z on the 29th June (day 179.181). *Viking* was located at 43º 36.274' N 59º 30.853 W (just south of point "A4" in Fig. 1) at 55.9 km range. The highest level occurred during an ~ 8 min. period of exceptionally high seismic signal levels outside of which 0-peak levels were of the order of 128 – 130 dB. The RMS level in a 1 s window centered on the highest peak signal, which would appear to correspond to the Sound Exposure Level (SEL) of Davis et al. (1998), was 128.8 dB. The SEL will be numerically much closer to the maximum RMS level for a distant seismic shot with a pulse envelope duration exceeding 1 s than for short range observed shots with envelope durations <<1 s. Maximum 0-peak levels at Stations #5 & 6 are estimated to lie in the vicinity of 146 and 150 dB respectively after making reasonable allowances for clipping in the strongest received signals. The above quoted levels utilize the full analog passbands of the OBS systems.

Power spectra of the ambient noise signals, $P(t)$, during one simultaneous, quiet, non-seismic shooting period (starting day 179.250) at Stations #1, 5, and 6 are shown in Fig. 17. A spectrum for an identical-length, non-simultaneous data set selected from a very quiet period (starting day 173.672) at Station #4 is also shown. At each station, 50 consecutive 32768 pt (5.46 min. total) Fast Fourier Transforms (FFTs) were squared and averaged, and the resultant raw signal powers divided by the frequency increment to yield power spectral densities, $S_{nn}(f)$, expressed in dB re 1μPa^2/Hz. For display purposes a rescaled variance conserving spectral density, $P_{nn}(f)$, is defined and utilized with the property[1]:

[1] An alternative convention (used for instance in MatLab) is to sum the squared transforms over +ve frequencies only resulting in the original spectral estimate, $S_{nn}(f)$, above which is a factor of 2 (3 dB) lower than $P_{nn}(f)$ (Clay & Medwin 1977).

$$\int_0^{\infty} P_{nn}(f).df = \int_{-\infty}^{+\infty} S_{nn}(f).df = 2\int_0^{\infty} S_{nn}(f).df = 1/T\int_0^{T} P(t).dt = Variance\ P(t) \qquad (11)$$

Spectral $P_{nn}(f)$ levels were subsequently further smoothed by averaging each spectrum over 1/3 octave bandwidths. Only estimates above 1 Hz, confidently believed to accurately represent true ambient background, are plotted. Lower frequency estimates are very subject to locally generated flow noise and as well as to calibration uncertainties.

From Fig. 17, noise spectral levels at all Stations are seen to be comparable between 12 – 80 Hz, a frequency range which tends to be dominated by shipping noise (Urick 1975). Above 80 Hz increasing divergence is observed. This is unlikely to be a consequence of greatly contrasting sea states (Urick 1975) since measured wind speeds at Sable Island were 9 km/hr during the common Stations #1, 5, and 6 analysis period and 19 km/hr for the selected period for Station #4.[1] Below 12 Hz, the "modified" OBS Stations #4, 5 & 6 noise levels maintain good agreement to 1 Hz while the "new" OBS Station #1 shows a considerably enhanced comparative response from about 2 – 10 Hz. This Station #1 enhancement does not appear totally explicable by the faster low end roll-off response of the "modified" OBS electronics (Fig. 2). The "new" Station #1 HTI hydrophone response has a manufacturer-listed low frequency cut-off of 2 Hz which is not included in the Fig. 2 electronics response as the preamp is an external component. Addition of the preamp roll-off should act to make the overall **acoustic** low end responses more similar but this has not been directly verified. Locally generated flow noise might well persist into the 5 – 10 Hz range. Therefore, some uncertainty must remain in the compatibility off the very-low frequency roll-off responses for the two differing OBS instruments. Fortunately, this low end cut-off region lies below the primary energy frequency range of exploration seismic signals and should have little influence on comparative observed seismic signal amplitudes.

Marine Mammal Vocalizations

At all four OBS recording sites a semi-continuous background of clicks presumed of biological origin could be detected on applying the digital derivative (DD) technique to the direct hydrophone channel. Clicks were also audible on playback of the corresponding WAVE files with or without DD pre-processing. This points to considerable click energy below 2 kHz. Clicks tended to repeat regularly at about 1 s intervals over durations of several minutes. Frequently, overlapping trains of clicks could be detected suggestive of multiple sources. Occasionally, an overlapping set of clicks repeated at a short fixed time delay from the primary train. This phenomenon appeared consistent with reflection of a primary train from the ocean surface. On the basis of their wide geographic distribution and inferred spectral and repetitive character, we tentatively identify these clicks as originating from sperm whales (Goold & Jones 1995, Richardson et al. 1995, Mullins et al. 1988, Watkins et al. 1985). Infrequent squeals or whistles of a swept-frequency variety were also detected by audible inspection and later verified by

[1] Wind speeds obtained from Internet meteorological archive accessed through "Weather Underground" at http://autobrand.wunderground.com/.

WAVE file sonograms. These swept-frequency signals remained unidentified, and due to their infrequent nature were not subjected to further study.

At Station #1, on utilizing the high frequency-sensitive click detector channel, a virtually identical pattern of two-sided (both +ve and –ve going component) clicks was observed to that obtained by applying the DD to the simultaneously sampled 5 kHz direct hydrophone channel (Fig. 18). The similarity is probably a consequence of nearly identical low frequency roll-offs for both the analog click detector and the DD conditioned direct hydrophone channel. Occasionally, the click detector channel revealed distinctive bursts (~ 10/s) of "one-sided" clicks without direct channel DD counterparts (Fig. 18). On the basis of our understanding of click detector characteristics we attribute to these contrasting clicks to the northern bottlenose whale (NBW). In Fig. 18, two bursts of 6-7 clicks characterized by a roughly 0.1 s inter-click separations are reasonably characteristic of "surface" type NBW clicks as described in Hooker & Whitehead (2002).

Another interesting click detector recording (Fig. 19) reveals an apparent close whale encounter with an OBS in which the recorder was driven to saturation during two successive clicks. Clicks were quite regularly spaced at about 1 s intervals, somewhat longer but still reasonably compatible with the ~ 0.4 s NBW "deep-water" inter-click intervals also reported by Hooker & Whitehead (2002). Assuming 20 log *R* type acoustical spherical spreading from the source, click pressure amplitudes should vary inversely with range. If an animal were to swim directly towards an OBS instrument at constant speed, range would decrease linearly with time to passage and, consequently, click amplitude should increase inversely with time to passage. The time dependence of Fig. 19 click amplitudes appears reasonably compatible with such a scenario[1]. Following the click amplitude maximum, amplitudes decline very rapidly (at least 15 – 20 dB over 1 s). Perhaps vocalizations tended to be suppressed after target identification at passage or, perhaps, the sound source was directional with the principal radiation lobe directed away from the instrument after passage.

[1]Assuming omni-directional surface and bottom click sources of equal intensity and the OBS having an identical amplitude response to both (unlikely due to hydrophone directivities), a typical 300 count OBS response at the immediate surface (Fig. 18) at 1 km range translates, with spherical spreading, to a 3000 count amplitude response on the bottom at 100 m range, or about 10 s from nearest approach using Fig. 19. This implies an unreasonably high OBS approach speed of 10 m/s or about 20 knots. However, Hooker & Whitehead show that "deep-water" clicks are generally significantly shorter (~ 0.3 ms) compared to "surface" clicks (0.5 to several ms). The OBS click detector has not been characterized for sub-millisecond pulse (click) durations but is likely to comparatively underestimate their true amplitudes. This would tend to place the true 3000 count amplitude, time range at more than 10 s swimming range reducing the need for excessively high swimming speeds. We emphasize the above arguments are highly speculative since little is known about NBW click amplitudes (or even if this particular instance of apparent deep-water clicks truly originate from the NBW) and laboratory click detector characterization is presently only partial.

Under the working assumption that the click detector can discriminate NBW clicks, Station #1 data was extensively analysed under contract to explore possible relationships between NBW clicks and periods of seismic shooting[1].

ACOUSTIC LEVELS MODELING

Propagation Considerations

From winter until May or June on the Scotian Shelf/Slope, near-surface origin sound is efficiently captured in a low temperature, low sound speed "sound channel" centered at about 70 m depth within which sound can travel to long ranges with minimal bottom interaction. Later, with growth of the seasonal thermocline, a high sound speed "lid" forms on the top of the channel. When the lid is fully developed, typically by mid-summer, sound originating from sources located within the shallow lid zone is refracted strongly downward passing through the low sound speed channel with limited trapping. For long range sound propagation, especially on the shallow continental shelf, this results in stronger sound interaction with the bottom and, consequently, more rapid sound attenuation with range. Such seasonal variation in Scotian Shelf propagation conditions have long been recognized (Macpherson & Fothergill 1962). Specifics of the sound speed structures and their effects on propagation will be further explored below.

The systematic seasonal change in water column temperature and sound speed profiles is illustrated in the measurements listed in Table 3, a subset of which are graphically displayed in Fig. 20. Reproduced for April and May are profiles from the two deep CTD casts reaching 2975 and 1616 m respectively. These profiles exhibit excellent agreement at depth, with sound speeds increasing essentially linearly from about 800 to at least 2000 m, the greatest depth of significance in this study. These profiles serve as the determinants of the default deep sound speed structure for this entire analysis. The June sound speed profile of Fig. 20 is from the Station #5 "deployment" XBT to 828 m conducted on June 19th. The Station #6 deployment XBT profile (not shown) was quite similar. The Station #3 deployment XBT (not shown) in the Whale Sanctuary was also reasonably similar except that the base of the seasonal thermocline extended about 20 m deeper i.e. a thicker mixed layer. Below 200 m depth, sound speeds for all three profiles matched closely. A limited number of sound velocity profiles were also gathered by Marathon Canada Ltd. from *Ramform Viking* in the shooting area to the west. A June 29th *Viking* temperature profile to about 1325 m at 43 20' N 59 20' W is also reproduced in Fig. 20. It shows a cold intermediate layer rather similar to the Station #5 deployment profile but with a more pronounced "cap" characterized by a 11.5º C water temperature at the surface and a 10.0º temperature at the seismic source depth of 6 m. This *Viking* station was the apparently origin for the sound speed profile reproduced in and utilized for the shallower depth propagation analysis of Austin et al. (2004).

[1] Laurinolli, M. H. and N. A. Cochrane. Hydroacoustic analysis of marine mammal vocalization data obtained using ocean bottom seismometers in the Gully. Environmental Studies Research Fund (ESRF) Report (in preparation).

In contrast, the July 3rd Station #5 recovery profile differs radically from any of the profiles previously examined. Although this XBT profile was the only one successfully obtained on the OBS recovery leg, nothing inherent to the data suggests instrumental malfunction; the derived sound speed profile below 400 m converges well with the earlier deep profiles. Insight into the anomalous Station #5 sound speed is afforded by an intensive IML CTD survey[1] to 550 m maximum conducted over the entire Gully area from July 5-14 immediately following OBS recovery. Most of the Gully region was still covered by the cold intermediate layer between 50 and 100-150 m. However, a shallow warm intrusion was detected impinging on the southern extremes of a grid of N-S profiles which lay just north of Stations #5 & 6. Profiles approaching these stations showed a "pinching out" or even total loss of the cold intermediate layer. The warm intrusion did not extend to Station #4 or the central Gully NBW whale concentration area. Additional shallow sound speed profiles (to 100 m) from the more westerly Cortland-Empire blocks, reproduced in the same document, showed the cold intermediate layer to persist during the entire month of July although the exact location of sampling stations is not indicated. An additional June 23rd Marathon profile at 43º 25'N 59º 23'W (not shown) revealed a profile intermediate in character between those of July 3rd and June 29th, the shallow sound channel still being present but the low sound speed, cold intermediate layer being less pronounced. Curiously, this structure had reverted to the more "normal" profile form by the June 29th measurement not far to the south. The general impression is that the sound speed structure was spatially complex with warmer slope waters impinging on the southernmost part of the region in an irregular fashion. An attempt to better decipher the oceanographic variability around the deployment period using thermal satellite imagery was not definitive.

We have chosen the June 19th "deployment" profile from Station #5 supplemented by the observations of deeper water velocity structure from the April *Hudson* offshore CTD observations to represent the primary velocity structure for initial modeling of regional propagation paths. Additional models have also been computed using the July 3rd "recovery" Station #5 sound speed profile and the June 29th *Viking* profile to determine how contrasting upper water column sound speeds might influence observed OBS seismic sound levels at depth. For modeling, all XBT and the Marathon CTD derived sound speed profiles were linearly extrapolated to maximum depth using the computed sound speed (Mackenzie 1981) of 1497 m/s at 2000 m from the *Hudson* April 2003 deep CTD profile.

Acoustic properties of the sub-bottom can have a substantial influence on long range sound propagation on the outer Shelf and Slope but are difficult to reliably parameterize. The outer Scotian Shelf/Slope seafloor is characterized by exposed sequences of sand and gravel on the outer shelf and extending down the uppermost slope to about 500-700 m water depth. Beyond the 700 m bathymetric contour, the seafloor consists predominately of surficial clay and silty clay, forming an approximately 2 m-thick, acoustically transparent drape over glacial-marine sediments consisting of silty-clay with sand (Mosher et al. 2004). For simplicity, our PE models assume a default infinite depth sub-

[1] McQuinn, I., D. Carrier, S. Lambert-Milot, and A. Robillard. 2004. Measure of seismic airgun array pulses in the Gully MPA. Internal DFO summary document.

bottom of 1750 m/s compressional velocity, 1.9 specific gravity (S.G.), and 0.7 dB/wavelength (λ) compressional wave attenuation. Values chosen are consistent with those for waterlogged sand/gravels as tabulated by Jensen et al. (2000) and Clay & Medwin (1977). These values are not greatly inconsistent with the observed acoustic properties of finer-grained deeper-water Scotian Slope sediments at depth of several meters, and are a fairly good match to more consolidated materials about 10 m down (David Mosher, GSC Canada, personal communication). The finer-grained Scotian Slope surficial sediment drape has acoustic properties more closely approaching those of the overlying seawater; velocity, 1500 m/s; S.G., 1.5; and attenuation 0.1 dB/λ. We have chosen to handle the surficial material, to first order, by simply elevating the modeled depth for OBS measurement in the water column to 2 m above the harder bottom as parameterized above. This simple procedure allows the effect of a variable thickness surficial sediment drape to be studied by examining modeled transmission loss as a function of height above the uniform "harder" underlying sediment without having to rerun the computation-intensive model.

Specific Applications

Four contrasting acoustic profiles were chosen to explore the predictability of observed acoustic levels (Fig. 1):

Profile #1 – Moderately downslope profile from point A1, passing near Station #6 at 31.4 km and across Station #5 at about 41.6 km range.

Profile #2 – Dominantly across-slope profile near 1000 m contour from point A2, crossing Stations #6 and #5 at ranges of 31.5 and 42.2 km respectively.

Profile #3 – Upslope from point A3, crossing Station #6 at 48 km range and then downslope to near Station #4 at 67.6 km range.

Profile #4 – Upslope from point A4, across a shallow (~90 m) portion of the outer Continental Shelf and then rapidly downwards into the Gully axis crossing Station #1 at 54.6 km range.

Since seismic shooting was confined to the western half of EL2410 while all OBS stations were located to the east, all profile choices necessarily involved across-Slope bathymetry and consequently a moderate to high degree of 3-dimensionality. Also, because the OBS stations were not located on any standard survey track line or track line extension, one is forced to continuously model new bathymetric profiles to study propagation variability over an extended time period (i.e. one modeled 2-D section cannot handle a continuous family of moving source – fixed receiver locations by modeling the loss from receiver to source and assuming *TL* reciprocity). Accordingly, this study confined itself to analysis of short data stretches (approximately 100 s) reasonably modeled by single bathymetric sections. In Table 4 are listed selected analysis profile origin times and *Viking* positions and east-of-north courses (at origin), the latter derived from *Viking* log GPS positions compared over 3.3 and 10 min intervals.

Seismic array orientations are assumed to align with GPS course but cross-track currents could introduce modest orientation errors.

The RAM PE model was used for the quantitative computation of transmission loss (*TL*) along the specified profiles. Five standard frequencies 25, 50, 100, 200, and 400 Hz, were chosen as representative of the exploration seismic spectrum. Above 400 Hz, little energy of consequence was recorded at observation ranges of 10's of km and modeled source levels are also quite uncertain.

Table 5 lists OBS station-specific modeled transmission loss (*TL*) for each profile above together with the "source", "observed", and "predicted" seismic spectral *SPL*s. To obtain the source spectral level a 32K pt., 5kHz sampling rate representation of the array far-field source pressure impulse at a reference distance of 1 m was generated at 10º off the horizontal plane at the appropriate OBS azimuth (Davis et al. 1998). Spectral source levels, smoothed over 1/3 octave bandwidths were computed from the simulated time domain signal using the methodologies and scaling conventions explained previously for use in Eq. 1. Over the frequency range of interest, smoothed array source strengths varied by only a few dBs within of ± 30º from the horizontal, an angular spread which should encompass most of the acoustic energy propagated to long ranges. Source energy radiated at higher angles is rapidly lost to refraction into the bottom on successive bottom bounces. "Predicted" OBS levels in Table 5 were obtained using Eq. 1 and tabulated spectral source levels and transmission losses, the latter also averaged over 1/3 octave as explained in the "METHODS" Section.

"Observed" spectral levels were obtained from discrete 32 K pt. (6.55 s) time series each beginning just before the initial rise of successive seismic impulses. FFTs from a total of 10 impulses were squared and averaged with scaling and 1/3 octave smoothing identical to those employed for the source spectra above. As seen below when profile station sonograms are considered, seismic signal components above approximately 100 Hz tend to decline rapidly into the ambient background noise over the course of the 6.55 s sampling window. To better estimate weak seismic spectral levels in the presence of a strong non-seismic ambient background it was assumed that background levels were reached at or before an elapsed time equal to 75% of the sampling window duration. "Noise" spectral levels were computed as above after first zeroing the first 75% of the 32K data series. Assuming the non-seismic background to be stationary, the "Noise Corrected" OBS spectral levels entered in Table 5 are given by

$$SPL_{\text{Noise Corrected}} = SPL_{\text{Observed}} - 4 \text{ x Noise Level} \qquad (12)$$

the stated operation performed with *SPL*s in their linear (non-decibel) form. Noise corrected *SPL*s should constitute superior estimates of true seismic origin signal provided signal ambient noise levels are reached before 75 % of the sampling window has elapsed. If some seismic signal remains in the noise-analysed final 25% of the window, as frequently happens below 100 Hz, the noise corrected levels will underestimate the true seismic levels. In many cases the difference between "observed" and "noise corrected" levels is small which signifies both that the seismic signal declines reasonably rapidly

compared to the window length and that the overall signal-to-noise ratio within the time series window is good. This constitutes the favoured situation signifying a reliable estimate. In the remaining cases, the best signal estimate choice for a particular spectral frequency and station profile should be made after reference to the pertinent sonogram.

Each profile is now examined in detail:

Profile #1 - The modeled Profile #1 is shown in Fig. 1. Before considering exploration seismic observations, it is instructive to explore the theoretical impacts of seasonally variant water column sound speed structures on long-range sound propagation using this profile (#1) as an example. Fig. 21 shows 2-D profile sections of modeled transmission loss at 100 Hz corresponding to the 4 differing temperature profiles in Fig. 20. In Fig. 21, decreasing (less negative) transmission loss or, equivalently, increasing *SPL*, with the fundamental 10 log *R* long-range cylindrical spreading losses removed to emphasize other range dependent propagation loss mechanisms, has been spectrally colour-coded from blue to red. In general, sound energy propagates (left to right) by a combination of sound entrapment and channelling within the low acoustic velocity layer centered at 70 m and by successive wide angle reflections off the ocean bottom and water surface of the continental slope. On moving down the Slope into waters of 1500 – 2000 m depth, increasing sound speed with depth causes deep plunging ray paths to be progressively refracted toward the horizontal and to eventually turn upward. Over longer ranges than illustrated above, deeper sound energy travels in a slow upward-downward oscillatory fashion about the 400 – 600 m deep sound speed minimum. The fraction of energy entrapped in the shallow sound channel centered at about 70 m is seen to progressively decrease from April to June as the channel high sound speed "cap" becomes more pronounced with growth of the seasonal thermocline (Fig. 20). For the final (July) sound speed profile, no pronounced surface channel exists. The July structure appears a likely consequence of the advective appearance of a contrasting water mass from the south as discussed earlier. Energy within a sound channel, whether shallow or deep, can potentially travel to long ranges with comparatively low attenuation since lossy interactions with the bottom are avoided. Seismic airgun sounds triangulated to originate off Nova Scotia and Newfoundland have been easily detected in the deep sound channel in the mid-Atlantic 3000 km distant (Nieukirk et al. 2004).

Profile #1 propagation specific to the OBS observations is now considered. Waveform visual inspection (Fig. 22) would suggest that seismic sound levels remain above ambient for at least 6 s following the initial impulse rise. Energy persistence is further explored using uncalibrated sonograms, based on successive 1024 pt FFTs, and computed using *Adobe Audition*[1] (Fig. 22). At 50 Hz and below, seismic energy is clearly seen to remain above ambient for 6 s, and probably longer. In contrast, most energy above 200 Hz arrives within about 1 second of the initial signal rise and merges into ambient background after only 2 – 3 s. Peaks and nulls are observed to occur in the frequency domain; broad peaks around 140, 260, 340, and 460 Hz; and nulls around 100, 225, 290, and 390 Hz. This frequency response pattern persists relatively unchanged over the time evolution of individual pulses and from pulse-to-pulse for at least the entire time interval

[1] *Adobe* and *Adobe Audition* are trademarks or registered trademarks of Adobe Systems Inc.

displayed. The imprint of the frequency dependent Lloyd-mirror source radiation pattern on the family of all possible source-to-receiver ray paths might be responsible.

The along-profile computed transmission losses to OBS Station #5 for five selected frequencies are shown in Table 5. Sample 2-D *TL* sections at 25 and 200 Hz[1], with the cylindrical spreading component removed as previously, appear in Fig. 23. Superimposed on each section is a profile of absolute *TL* (i.e. cylindrical spreading included) vs. depth computed at the range of Station #5. Transmission losses increase (i.e. become more negative) at lower acoustic frequencies throughout most of the water column. This is probably a consequence of surface Lloyd Mirror reflections of the shallow point source which at lower frequencies tends to direct radiated energy strongly downwards with consequent higher bottom losses. Sound entrapment in the shallow channel is seen to be more pronounced at 200 than at 25 Hz. Detailed inspection of *TL* sections shows that the deep sound energy in the general vicinity of the Station #5 OBS tends to follow relatively narrow isolated ray paths largely governed by the profile reflective geometry and the deep sound speed structure. This suggests that observed OBS levels are determined by a "hit or miss" mechanism of high spatial variability..

The agreement between "Observed" and "Noise Corrected" OBS levels is good at all frequencies, suggesting meaningful estimates. Predicted OBS signal levels tend to modestly exceed the (noise corrected) observed levels except at 400 Hz where the excess is relatively large (24 dB). Data from Station #6 has not yet been quantitatively analysed but visual inspection of graphical records reveal peak waveforms amplitudes about 6 dB higher than at Station #5 during the identical analysis interval. This would appear consistent with the somewhat higher acoustic levels expected for Station # 6 from the colour-coded sections of Fig. 23.

Profile #2 - Profile #2, the across-slope example, is in reality mildly down-slope but with the source region lying in deeper water than in Profile #1 (Fig. 1). While the Station #5 waveform and sonogram (Fig. 24) appear superficially similar to those for Profile #1, higher frequency spectral energy maxima tend to arrive slightly earlier than energy maxima at lower frequencies. The 25 and 200 Hz transmission loss sections (Fig. 25) both show isolated ray paths at range. Again the signal-to-noise ratio is good. Predicted and observed levels are in reasonable agreement at 25 and 50 Hz (Table 5). At 100 Hz and above, predicted levels are considerably higher than observed. The 200 Hz computed section (Fig. 25) reveals narrow ray paths converging in the vicinity of the Station #5 OBS resulting in very high predicted values. A slight upward displacement of these ray paths in would result in much lower predicted levels. The corresponding Station #6 file did not record.

Profile #3 - Profile #3 (Fig. 1) is strongly upslope to Station #6 but ends with a rapid downslope section to Station #4. The Station #6 waveform (Fig. 26) is reasonably

[1] Actually shown is the colour-coded *TL* at the single end frequency (nominal + 1/6 octave) for 1/3 octave averaging or about 12% higher than nominal frequency. The superimposed fully calibrated *TL* profile is averaged over the full 1/3 octave interval about the nominal frequency.

conventional except successive pulses vary slightly in amplitude in a low-high-low-high-low pattern. This could result from the two alternating airgun source arrays differing slightly in strength (several guns may be inoperative in a given source array) or being displaced spatially so that their respective propagation multi-path interference patterns differ. The sonogram (Fig. 26) reveals additional peculiarities. Seismic energy appears to be arriving from two differing sources. The initial arrival from the weaker (denoted 2^{nd}) source arrives about 5 s later than that from the stronger. In the frequency range 170 – 300 Hz the two source strengths are more comparable. The 2^{nd} source may arise from the in-progress Encana "Stonehouse" survey 110 to 170 km to the east, largely in EL 2414. A less probable alternative is a single survey with a strong 3-D wide-angle reflection from an isolated scattering feature on the continental slope. The visual appearance of signal 1^{st} derivative waveforms (not shown) over an extended time period seems more consistent with a 2^{nd} survey with a shot repetition interval about 10.5 s.

Another curious sonogram feature is the multiple character of the peak of the primary arrival and possibly that of the 2^{nd} source arrival as well. The primary peak, which extends over nearly 2 s, is composed of three discrete arrivals of broad frequency content. The composite character may indicate propagation via a small number of differing ray paths of comparable intensity. Inspection of the 200 Hz *TL* plot (Fig. 27) suggests that because of the deep water path extending from the source to OBS Station #6 the bulk of acoustic energy is transferred between source and receiver with fewer bottom and surface reflections than is the case for Profiles #1 & 2 where the sources lay in shallower water. This may result in the better time domain resolution of component path "eigenrays" in the sonogram. A ray trace model, while not quantitatively valid at the lower seismic frequencies, might still be helpful in elucidating time-domain eigenray possibilities not easily provided by PE models.

Seismic levels at Profile #3 Station #4 (Figs. 28) are very low, in fact, sufficiently buried in noise to preclude quantitative estimates. Hints of both a "primary" and "secondary" source, as at Station #6, are discernable on the sonogram. The *TL* sections (Fig. 27) show local weakening of the near-bottom pressure field at a rate in excess of cylindrical spreading due to the immediate downslope bathymetry leading to Station #4 (this is to be contrasted with sound propagated in the near-surface sound channel where *TL* is essentially range-independent with cylindrical spreading removed).

The Station #6 dataset was analysed in the standard manner since the primary arrival appears dominant at our standard analysis frequencies – with the possible exception of 200 Hz. Reference to Table 5 shows that observed OBS levels are well predicted at 25 Hz and perhaps 100 Hz, if one uses the non noise-corrected value, but underestimated at 50 Hz, and significantly overestimated at 200 and 400 Hz in spite of the energy contribution from the apparent 2^{nd} source arrival. Nevertheless, the considered secondary arrival does contribute sufficient power in the final 25% of the analysis window to totally disrupt the standard noise correction at 200 Hz and to cause an excessive correction at 100 Hz. For the present Profile #3, as for Profile #2 above, predicted levels at the highest frequencies are overestimated. The fewer bottom bounces associated with source to receiver paths in increasingly deeper water in combination with an unrealistically low

bottom attenuation and/or assumed planar (too smooth) bottom and water surface interfaces could result in insufficient modeled transmission loss at higher acoustic frequencies. These effects do not appear strongly dependent on the sound speed structure in the upper few hundred meters of the water column which define the character of the shallow sound channel. To explore the latter question, Profile #3 predicted levels were re-computed (Table 6) using the Station #5, July 3rd (Fig. 20) XBT derived sound speed profile which was characterized by the virtual absence of a shallow sound channel. Predicted OBS levels are observed to change only 1 - 2 dB, some up, some down, suggesting the shallower sound speed structures have a minimal effect on acoustic intensities near-bottom at range.

Profile #4 – The final profile (Fig. 1), like previous Profile #3, involves a rapid local downslope to the observing OBS (Station #1). The broadband seismic signal levels at Station #1 (Fig. 29) are comparable to those reproduced in Fig. 7 recorded about 30 min. later just prior to the cessation of shooting. The corresponding sonogram (Fig. 29) demonstrates considerable pulse-to-pulse variability, a suggestion of comparatively less low frequency power than for our three earlier-examined profiles, and a rapid fall-off of seismic energy above 300 Hz into the ambient noise background. As the case for the preceding profiles, modeled transmission losses decline with increasing frequency. Again this is a probable consequence of more favourable Lloyd-Mirror coupling of energy into horizontal transmission modes at higher frequencies (compare the 25 and 200 Hz *TL* sections of Fig. 30). Observed levels are under-estimated except for a single significant overestimate at 400 Hz (Table 5 includes an additional estimate at 250 Hz). The 200 Hz *TL* section (Fig. 30) reveals that on reaching the downslope to the central Gully, sound paths are concentrated into a relatively small number of narrow isolated "rays". Consequently near-bottom sound intensities might be expected to be spatially "spotty" as observed in the computed sections for Profiles #1 & 2.

Reasons underlying the general underestimation of Profile #4 Station #1 observed levels (Table 5) have been explored. Unique to this profile is the extended shallow water path across the Shelf. As in the case of Profile #3, the modeled effect of a missing near surface (< 100 m) low sound speed channel was explored (Table 6) by using the alternative "July 3rd" sound speed profile of Fig. 20. Unlike the case for the completely deep water path of Profile #3, the absence of a sound channel in Profile #4 significantly increased discrepancies between observed and predicted levels. For Profile #4, absence of a sound channel results in a quite significant attenuation of modeled acoustic energy due to enhanced bottom interaction over the shallow water (< 200 m) portions of the profile. Better agreement between predicted and observed levels might results from use of the June 19th sound speed profile together with a more reflective or less attenuating bottom - at least for the continental shelf depth profile portion where bottom interactions are expected to be most intense.

Previous modeling investigations, especially the modeled shallow "S1" Profile of Davis et al. (1998), have used a "harder" bottom than assumed above. Davis et al. consider glacial till (c = 1900 m/s & S.G. = 2.1) and sedimentary bedrock (c = 2050 m/s & S.G. = 2.2) at shallow depths in proximity to the Gully edge and persisting to depth in the central

Gully. Our Profile #4 has been recomputed (Table 6) assuming the "Moraine" bottom type of Jensen et al. (2000) parameterized by c = 1950 m/s, S.G. = 2.1, and attenuation = 0.4 dB/wavelength. Agreement between observed and predicted levels are observed to improve markedly although predicted 400 Hz levels remain excessively high.

All PE modeling results presented so far have assumed a 2 m layer of "transparent" sediments under the OBS with properties matching those of seawater. If the bottom depth was nominally 1700 m as at Profile #1 Station #5 the presence of a transparent sediment layer was simulated by utilizing the modeled pressure at 1698 m to establish the *TL*. Alternatively, absence of this layer can be simulated by utilizing the pressure at 1700 m (the recording hydrophone is actually about 0.5 m above bottom but this effect is ignored). The final sub-table in Table 6 shows the effect of a missing transparent layer for Profile #1. Transmission losses increase with increasing frequency to about 4 dB at 400 Hz. Overall observed – predicted agreement is improved but remains far from perfect. This demonstration should not be construed as implying the absence of the "transparent layer" but merely places some bounds on its quantitative importance. The effect of OBS bottom proximity on transmission loss is further treated in the next section.

Alternative Sound Speed Parameterization - For completeness, one additional alternative water column sound speed parameterization has been explored in connection with Profiles #3 & 4. It is based on the June 29th Marathon *Viking* observed sound speed profile which is quite similar to the June 19th profile except for a more pronounced high sound speed "cap" resulting from water temperatures reaching 11.5º C at the sea surface. Profiles with a similar high sound speed cap were observed from *Viking* in the seismics shooting area to the west of the OBS deployments and also in wider Gully area surveys by the IML team initiated shortly after recovery of the OBSs. The issue addressed is the possibility of the Station #5 deployment XBT sound profile being unrepresentative of the propagation path as a whole. Recomputed model-predicted OBS levels analogous to those reported in Table 5 are presented in Table 7. Differences between "Predicted" and "Observed" levels tabulated in both Tables 5 and 7 are compared in Table 8. It is noted that while some differences change by 1 – 2 dB between use of the two differing sound speed structures, no radical change is evident, and the overall agreements between observed and predicted levels quantified by the "Average Difference" and "Average | Difference|" measures are little changed. Even for Profile #4, where seismic energy propagates a comparatively long distance across the continental shelf, the change is comparatively minor compared to that resulting from use of the July Station #5 sound speed profile in which the shallow sound channel is totally absent.

A word of caution – Profile #4 was recorded on the survey transect immediately following the unexplained, sudden ~10 dB drop in signal levels detected at Stations #5 & 6.

DISCUSSION

OBS deployments in the Gully area have produced informative acoustic data sets which capture marine mammal vocalizations, exploration seismic origin signals, and, during frequent seismic non-shooting intervals, ambient background noise levels.

The fact that the 4 operational instruments repeatedly displayed similar ambient background total noise levels during the quieter non-shooting periods and similar spectra in the 12 – 80 Hz frequency range usually dominated by distant shipping noise would argue for no major discrepancies in instrument calibration at lower frequencies. During periods of regionally light winds, spectral noise levels above 100 Hz are more discordant. Possible systematic influences on the overall high frequency calibration of OBS hydrophones arising from the mounting methodologies employed cannot be ruled out. All OBS hydrophones were enclosed in protective perforated metal chambers mounted directly on the OBS superstructure. Significant distortions in hydrophone directional sensitivities could arise from the OBS unit superstructure becoming a progressively more interactive acoustic scatter toward the higher end of the recorded frequency range. OBS structural dimensions are about 1.1 x 1.2 x 0.6 m. If the OBS is crudely modeled as an equi-volume sphere of 1.1 m diameter, D, the relatively non-interactive "Raleigh" scattering regime would nominally cease at a frequency of $c/\pi D$ or about 430 Hz. However, effects might be expected to extend to lower frequencies and could impact observed levels at 200 Hz and above.

Periods of seismic shooting do clearly correlate with enhanced acoustic levels at Stations #5 and 6. A much reduced visual correlation is observed for Stations #1 & 4, though the quantity of "shooting" data available from the former station was limited. Propagation paths from the western half of EL 2410 to Stations #5 & 6 (Fig. 1) are either dominantly upslope, regionally downslope, or follow a roughly constant bathymetric contour. In contrast, corresponding paths to Stations #1 & 4, in or near the central Gully, generally involve rapid downslopes on at least the final 7 – 8 km of approach to the OBS site. Lower observed seismic levels at Stations #1 & 4 demonstrate the efficacy of suddenly initiating local downslope conditions in combination with otherwise extended shallow water propagation paths associated with the more northern portions of the source transects in partially shielding near-bottom acoustic sensors from long range seismics over a wide range (at least 50º) of source azimuths. These effects are supported by the modeled *TL* sections for Profile #3 (Fig. 27) and for Profile #4 (Fig. 30).

In regard to possible disturbance to the Gully northern bottlenose whale population by the Marathon survey, it can be pointed out that the maximum measured seismic levels of about 129 dB RMS (1 s window) observed at 56 km range in the Gully Whale Concentration Area (Station #1) are much below the 150 - 160 dB RMS levels at which strong behavioural responses have been noted for baleen whales as summarized by Davis et al. (1998). The behavioural response acoustic thresholds for toothed whales, including the northern bottlenose whale, are unknown but are anticipated to be higher than those for baleen whales. This would seem to guarantee an even larger safety margin.

Unfortunately, no acoustic measurements were conducted at Station #1 when *Viking* was shooting in the easternmost portion of EL 2411 (Empire) where less shielded, deep water paths into the Gully whale concentration area would be only about 35 km in length. One might speculate that resultant acoustic levels would be more comparable to the maximum observed (allowing for clipping) at Stations #5 & 6 in the present dataset. The maximum observed 1 s RMS levels at Station #5 **from seismics** are about 135 dB (with slight clipping) but more typically peak at about 130 dB RMS, near the mid-points of the north to south survey transects with *Viking* about 45 km distant over a deep water path. Cylindrical (10 log R) spreading loss differences between 35 and 45 km range are only about 1 dB. Curiously, levels at Station #5 were about 5 dB lower for south-to-north transects, a discrepancy which appears not totally explicable in terms of **modeled** asymmetries in the *Viking* array radiation pattern (Fig. 6). The south-to-north lines lie only about 8 km west of the north-to-south lines (Fig. 1) so differential spreading losses should be almost negligible. There is some evidence (the charts are not absolutely definitive) that regional bottom slopes on the north-to-south lines within a few kilometers of the mid-profile acoustic maxima tilt toward Station #5 but away from Station #5 on south-to-north transects. Maximum measured RMS levels at Station #6 are about 137 dB RMS and, in reality, probably 1 – 2 dB higher on making reasonable allowances for signal clipping. Again, at Station #6, levels for north-to-south transects are about 5 dB higher than for south-to-north transects.

The agreement between observed and predicted OBS seismic acoustic levels is, on the whole, definitely inconsistent. Average absolute differences (Table 8) are large, between 10 and 11 dB, for both the June 19th and June 29th sound speed structures. There is a consistent and marked overestimate of predicted levels at 400 Hz on all four profiles. The latter could arise from several causes: 1) A systematic inaccuracy in the source model such as the assumption of too rapid initial impulse rise times for the array airguns 2) Measured acoustic levels being systematically depressed at this frequency due to the perforated OBS hydrophone enclosures. All hydrophones were calibrated minus the holders 3) The 2 m "transparent" layer of sediment underlying the OBSs having a more contrasting character to the water column than assumed, the effect becoming more pronounced at higher frequencies (this could explain part but not all of the discrepancy).

Excepting 25 Hz, predicted levels for Profiles #1 & 2 are too high, an effect which, in general, appears to increase with increasing frequency. This could be a consequence of using 2-D PE models for profiles oblique to the shelf where the structure is clearly 3-dimensional. The general non-parallelism of the surface and bottom interfaces out of the plane of the model may systematically deflect acoustic energy seaward reducing acoustic levels at range. However, this does not fully explain the apparent frequency dependence which is more suggestive of a lossy incoherent scattering process.

At times, OBS signal levels varied rapidly over time, i.e. along the source transect, which again suggests that the level of detail in model parameterizations may be inadequate. However, it seems unlikely that the very sudden (within 11 s) ~10 dB drop in signal

levels at day 178.758 can be explained in terms of a natural process, as for instance, the source arrays passing through a sharp oceanographic front in the upper water column.

Possible sources of inconsistency can be briefly summarized:

1) Observed signal levels
Uncertainty exists in the calibration and directional response of OBS hydrophones, especially above 100 Hz, due to the mounting and protective methodologies employed.

2) Source Model (affecting predicted levels)
The rise times of individual airgun signatures are imprecisely known, injecting significant uncertainty into the array spectral "tail" above 200 Hz. Source operating parameters may differ subtly (i.e. one or more airguns inoperative) or perhaps significantly (i.e. one or more subarrays inoperative) from those assumed. Documented shifts in operating parameters can be incorporated into the source model. However, observational evidence exists for at least one undocumented, sudden, and large change in observed levels highly suggestive of an origin at source.

3) Propagation Model (affecting predicted levels)

a) Both observed and modeled signal levels at > 200 m depth are critically dependent on the deep-water sound velocity profile(s). Modeled deep-water sound frequently follows isolated, narrow ray paths with spatially localized convergent zones resulting in a "spotty" distribution of sound intensities at depth. The effectiveness of frequency domain averaging in reducing this spatial variability is uncertain.

b) Modeled near-bottom signal levels are sensitive to sub-bottom acoustic parameters. The local variation in bottom sediment parameters (i.e. deviations from the assumed regional average properties) at specific OBS sites is unknown injecting consequent uncertainty into the modeling process. The effect of ignoring shear waves in the bottom sediments is also unknown.

c) The 2-D bathymetric sections employed are based on low resolution spatial sampling and should be regarded at best as crude and highly smoothed representations of reality. Better bathymetric data is becoming available from multibeam surveys.

d) Two-dimensional PE models are employed for sections running obliquely to the continental slope where bathymetric structure is strongly three-dimensional.

e) Omnidirectional acoustic sources are employed within the PE propagation models in contrast to the complex radiation patterns characterizing the simulated airgun array sources. The two can related quantitatively only by "hand-waving" assumptions, with uncertainties increasing with rising acoustic frequency.

It should be stated that, to date, our intercomparisons of observed and modeled OBS levels have been extremely limited and by no means exhaust the possibilities offered by

the available dataset. More extensive intercomparisons would have been facilitated by survey profiles running directly along the modeled propagation sections rather than obliquely as dictated by the geometry of the current experiment.

As an initial step in exploring measurement uncertainties and modeling close to the bottom interface (items 3b, c & d above), near-bottom *TL* vs. Depth profiles at five different frequencies were computed for Profile #3 at a range of 36 km (Fig. 31). The model bathymetry remains flat for several kilometers on both sides of the chosen location and the computed near-bottom pressure fields also show little lateral variability in the graphical sections (Fig. 27). Encouragingly - at least for this chosen example - the acoustic pressure field accommodation to the bottom appears to occur mostly at or below the bottom interface. It will be remembered that the "Predicted" OBS levels of Tables 5 and 6 assume an observation point 2 m above the 1750 m/s 1.9 S.G. interface to simulate a layer of very soft surficial sediment below the OBS with acoustic properties approximating those of seawater. The near-bottom curvature of the *TL* profiles of Fig. 31 suggests that small variations in the thickness of the acoustically "transparent" sediments underlying the OBS probably would not strongly affect observed acoustic levels although the effect becomes more critical with increasing acoustic frequency.

CONCLUSIONS

1) New calibrated ocean bottom instrumentation for long-term, autonomous, low ambient noise acoustic monitoring of both seismic signals and marine mammal vocalizations has been constructed, calibrated (for at least the lower frequency portions of its measurement range), and field tested.

2) A bottom instrument integral "click detector" reveals whale clicks of dominantly high frequency content (> 2 kHz) while avoiding the necessity of extremely high sampling rates, massive digital storage requirements, or sophisticated real-time digital processing to otherwise separate such vocalizations directly from their spectral signatures. There are promising, but not fully verified, indications that the click detector can distinguish northern bottlenose whale clicks from a background of more common sperm whale clicks.

2) Exploration seismic sources can be detected by bottom-mounted hydrophone sensors at ranges of many 10's of kilometers. Seismic impulses observed at such ranges are highly elongated in time due to path reverberation and frequently define acoustic background levels during the entire seismic interpulse interval (11 s).

3) The model predictability of ocean-bottom seismic acoustic levels at representative frequencies is not particularly good. This is most likely explicable by our inability to accurately parameterize our source and propagation (*TL*) models but questions about OBS calibration at higher frequencies, and therefore the accuracy of field measured levels, remain. Analysis complexities severely limit the number of intercomparisons which are practical.

3) Flexible analytical tools have been developed and currently reside within DFO to display OBS recordings and to perform various types of time domain and spectral signal characterizations. Tools have also been developed and adapted to quantitatively model typical exploration seismic sources in both the time and frequency domains and to model seismic sound propagation within range-dependent ocean environments. The latter tools function within an interactive MS Windows environment and accept data inputs from DFO oceanographic sensors.

Recommendations for future work include:

1) Improvements to the OBS recording systems:
a. Specifically, OBS firmware should be upgraded to enable data recording in FAT 32 rather than the current FAT 16 file format. This would allow more efficient use of present mass storage recording media resulting in extended recording endurance and/or higher data sampling rates.
b. A higher dynamic range (> 16 bit) A-D converter is required to accommodate close passes of the seismic vessel while maintaining ambient background noise-limited recording during non-shooting periods.
c. Greater "built-in" instrument intelligence would allow the gathering of short "triggered" (perhaps by using a click detector or other frequency/amplitude sensitive device) high-rate samples of marine mammal vocalizations. These could be either directly stored or spectrally analysed in real-time. Triggered sampling would enable more critical species identification using sonogram-like approaches rather than use of the current click detector in isolation.
d. Hydrophones should be mounted more remote from the OBS body in a fully exposed condition. "Floating" recording hydrophones at least ¼ wavelength above the OBS at the lowest critical frequency would substantially alleviate the present analytical uncertainties associated with sampling too close to the water-sediment interface and also ensure that hydrophone sensitivities and patterns are not unduly influenced by the proximity of the OBS (some monitoring objectives may still require measurement very close to the bottom).
e. Accuracy of the OBS recorded time base should be improved, particularly if triangulation is to be employed for localizing and tracking mammalian vocalizations.

2) Future seismic monitoring should aim at acoustic characterization of the entire water column over extended temporal periods. This need could be met by well-engineered (low noise) deep-water acoustic moorings equipped with multiple fixed-depth autonomous sensors/recorders of a roughly similar nature to the OBS systems. At present, only the near-bottom and surface regions (< 200 m) are accessible with instrumentation readily available on the East Coast. With "intelligent" signal processing, real-time statistical summaries of acoustic levels or warnings of excessive levels from at least sensors in the shallow sound channel - where acoustic levels are frequently expected to be the highest - could be telemetered to responsible authorities via *Iridium* satellite link.

3) A need exists to model the time domain evolution of seismic pulses observed at ranges of 10's of kilometers. Existing PE models operate in the frequency domain and are

extremely inefficient for predicting time domain transmission effects. The PROSIM model as utilized by Simons et al. (2001) would appear better suited to time domain problems and might be adaptable to the deep water environment provided the substantial bathymetry in the slope region can be efficiently accommodated.

Finally it should be noted that future instrumentation development could be materially assisted by parallel DFO programs on the West Coast. Long duration moored whale recording systems have been developed (Vagle et al. 2004) with triggered high rate sampling for capturing killer whale calls with characteristics which mirror some of our projected requirements.

ACKNOWLEGDEMENTS

Many thanks must go to Dr. Ken Lee of DFO's Center for Offshore Oil and Gas Environmental Research for conceiving this project, and arranging the participation of diverse government, industry, and academic groups, and the underlying complex funding infrastructure making this possible. David Heffler of the Geological Survey of Canada (GSC) –Atlantic did a commendable job of overseeing the basic design and construction of the OBSs including conceptualization of the "click detector". George States of the Ocean Physics Section of DFO's Ocean Sciences Division (OSD) performed vital lab measurements of OBS performance. David Morse of the Canadian Coast Guard arranged both the OBS deployment and recovery cruises on board the *Edward Cornwallis* in spite of "last minute" scheduling. Conversations and advice from David Thomson, Defence Research and Development (DRDC) – Atlantic, and David Mosher, of the GSC-Atlantic in regard to acoustic modeling techniques and the proper parameterization of seafloor sediments respectively are also acknowledged. DRDC – Atlantic, and Allyn Clarke of DFO's OSD generously provided XSV and XBT probes for this mission.

The funding support of Petroleum Research Atlantic Canada, the Environmental Studies Research Funds (ESRF), the DFO Species at Risk (SARCEP) fund, and the GSC - Atlantic are gratefully acknowledged.

REFERENCES

Austin, M. E. A.O. MacGillivary, D. E. Hannay, and S. Carr. 2004. Acoustic Monitoring of Marathon Canada Petroleum ULC 2003 Cortland/Empire 3-D Seismic Program. JASCO Rep. JRL04 001, Rep. by JASCO Research Ltd. for Marathon Canada Petroleum ULC, Halifax, N.S., Jan. 2004: 65 p.

Canadian Hydrographic Service. 1986. Sable Island Bank to St. Pierre Bank. Atlantic Coast bathymetric chart L/C 4045 (Metric). Scale 1:400,000, Mercator Projection.

Chapman, N. R. 1985. Measurement of the waveform parameters of shallow explosive charges. J. Acoust. Soc. Am. 78(2): 672-681.

Clay, C. S. and H. Medwin. 1977. Acoustical Oceanography: Principles and Applications. New York, John Wiley & Sons: 544 p.

Cochrane, N. A. 2005. Near-bottom ocean acoustic observations in the Scotian Shelf Gully Marine Protected Area during an exploration seismic survey. *In*: K. Lee, H. Bain, and G. V. Hurley, Eds. Acoustic Monitoring and Marine Mammal Surveys in the Gully and Outer Scotian Shelf Before and During Active Seismic Programs. Environmental Studies Research Funds Report No. 151: 75-88.

Collins, M. D. 1989. Applications and time-domain solution of higher-order parabolic equations in underwater acoustics. J. Acoust. Soc. Am. 86: 1097-1102.

Collins, M. D. 1992. A self starter for the parabolic equation method. J. Acoust. Soc. Am. 92: 2069-2074.

Collins, M. D. 1993. A split-step Padé solution for the parabolic equation method. J. Acoust. Soc. Am. 93(4): 1736-1742.

Davis, R. A., D. H. Thomson, and C. I. Malme. 1998. Environmental Assessment of Seismic Exploration on the Scotian Shelf. Rep. by LGL Ltd. and C.L. Malme for Mobile Oil Properties Ltd., Shell Canada Ltd., and Imperial Oil Ltd., Calgary for Submission to the Canada/Nova Scotia Offshore Petroleum Board, 5 Aug. 1998: 181 p. + Appendices.

Francois, R. E., and Garrison, G. R. 1982a. Sound absorption based on ocean measurements: Part I: Pure water and magnesium sulfate contributions. J. Acoust. Soc. Am. 72(3): 896-907.

Francois, R. E., and Garrison, G. R. 1982b. Sound absorption based on ocean measurements: Part II: Boric acid contribution and equation for total absorption. J. Acoust. Soc. Am. 72(6): 1879-1890.

Giles, B. F. and R. C. Johnston. 1973. System approach to air-gun array design. Geophysical Prospecting 21: 77–101.

Goold, J. C. and S. E. Jones. 1995. Time and frequency domain characteristics of sperm whale clicks. J. Acoust. Soc. Am. 98(3): 1279-1291.

Hooker, S. K. and H. Whitehead. 2002. Click characteristics of northern bottlenose whales (*Hyperoodon ampullatus*). Marine Mammal Science 18(1): 69-80.

Hooker, S. K., H. Whitehead, and S. Gowans. 1999. Marine Protected Area design and the spatial and temporal distribution of Cetaceans in a submarine canyon. Conservation Biology 13(3): 592-602.

Jensen, F. B., W. A. Kuperman, M. B. Porter, and H. Schmidt. 2000. Computational Ocean Physics. AIP Series in Modern Acoustics and Signal Processing. New York, Springer-Verlag: 578 p.

Johnston, R. C. 1980. Performance of 2000 and 6000 psi air guns: Theory and experiment. Geophysical Prospecting 28: 700-715.

Laws, R. M., L. Hatton, and M. Haartsen. 1990. Computer modelling of clustered airguns. First Break 8(9): 331–338.

Mackenzie, K. V. 1981. Nine-term equation for sound speed in the oceans. J. Acoust. Soc. Am. 70: 807-812.

Macpherson, J. D. and N. O. Fothergill. 1962. Study of low-frequency sound propagation in the Hartlen Point region of the Scotian Shelf. J. Acoust. Soc. Am. 34(7): 967-971.

Mosher, D. C., D. J. W. P. Piper, D. C. Campbell, and K. A. Jenner. 2004. Near surface geology and sediment failure geohazards of the central Scotian Slope. American Association of Petroleum Geologists Bulletin 88: 703-723.

Moulton, V. D., R. A. Davis, J. A. Cook, M. Austin, M. L. Reece, S. A. Martin, A. MacGillivary, D. Hannay, and M. W. Fitzgerald. 2003. Environmental Assessment of Marathon Canada Limited's 3-D Seismic Program on the Scotian Slope, 2003. LGL Rep. SA744-1, Rep. by LGL Ltd., St. John's, Newfoundland, for Marathon Canada, Ltd., Halifax, Nova Scotia, 17 Jan. 2003: 173 p. + Appendices.

Mullins, J., H. Whitehead, and L. S. Weilgart. 1988. Behaviour and vocalizations of two single sperm whales, *Physeter macrocephalus*, off Nova Scotia. Can. J. Fish. Aquat. Sci. 45: 1736-1743.

Nieukirk, S. L., K. M. Stafford, D. K. Mellinger, R. P. Dziak, and C. G. Fox. 2004. Low-frequency whale and seismic airgun sounds recorded in the mid-Atlantic Ocean. J. Acoust. Soc. Am. 115(4): 1832-1843.

Nooteboom, J. J. 1978. Signature and amplitude of linear airgun arrays. Geophysical Prospecting 26: 194-201.

Oakwood Computing Services. 2004. Gundalf Calibration data, January 2004 – Sleeve and Sodera G gun. http://www.gundalf.com/calib.html#sodera

Richardson, W. J., C. R. Greene, Jr., C. I. Malme, D. H. Thomson, S. E. Moore, and B. Wursig. 1995. Marine Mammals and Noise. San Diego, Academic Press: 576 p.

Seismic Systems Inc. and SODERA. 2004. G. GUN – The Recoilless Air Gun. http://moveout.ifjf.uib.no/equipment/seismic/airguns/sodera/GGbrochure_11_99.pdf

Simons, D. G., R. McHugh, M. Snellen, N. H. McCormick, and E. A. Lawson. 2001. Analysis of shallow-water experimental acoustic data including a comparison with a broad-band normal-mode-propagation model. IEEE Journal of Ocean Engineering 26(3): 308-323.

Thomson, D. J. 1990. Wide-angle parabolic equation solutions to two range-dependent benchmark problems. J. Acoust. Soc. Am. 87(4): 1514-1520.

Thomson, D. J. and N. R. Chapman. 1983. A wide-angle split-step algorithm for the parabolic equation. J. Acoust. Soc. Am. 74(6): 1848-1854.

Vaage, S., K. Haugland, and T. Utheim. 1983. Signatures from single airguns. Geophysical Prospecting 31: 87-97.

Vaage, S., B. Ursin, and K. Haugland. 1984. Interaction between airguns. Geophysical Prospecting 32: 676-689.

Vagle, S., J. K. B. Ford, N. Erickson, N. Hall-Patch, and G. Kamitakahara 2004. Acoustic recording systems for baleen whales and killer whales on the West Coast of Canada. Canadian Acoustics 32(2): 23-32.

Verbeek, N. H. and T. M. McGee. 1995. Characteristics of high-resolution marine reflection profiling sources. Journal of Applied Geophysics 33: 251-265.

Wardle, C. S., T. J. Carter, G. G. Urquhart, A. D. F. Johnstone, A. M. Ziolkowski, G. Hampson, and D. Mackie. 2001. Effects of seismic air guns on marine fish. Continental Shelf Research 21: 1005-1027.

Watkins, W. A., K. E. Moore, and P. Tyack. 1985. Sperm whale acoustic behaviours in the southeast Caribbean. Cetology 49: 1-15.

Ziolkowski, A., G. Parkes, L. Hatton, and T. Haugland. 1982. The signature of an air gun array: Computation from near-field measurements including interactions. Geophysics 47(10): 1413-1421.

Table 1. Calibration properties of OBSs and associated hydrophones

Station #	1	2	3	4	5	6
OBS #	S (new)	M (new)	Z (new)	T (mod)	A (mod)	P (mod)
Hydrophone Type	HTI-90U inc. preamp	HTI-90U inc. preamp	HTI-90U inc. preamp	OAS E-2SD	OAS E-2SD	OAS E-2SD
Hydrophone #	363001	363003	363002	1341	1420	1345
Hydrophone Sens. (dB re 1 V/μPa)	-149.7	-149.5	-149.3	-187.0	-187.0	-187.0
Gain Mid-Band (dB)	6.02	6.02	6.02	47.90	47.90	47.90
Total Sensitivity (dB re 1 V/μPa)	-143.68	-143.48	-143.28	-139.10	-139.10	-139.10
Voltage Sensitivity (V/μPa)	6.55E-08	6.70E-08	6.85E-08	1.11E-07	1.11E-07	1.11E-07
Quantization (V/digit. Int.)	6.10E-05	6.10E-05	6.10E-05	6.10E-05	6.10E-05	6.10E-05
Calibration (μPa/digit. int.)	9.32E+02	9.11E+02	8.90E+02	5.50E+02	5.50E+02	5.50E+02
DC Offset (digit. int.)	-223.3	?	?	5.4	-87.6	-186.9
Saturation Level (dB re 1 μPa 0-p)	149.7	149.5	149.3	145.1	145.1	145.1

Table 2. Locations, depths, and recording periods of deployed OBSs.

Stat.	Lat.	Long.	Depth	Ch.	Start Z	Stop Z	Status
1	43º 55.434'	58º 58.592'	1000 m	2	28/06/2003 15:00	03/07/2003 18:22	Good
2	43º 51.500'	58º 55.879'	1300	2			Inoperative
3	43º 50.483'	58º 55.198'	1300	2			Inoperative
4	43º 48.521'	58º 58.057'	1200	1	23/06/2003 15:00	26/06/2003 19:26	Partial
5	43º 39.599'	58º 54.896'	1700	1	23/06/2003 15:00	03/07/2003 10:06	Good
6	43º 38.144'	59º 02.735'	1200	1	23/06/2003 15:57	03/07/2003 13:04	Good

Table 3. Primary CTD & XBT profiles for establishing sound speed profiles.

Profile Type	Date	Time Z	Latitude	Longitude	Max. Depth m
CTD	15/04/ 2003	20:32:23	44º 01.032’	59º 02.538’	502
CTD	16/04/2003	03:14:19	44 07.848	58 10.032	927
CTD	16/04/2003	07:44:33	43 46.710	57 50.232	2975
CTD	25/05/2003	09:54:13	43 51.390	58 56.202	1616
XBT	19/06/2003	18:18	STN 6		569
XBT	19/06/2003	23:57	STN 5		828
XBT	20/06/2003	00:09	STN 3		828
XBT	03/07/2003	15:01	STN 5		828

Table 4. Details of selected analysis profiles including assumed bathymetry compiled from Canadian Hydrographic Service (1986) bathymetric chart L/C 4045.

PROFILE #1

Time – 25 June 2003 17:15:18 Z (Day 175.719)
Viking Position – 43º 37.426' N 59º 25.943' W
Course – 166.30º
Profile Direction – 84.58º
Profile Direction to Starboard of Course – 278.28º

RANGE KM	DEPTH M	COMMENTS
0	550	Source
2.4	500	
5.4	400	
7.6	500	
10.5	550	
13.1	600	
15.3	600	
17.4	700	
19.2	600	
20.9	700	
22.2	800	
23.7	950	
24.8	800	
25.5	700	
26.1	900	
26.6	1000	
28.3	1000	
31.4	1200	Stn 6
35.7	1200	
37.9	1400	
40.5	1600	
41.6	1700	Stn 5
47.1	1800	
52.7	2000	
56.6	2500	
60.0	2500	

PROFILE #2

Time – 24 June 2003 05:04:10 Z (Day 174.211)
Viking Position – 43º 34.269' N 59º 25.717' W
Course – 163.05º
Profile Direction – 76.66º

Profile Direction to Starboard of Course – 273.61º

RANGE KM	DEPTH M	COMMENTS
0	1100	Source
3.7	1000	
5.6	1000	
7.4	800	
9.3	1000	
14.8	800	
16.7	1000	
25.9	1000	
31.5	1200	Stn 6
35.2	1400	
40.7	1600	
42.2	1700	Stn 5
50.0	1900	
55.6	2500	
60.0	2500	

PROFILE #3

Time – 24 June 2003 09:37:00 Z (Day 174.401)
Viking Position – 43º 14.721' N 59º 18.732' W
Course – 166.10º
Profile Direction – 23.92º (through Stn 4)
- 26.38º (through Stn 6)
Profile Direction to Starboard of Course – 217.82º (through Stn 4)
- 220.28º (through Stn 6)

RANGE KM	DEPTH M	COMMENTS
0	2500	Source
20.4	2000	
30.6	1800	
33.3	1600	
38.9	1600	
49.1	1000	
53.7	700	
59.3	600	
61.1	600	
64.8	1000	
67.6	1200	Stn 4
70.0	1371	

Note: Stn 6 is slightly offset from the above profile at 48.5 km range and 1200 m water depth. Using the above profile, Stn 6 can be reasonably simulated by a station at 48.5 km where the interpolated water depth is 1035.3 m.

PROFILE #4

Time – 29 June 2003 04:43:00 Z (Day 179.197)
Viking Position – 43º 37.88' N 59º 31.34' W
Course – 348.47º
Profile Direction – 53.41º
Profile Direction to Starboard of Course – 64.94º

RANGE KM	DEPTH M	COMMENTS
0	500	Source
3.3	300	
5.9	200	
9.8	150	
28.5	100	
39.8	90	
44.6	100	
46.7	150	
47.8	200	
49.6	500	
52.0	1000	
52.8	1200	
54.6	1000	Stn 1
55.6	700	
57.4	500	
60.0	221	

Table 5. Comparison of observed and predicted seismic spectral levels at OBS stations lying on selected profiles using June 19th Station #5 (deployment) sound speed profile.

Profile 1 Station 5 June 19th Sound Speed Structure (RAM Model 1/3 Octave Averaged Values)						
Freq Hz	Source Level Bar-m^2/Hz	Source Level dB re 1 μPa^2/Hz	*TL* dB	Observed OBS Level dB re 1 μPa^2/Hz	Noise Corrected OBS Level dB re 1 μPa^2/Hz	Predicted OBS Level dB re 1μPa^2/Hz
25	5.208E-03	197.17	-105.60	93.99	93.27	91.57
50	1.908E-03	192.81	-98.70	88.22	86.70	94.11
100	2.000E-03	193.01	-92.10	92.57	92.22	100.91
200	1.069E-04	180.29	-92.20	81.22	80.97	88.09
400	4.206E-05	176.24	-86.20	66.65	66.05	90.04

Profile 2 Station 5 June 19th Sound Speed Structure (RAM Model 1/3 Octave Averaged Values)						
Freq Hz	Source Level Bar-m^2/Hz	Source Level dB re 1 μPa^2/Hz	*TL* dB	Observed OBS Level dB re 1 μPa^2/Hz	Noise Corrected OBS Level dB re 1 μPa^2/Hz	Predicted OBS Level dB re 1μPa^2/Hz
25	5.064E-03	197.04	-98.60	100.28	99.70	98.44
50	2.093E-03	193.21	-95.20	93.01	92.09	98.01
100	2.373E-03	193.75	-89.20	89.94	89.46	104.55
200	1.535E-04	181.86	-84.80	80.54	80.30	97.06
400	3.375E-05	175.28	-84.10	65.76	65.32	91.18

Profile 3 Station 6 June 19th Sound Speed Structure (RAM Model 1/3 Octave Averaged Values)						
Freq Hz	Source Level Bar-m^2/Hz	Source Level dB re 1 μPa^2/Hz	*TL* dB	Observed OBS Level dB re 1 μPa^2/Hz	Noise Corrected OBS Level dB re 1 μPa^2/Hz	Predicted OBS Level dB re 1μPa^2/Hz
25	1.230E-02	200.90	-97.70	104.63	98.07	103.20
50	2.624E-04	184.19	-91.40	102.01	100.39	92.79
100	4.649E-05	176.67	-86.10	87.65	80.36	90.57
200	3.974E-05	175.99	-79.80	82.20	-	96.19
400	6.076E-06	167.84	-81.00	73.53	72.67	86.84

Profile 4 Station 1 June 19th Sound Speed Structure (RAM Model 1/3 Octave Averaged Values)						
Freq Hz	Source Level Bar-m^2/Hz	Source Level dB re 1 μPa^2/Hz	*TL* dB	Observed OBS Level dB re 1 μPa^2/Hz	Noise Corrected OBS Level dB re 1 μPa^2/Hz	Predicted OBS Level dB re 1μPa^2/Hz
25	8.791E-03	199.44	-115.80	90.33	87.18	83.64
50	8.851E-04	189.47	-118.60	85.56	82.26	70.87
100	1.902E-04	182.79	-110.10	86.28	85.58	72.69
200	2.435E-06	163.86	-101.80	77.93	77.30	62.06
250	1.092E-05	170.38	-100.10	75.55	75.04	70.28
400	8.768E-06	169.43	-99.10	64.12	63.06	70.33

Table 6. Comparison of observed and predicted seismic spectral levels at OBS stations lying on selected profiles for variant propagation model parameterizations.

Profile 3 Station 6 July 3rd Sound Speed Structure (RAM Model 1/3 Octave Averaged Values)						
Freq Hz	Source Level Bar-m^2/Hz	Source Level dB re 1 μPa^2/Hz	*TL* dB	Observed OBS Level dB re 1 μPa^2/Hz	Noise Corrected OBS Level dB re 1 μPa^2/Hz	Predicted OBS Level dB re 1μPa^2/Hz
25	1.230E-02	200.90	-98.30	104.63	98.07	102.60
50	2.624E-04	184.19	-89.90	102.01	100.39	94.29
100	4.649E-05	176.67	-85.40	87.65	80.36	91.27
200	3.974E-05	175.99	-79.40	82.20	-	96.59
400	6.076E-06	167.84	-78.70	73.53	72.67	89.14

Profile 4 Station 1 July 3rd Sound Speed Structure (RAM Model 1/3 Octave Averaged Values)						
Freq Hz	Source Level Bar-m^2/Hz	Source Level dB re 1 μPa^2/Hz	*TL* dB	Observed OBS Level dB re 1 μPa^2/Hz	Noise Corrected OBS Level dB re 1 μPa^2/Hz	Predicted OBS Level dB re 1μPa^2/Hz
25	8.791E-03	199.44	-126.50	90.33	87.18	72.94
50	8.851E-04	189.47	-123.60	85.56	82.26	65.87
100	1.902E-04	182.79	-117.60	86.28	85.58	65.19
200	2.435E-06	163.86	-113.70	77.93	77.30	50.16
250	1.092E-05	170.38	-113.90	75.55	75.04	56.48
400	8.768E-06	169.43	-112.00	64.12	63.06	57.43

Profile 4 Station 1 June 19th-Moraine Sound Speed Structure (RAM Model 1/3 Octave Averaged Values)						
Freq Hz	Source Level Bar-m^2/Hz	Source Level dB re 1 μPa^2/Hz	*TL* dB	Observed OBS Level dB re 1 μPa^2/Hz	Noise Corrected OBS Level dB re 1 μPa^2/Hz	Predicted OBS Level dB re 1μPa^2/Hz
25	8.791E-03	199.44	-110.40	90.33	87.18	89.04
50	8.851E-04	189.47	-110.00	85.56	82.26	79.47
100	1.902E-04	182.79	-100.70	86.28	85.58	82.09
200	2.435E-06	163.86	-92.50	77.93	77.30	71.36
250	1.092E-05	170.38	-94.30	75.55	75.04	76.08
400	8.768E-06	169.43	-92.50	64.12	63.06	76.93

Profile 1 Station 5 June 19th Sound Speed – 1700 m (RAM Model 1/3 Octave Averaged Values)						
Freq Hz	Source Level Bar-m^2/Hz	Source Level dB re 1 μPa^2/Hz	*TL* dB	Observed OBS Level dB re 1 μPa^2/Hz	Noise Corrected OBS Level dB re 1 μPa^2/Hz	Predicted OBS Level dB re 1μPa^2/Hz
25	5.208E-03	197.17	-105.20	93.99	93.27	91.97
50	1.908E-03	192.81	-99.50	88.22	86.70	93.31
100	2.000E-03	193.01	-94.10	92.57	92.22	98.91
200	1.069E-04	180.29	-94.80	81.22	80.97	85.49
400	4.206E-05	176.24	-90.70	66.65	66.05	85.54

Table 7. Comparison of observed and predicted seismic spectral levels at OBS stations lying on selected profiles using Marathon Canada June 29th sound speed profile

Profile 1 Station 5 June 29th Sound Speed Structure (RAM Model 1/3 Octave Averaged Values)						
Freq Hz	Source Level Bar-m^2/Hz	Source Level dB re 1 μPa^2/Hz	*TL* dB	Observed OBS Level dB re 1 μPa^2/Hz	Noise Corrected OBS Level dB re 1 μPa^2/Hz	Predicted OBS Level dB re 1μPa^2/Hz
25	5.208E-03	197.17	-105.90	93.99	93.27	91.27
50	1.908E-03	192.81	-97.70	88.22	86.70	95.11
100	2.000E-03	193.01	-93.40	92.57	92.22	99.61
200	1.069E-04	180.29	-89.20	81.22	80.97	91.09
400	4.206E-05	176.24	-87.00	66.65	66.05	89.24

Profile 2 Station 5 June 29th Sound Speed Structure (RAM Model 1/3 Octave Averaged Values)						
Freq Hz	Source Level Bar-m^2/Hz	Source Level dB re 1 μPa^2/Hz	*TL* dB	Observed OBS Level dB re 1 μPa^2/Hz	Noise Corrected OBS Level dB re 1 μPa^2/Hz	Predicted OBS Level dB re 1μPa^2/Hz
25	5.064E-03	197.04	-98.90	100.28	99.70	98.14
50	2.093E-03	193.21	-97.10	93.01	92.09	96.11
100	2.373E-03	193.75	-91.20	89.94	89.46	102.55
200	1.535E-04	181.86	-84.80	80.54	80.30	97.06
400	3.375E-05	175.28	-84.30	65.76	65.32	90.98

Profile 3 Station 6 June 29th Sound Speed Structure (RAM Model 1/3 Octave Averaged Values)						
Freq Hz	Source Level Bar-m^2/Hz	Source Level dB re 1 μPa^2/Hz	*TL* dB	Observed OBS Level dB re 1 μPa^2/Hz	Noise Corrected OBS Level dB re 1 μPa^2/Hz	Predicted OBS Level dB re 1μPa^2/Hz
25	1.230E-02	200.90	-98.30	104.63	98.07	102.60
50	2.624E-04	184.19	-90.00	102.01	100.39	94.19
100	4.649E-05	176.67	-85.70	87.65	80.36	90.97
200	3.974E-05	175.99	-81.50	82.20	-	94.49
400	6.076E-06	167.84	-79.60	73.53	72.67	88.24

Profile 4 Station 1 June 29th Sound Speed Structure (RAM Model 1/3 Octave Averaged Values)						
Freq Hz	Source Level Bar-m^2/Hz	Source Level dB re 1 μPa^2/Hz	*TL* dB	Observed OBS Level dB re 1 μPa^2/Hz	Noise Corrected OBS Level dB re 1 μPa^2/Hz	Predicted OBS Level dB re 1μPa^2/Hz
25	8.791E-03	199.44	-117.30	90.33	87.18	82.14
50	8.851E-04	189.47	-110.60	85.56	82.26	78.87
100	1.902E-04	182.79	-114.10	86.28	85.58	68.69
200	2.435E-06	163.86	-105.30	77.93	77.30	58.56
250	1.092E-05	170.38	-107.50	75.55	75.04	62.88
400	8.768E-06	169.43	-96.70	64.12	63.06	72.73

Table 8. (Predicted – Observed) OBS levels in dB re 1μPa^2/Hz .

STN #5 June 19th (Deployment) Sound Speed Profile

Freq. Hz	Profile #1	Profile #2	Profile #3	Profile #4
25	-1.7	-1.3	5.1	-3.5
50	7.4	5.9	-7.6	-11.4
100	8.7	15.1	10.2	-12.9
200	7.1	16.8	In noise	-15.2
250	-	-	-	-4.8
400	24.0	25.9	14.2	7.3

Average |Difference| = 10.3 dB

Marathon June 29th Marathon *Viking* Sound Speed Profile

Freq. Hz	Profile #1	Profile #2	Profile #3	Profile #4
25	-2.0	-1.6	4.5	-5.0
50	8.4	4.0	-6.2	-3.4
100	7.4	13.1	10.6	-16.9
200	10.1	16.8	In noise	-18.7
250	-	-	-	-12.2
400	23.2	25.7	15.6	9.7

Average |Difference| = 10.8 dB

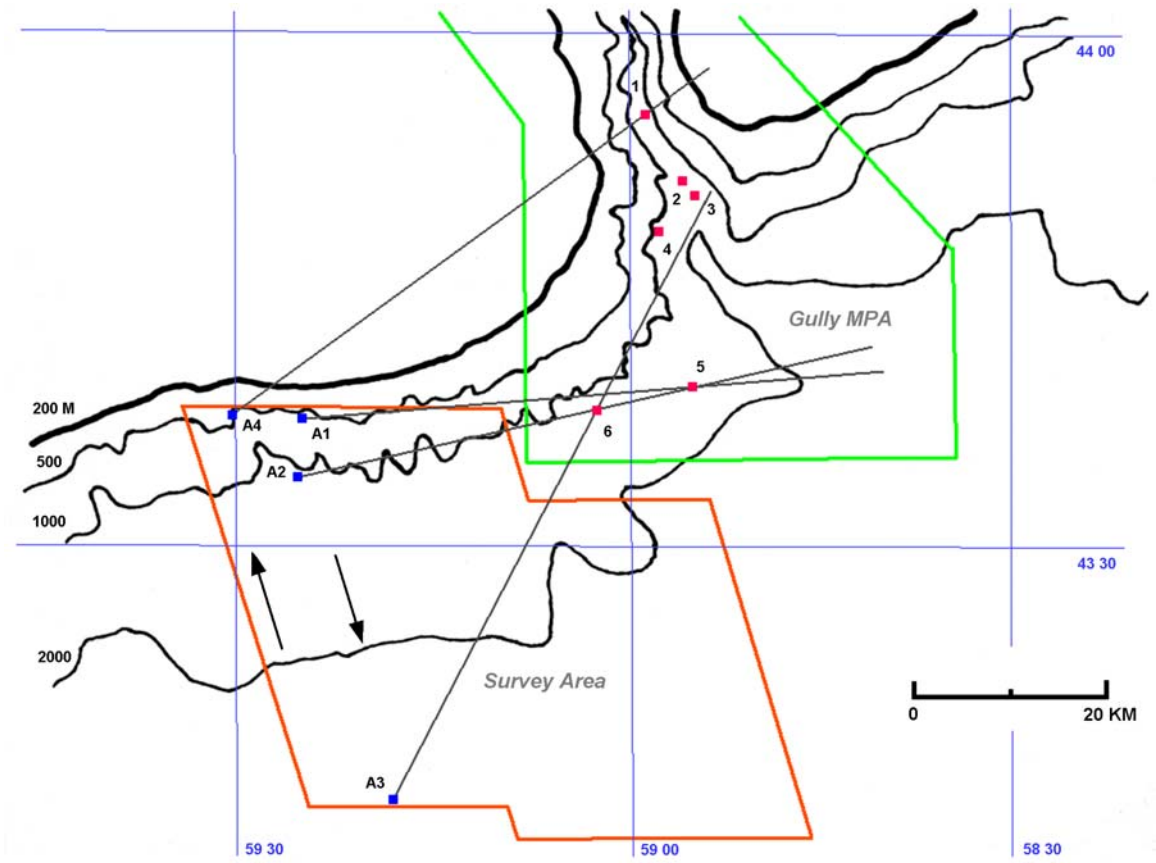

Figure 1. Gully survey area. The orange enclosed area outlines Exploration Leases (EL) 2410 and 2411 (Cortland & Empire from west to east). The green enclosed area is the southern portion of the Gully Marine Protected Area. Red square symbols show the 6 OBS deployments. Blue square symbols A1 – A4 show the location of seismic vessel M/V *Ramform Viking* for selected analysis profiles #1 through 4 respectively (grey lines). Arrows show approximate locations of *V*iking N-S and S-N shooting transects during OBS recording.[1]

[1] Figure 1 is a sketched rather than digitally produced map and should not be relied upon for highly precise station locations or bathymetry.

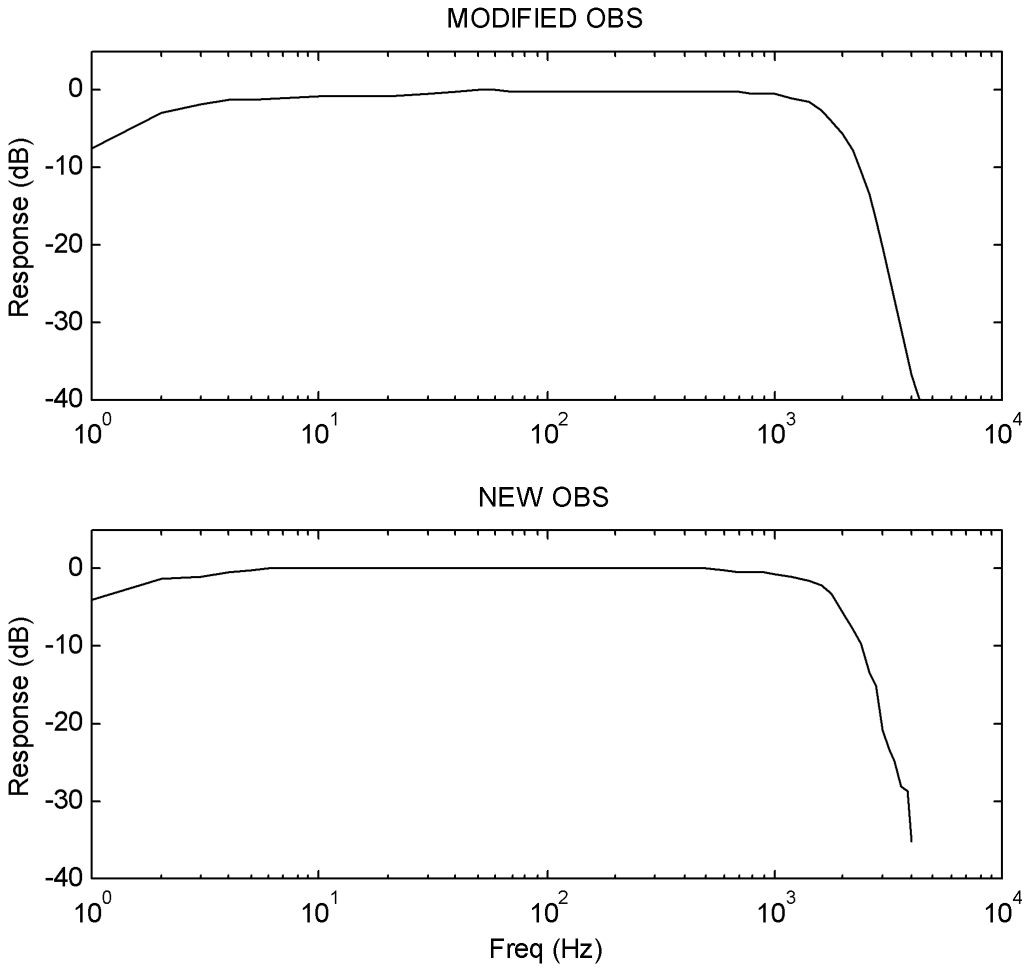

Figure 2. Measured frequency response of "Modified" and "New" OBS electronics not including hydrophones.

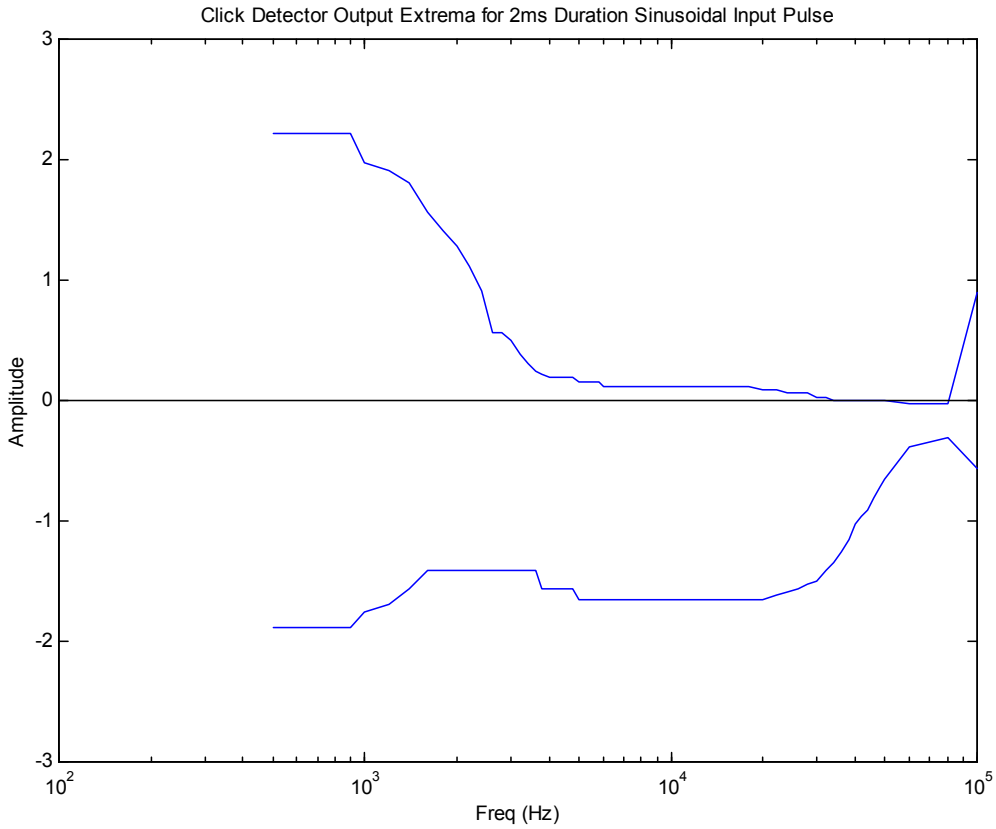

Figure 3. Extreme +ve and –ve going outputs of "click detector" for a 2 ms sinusoidal burst at frequency shown on horizontal axis.

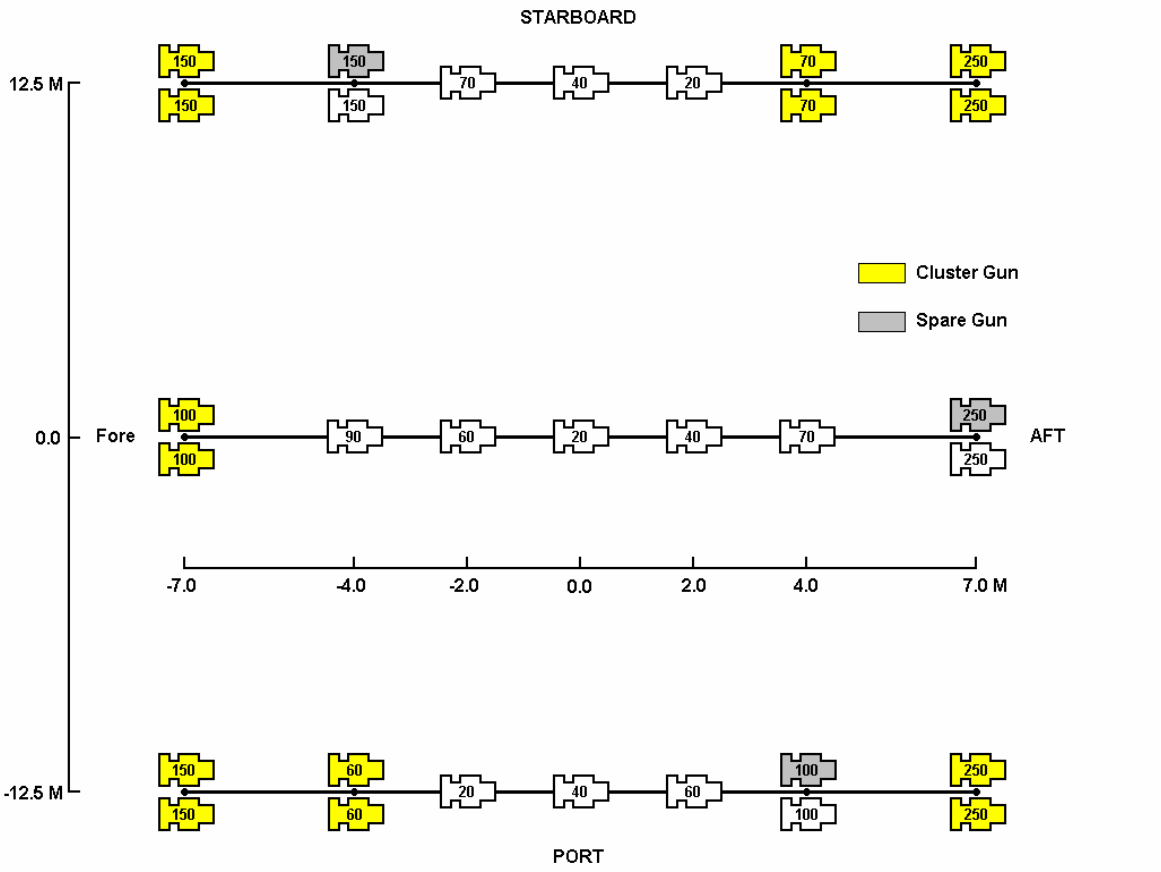

Figure 4. *Ramform Viking* airgun array configuration. Airgun capacities marked in cubic inches.

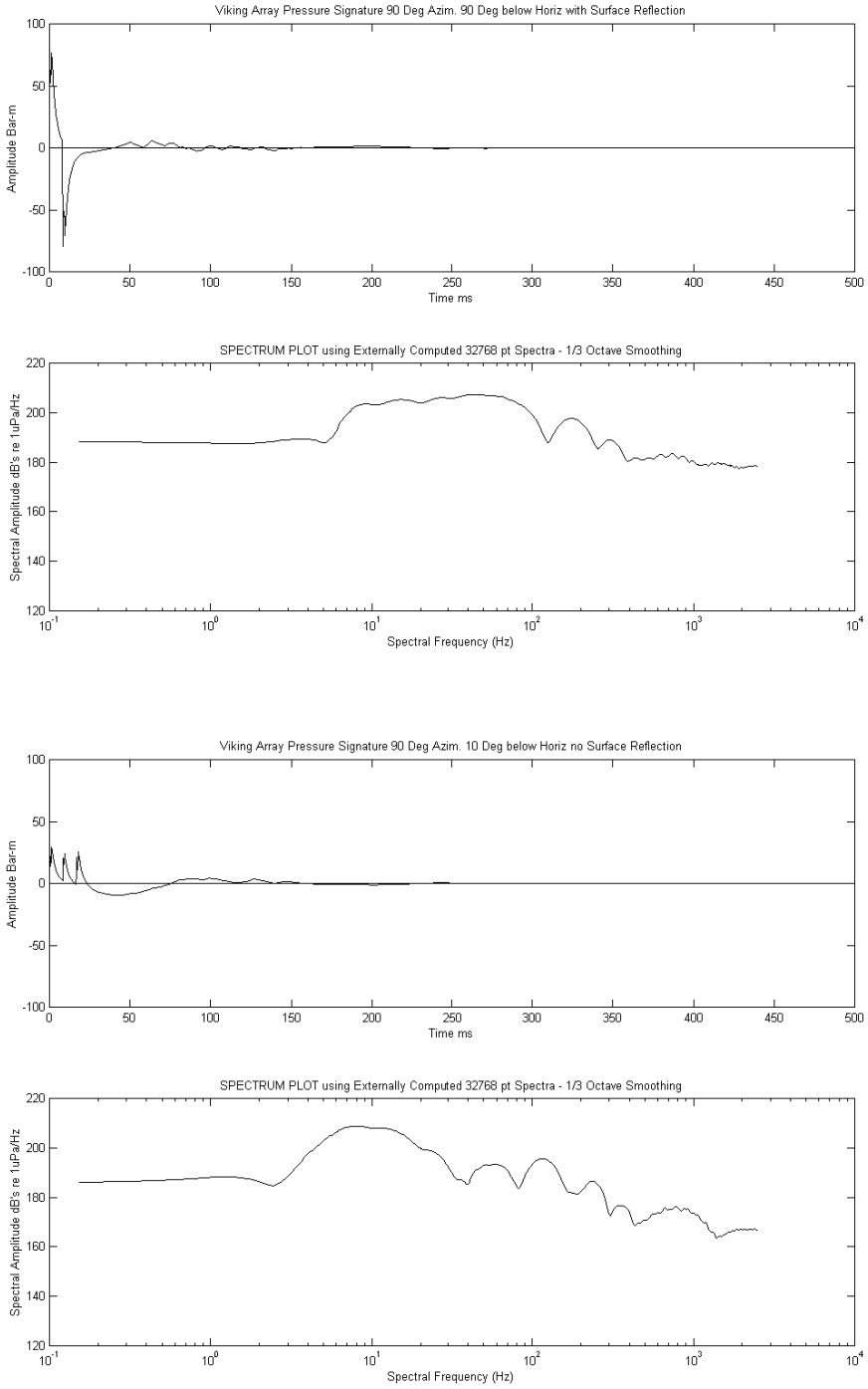

Figure 5. *Ramform Viking* far field airgun array pressure signature and power spectrum: Top) At 90º below horizontal (main beam) with surface reflection included; Bottom) At 10º below horizontal (side radiation) at azimuth of 90º (directly starboard of array), surface reflection **not** included. Parameters: Gun depth – 6m, gun pressure 2500 psi.

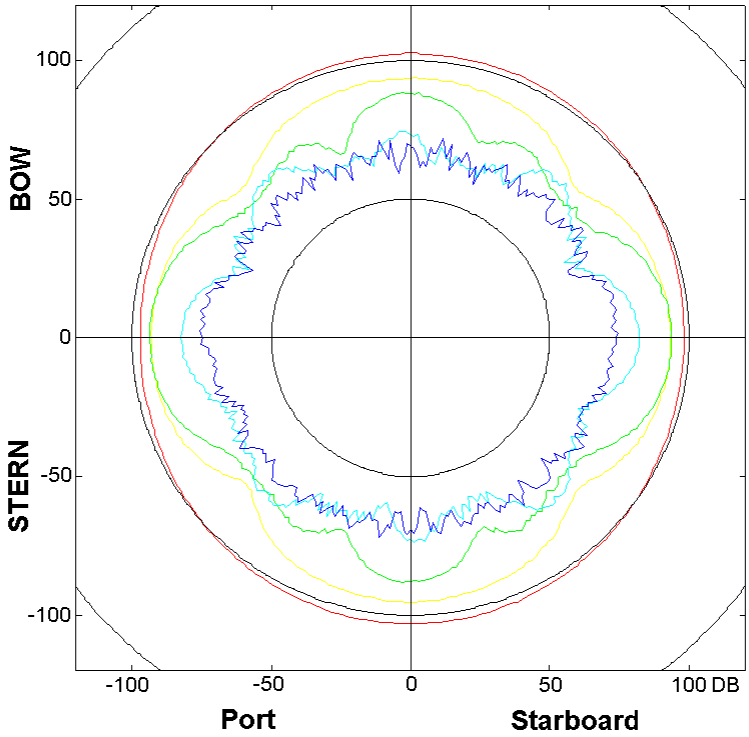

Figure 6. *Ramform Viking* far field airgun array radiation pattern at 10º below horizontal plane for: 25 Hz (red); 50 Hz (yellow); 100 Hz (green); 200 Hz (lt. blue); and 400 Hz (dark blue). Radiated pressures are in dB re 1μPa^2/Hz @ 1 m above a 100 dB baseline (center origin). Radiated pressure spectra are derived from 32768 pt. synthesized time series (6.55 s) averaged (smoothed) over 1/3 octave bands centered on the nominal frequencies. Towing direction is toward top of diagram. Water surface reflections are **not** included.

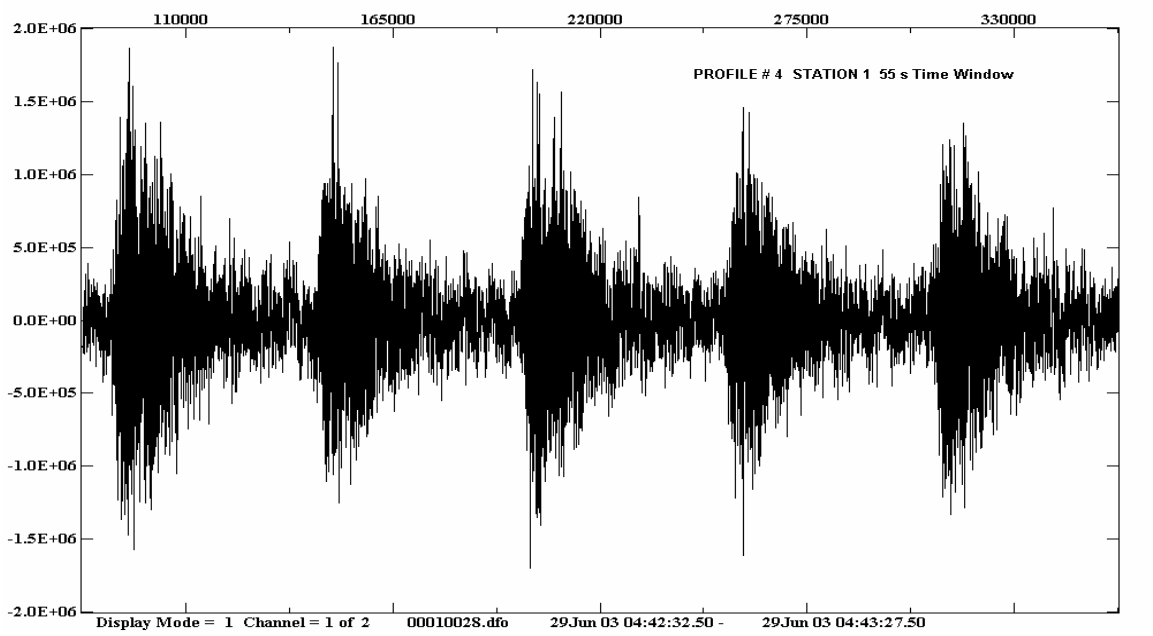

Figure 7. Typical OBS echogram during seismic shooting recorded at Station #1 (Channel 1) in Gully whale concentration area. Vertical axis shows acoustic pressure in μPa. Horizontal axis shows sample number (5 kHz sampling rate).

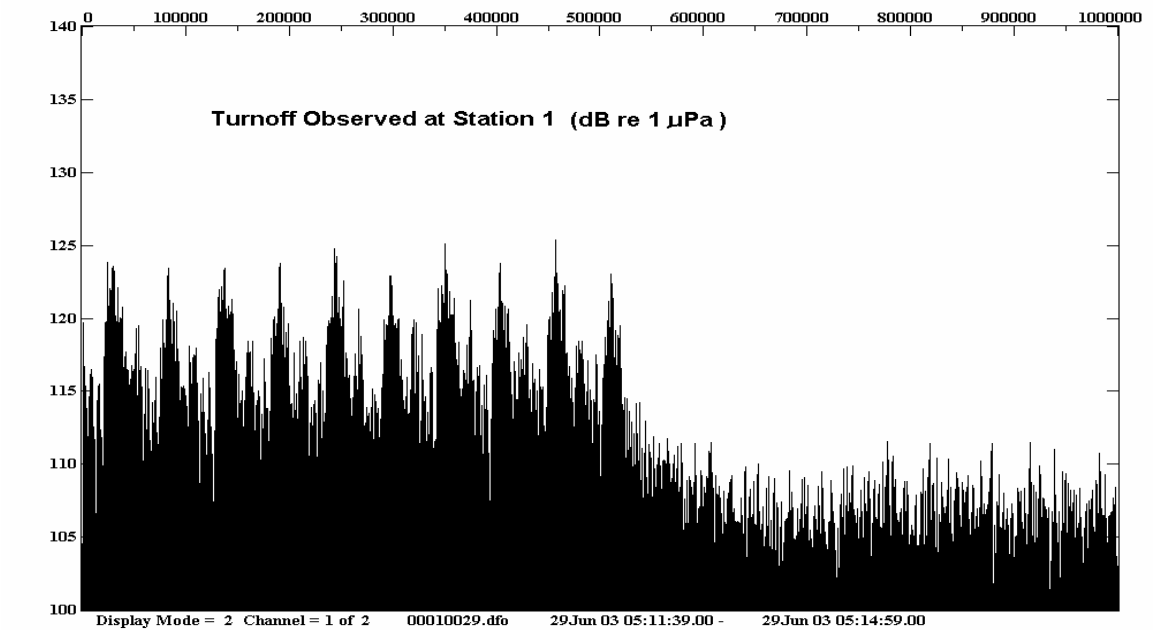

Figure 8. Cessation of seismic shooting at Station #1. Vertical axis shows absolute acoustic amplitude in dB re 1μPa. Horizontal axis shows sample number (5 kHz sampling rate). Acoustic levels decline to non-seismic ambient over approximately 20 s after last received seismic impulse.

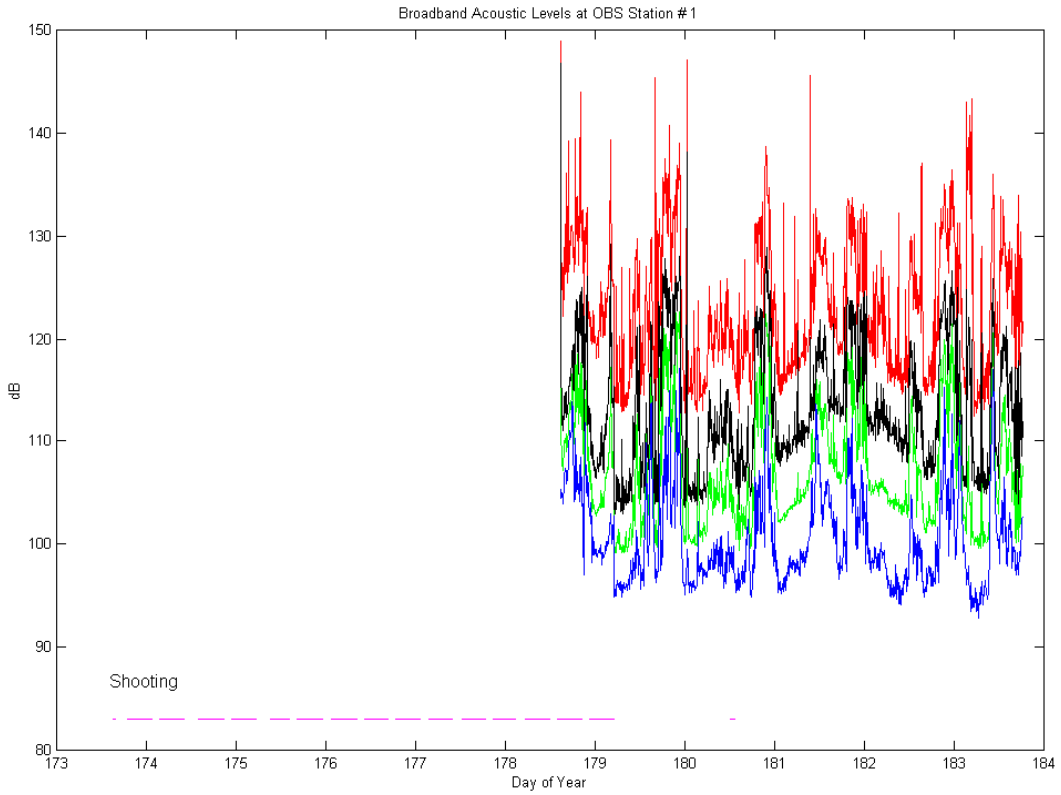

Figure 9. Broadband acoustic levels at OBS Station #1. Red – Maximum instantaneous 0-peak acoustic amplitude over consecutive 300 s intervals. Green – RMS amplitude averaged over same 300 s interval. Black – Maximum RMS amplitude averaged over any consecutive 1 s interval within 300 s interval. Blue – Minimum RMS amplitude averaged over any consecutive 1 s interval within 300 s interval. Magenta horizontal lines indicate active shooting periods.

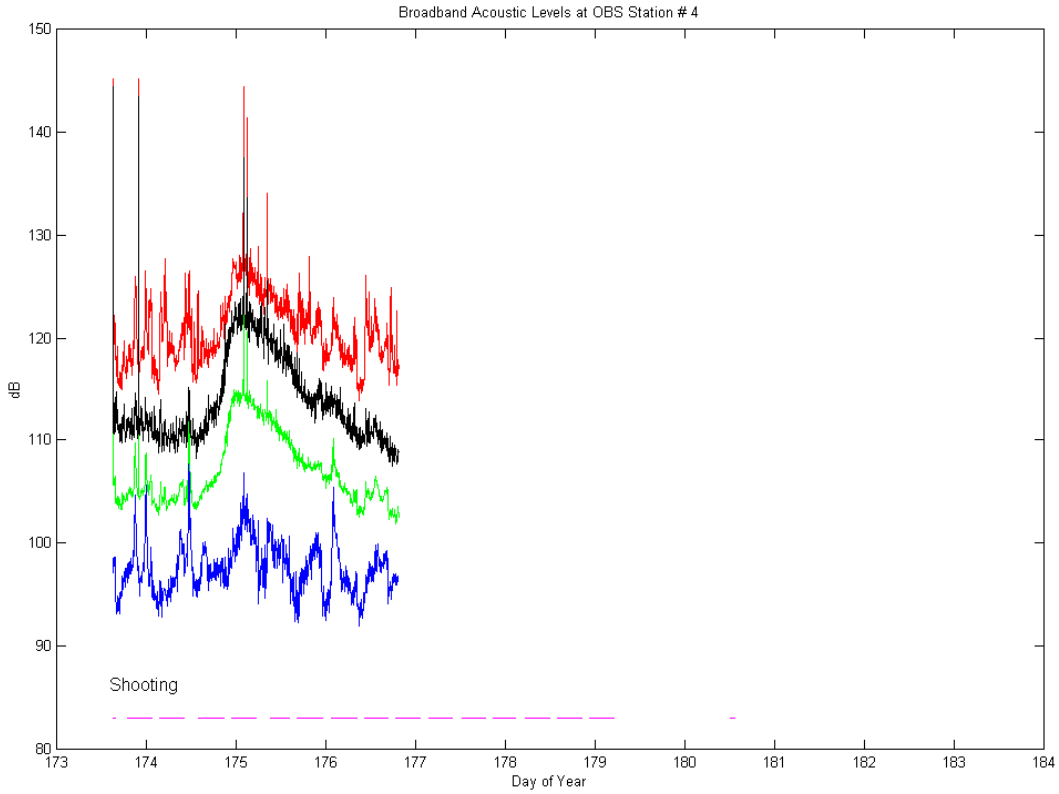

Figure 10. Broadband acoustic levels at OBS Station #4. Red – Maximum instantaneous 0-peak acoustic amplitude over consecutive 300 s intervals. Green – RMS amplitude averaged over same 300 s interval. Black – Maximum RMS amplitude averaged over any consecutive 1 s interval within 300 s interval. Blue – Minimum RMS amplitude averaged over any consecutive 1 s interval within 300 s interval. Magenta horizontal lines indicate active shooting periods.

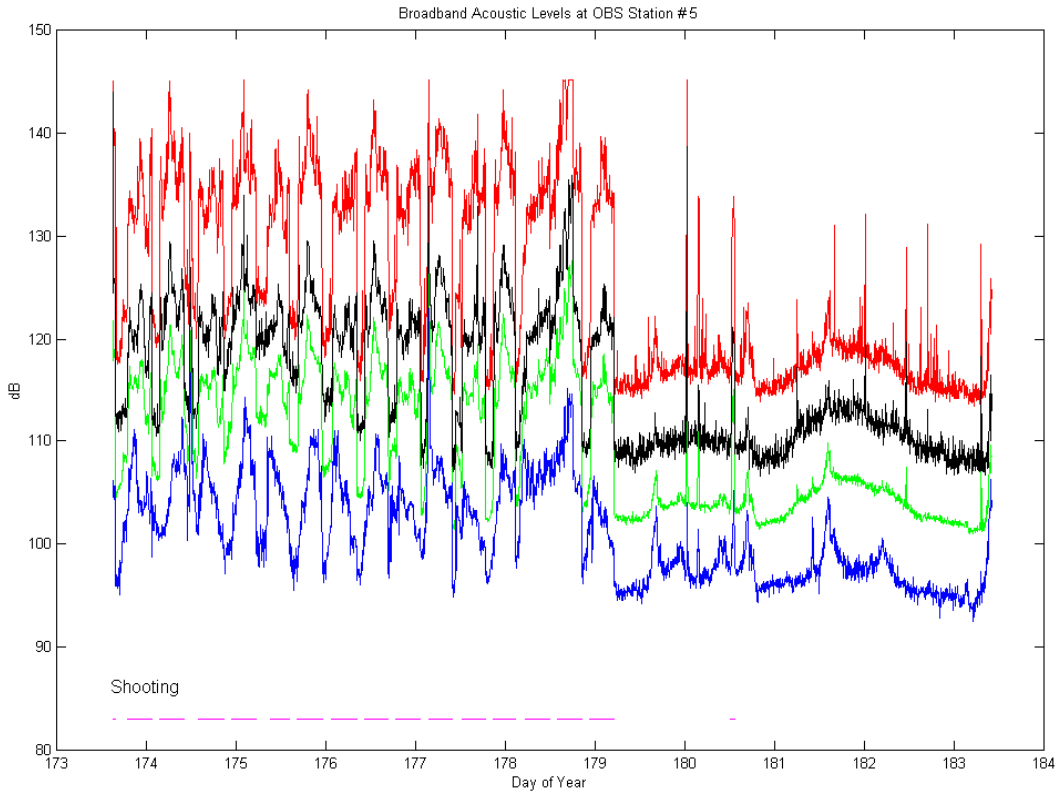

Figure 11. Broadband acoustic levels at OBS Station #5. Red – Maximum instantaneous 0-peak acoustic amplitude over consecutive 300 s intervals. Green – RMS amplitude averaged over same 300 s interval. Black – Maximum RMS amplitude averaged over any consecutive 1 s interval within 300 s interval. Blue – Minimum RMS amplitude averaged over any consecutive 1 s interval within 300 s interval. Magenta horizontal lines indicate active shooting periods.

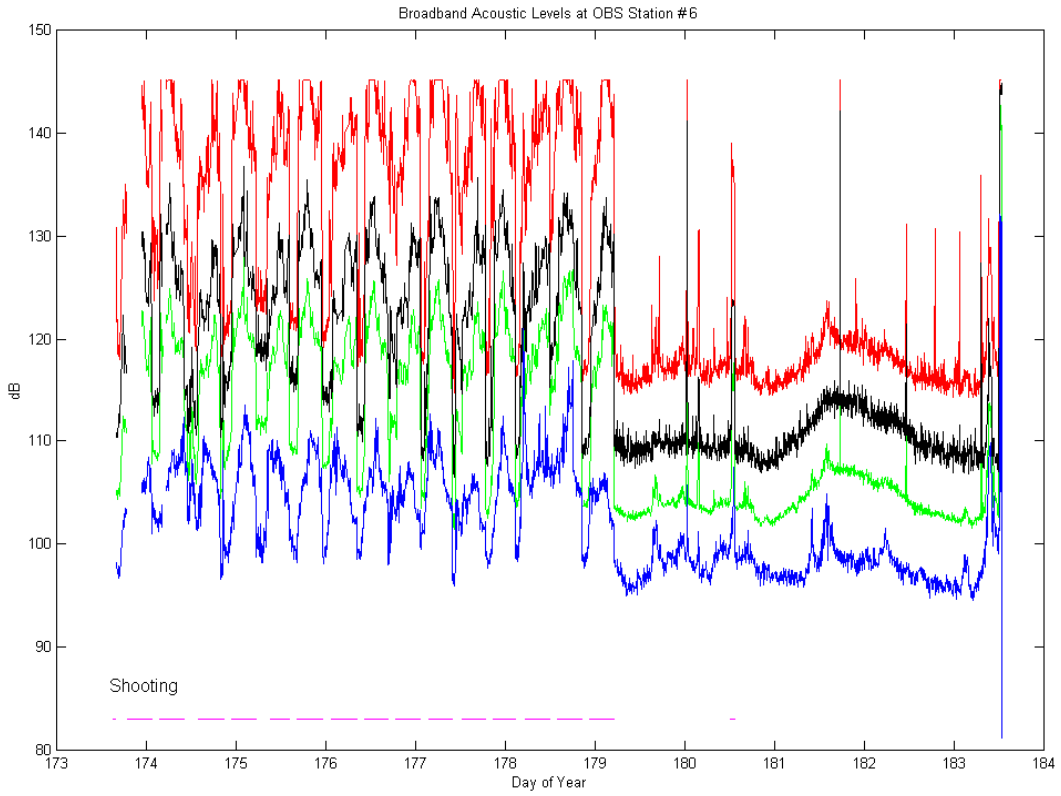

Figure 12. Broadband acoustic levels at OBS Station #6. Red – Maximum instantaneous 0-peak acoustic amplitude over consecutive 300 s intervals. Green – RMS amplitude averaged over same 300 s interval. Black – Maximum RMS amplitude averaged over any consecutive 1 s interval within 300 s interval. Blue – Minimum RMS amplitude averaged over any consecutive 1 s interval within 300 s interval. Magenta horizontal lines indicate active shooting periods.

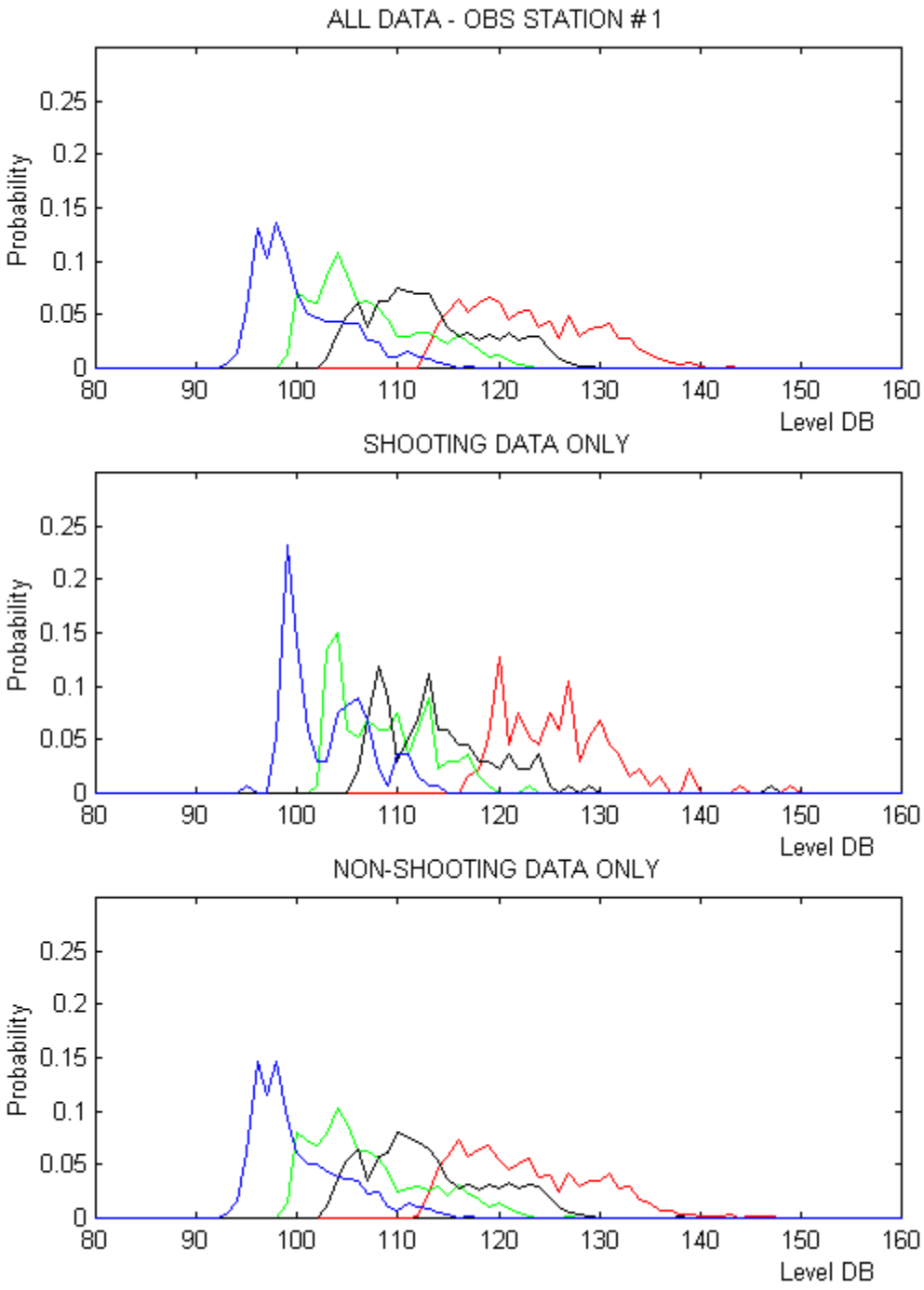

Figure 13. Probability distribution function of acoustic levels at OBS Station #1 for total observation period, and for seismic shooting and non-shooting intervals. Red – Maximum 0-peak acoustic amplitude over consecutive 300 s intervals. Green – RMS amplitude averaged over same 300 s interval. Black – Maximum RMS amplitude averaged over any consecutive 1 s interval within 300 s interval. Blue – Minimum RMS amplitude averaged over any consecutive 1 s interval within 300 s interval.

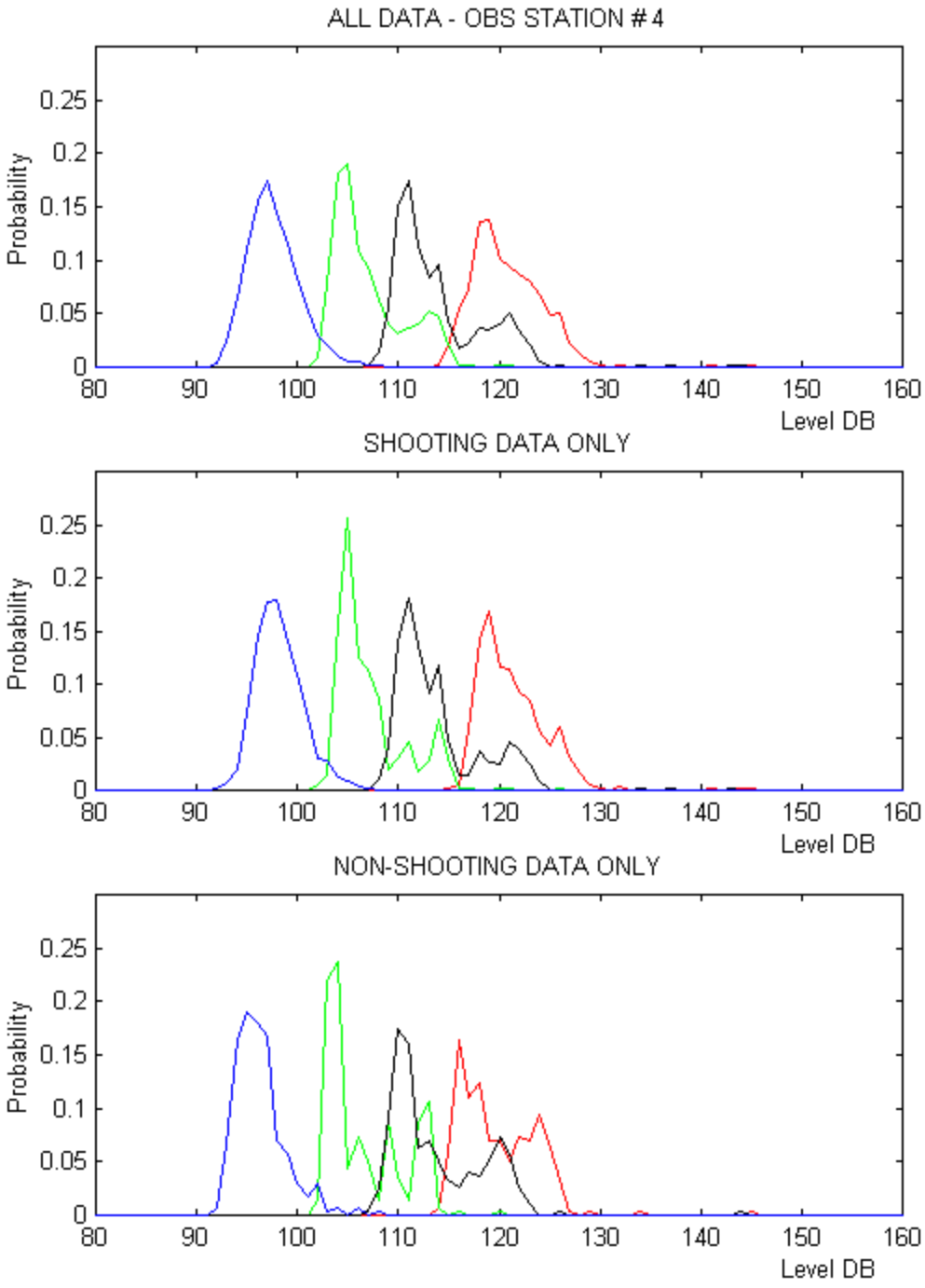

Figure 14. Probability distribution function of acoustic levels at OBS Station #4 for total observation period, and for seismic shooting and non-shooting intervals. Red – Maximum 0-peak acoustic amplitude over consecutive 300 s intervals. Green – RMS amplitude averaged over same 300 s interval. Black – Maximum RMS amplitude averaged over any consecutive 1 s interval within 300 s interval. Blue – Minimum RMS amplitude averaged over any consecutive 1 s interval within 300 s interval.

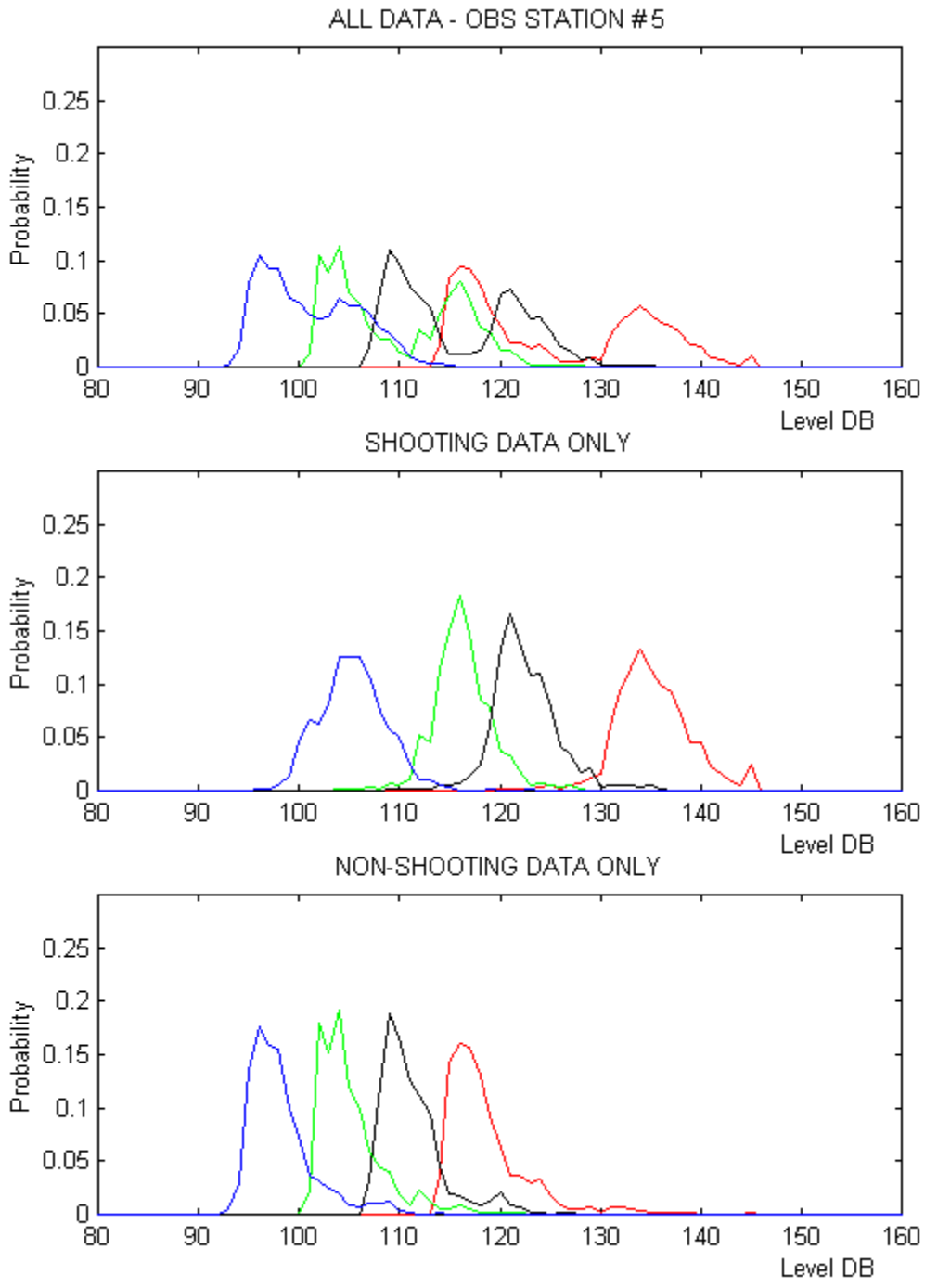

Figure 15. Probability distribution function of acoustic levels at OBS Station #5 for total observation period, and for seismic shooting and non-shooting intervals. Red – Maximum 0-peak acoustic amplitude over consecutive 300 s intervals. Green – RMS amplitude averaged over same 300 s interval. Black – Maximum RMS amplitude averaged over any consecutive 1 s interval within 300 s interval. Blue – Minimum RMS amplitude averaged over any consecutive 1 s interval within 300 s interval.

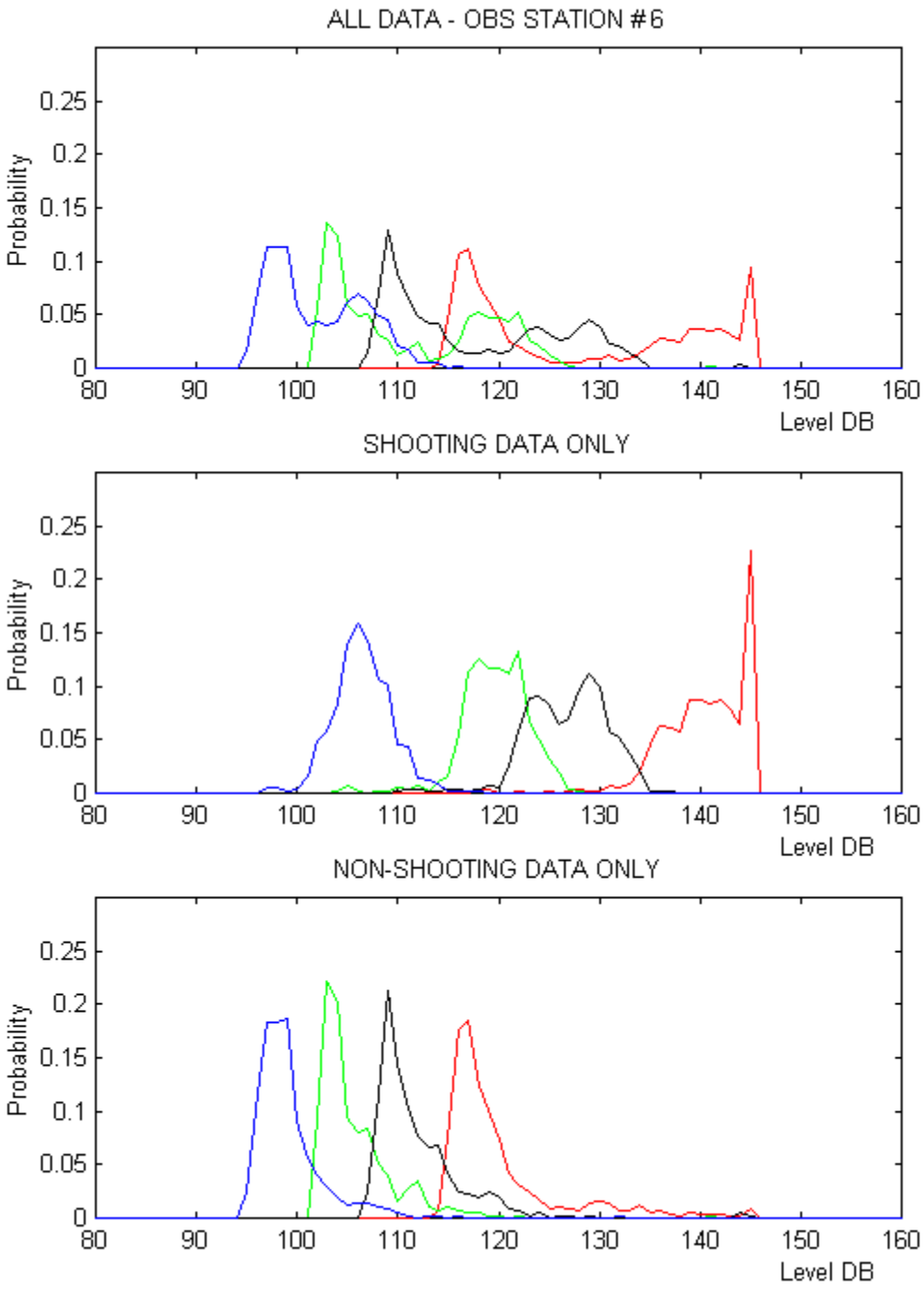

Figure 16. Probability distribution function of acoustic levels at OBS Station #6 for total observation period, and for seismic shooting and non-shooting intervals. Red – Maximum 0-peak acoustic amplitude over consecutive 300 s intervals. Green – RMS amplitude averaged over same 300 s interval. Black – Maximum RMS amplitude averaged over any consecutive 1 s interval within 300 s interval. Blue – Minimum RMS amplitude averaged over any consecutive 1 s interval within 300 s interval.

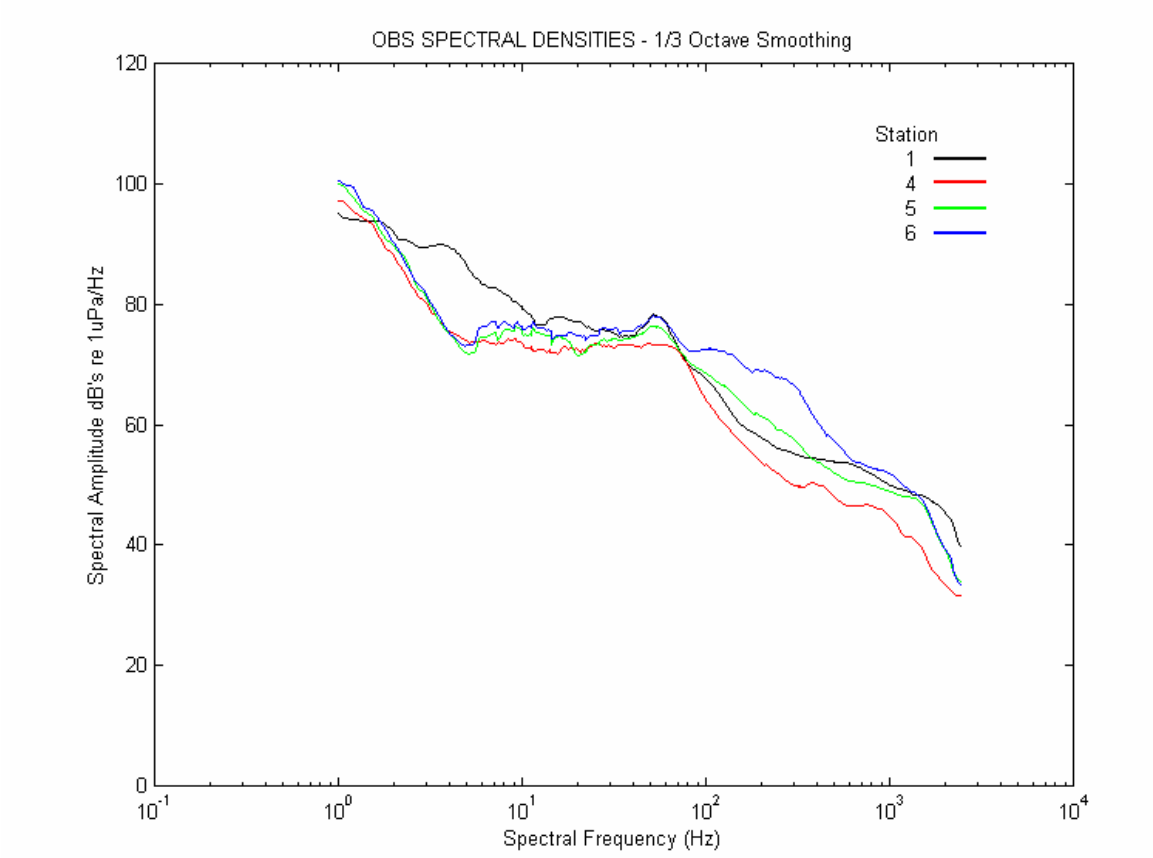

Figure 17. Power spectral densities for data recorded simultaneously at Stations #1 (black), 5 (green), and 6 (blue) during a low wind non-seismic-shooting period. A non-simultaneous spectrum for Station #4 (red) during a quiet non-seismic-shooting period is also shown.

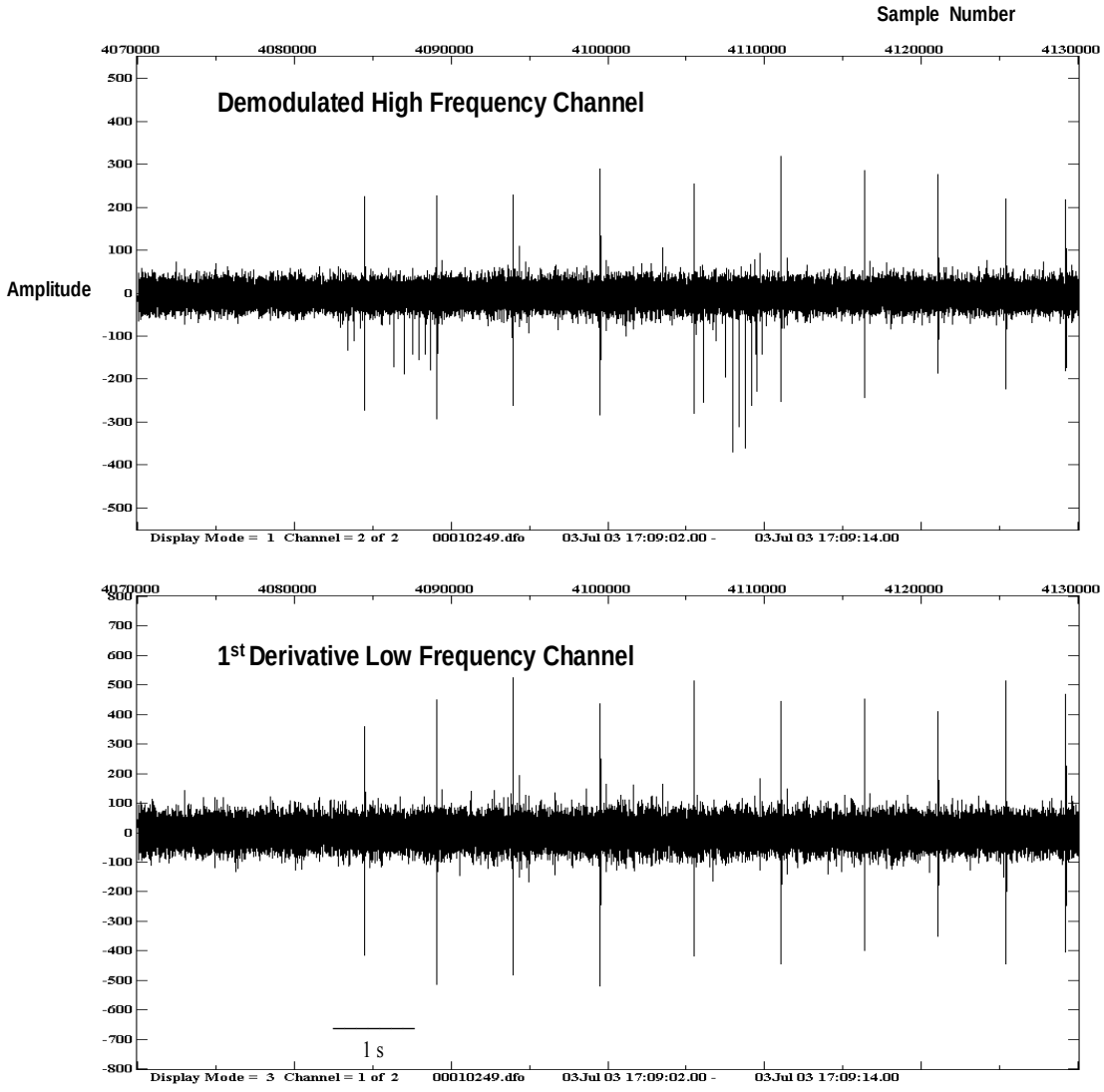

Figure 18. Station #1 time series comparing output of click detector (top) and digital derivative, 5 kHz sampled hydrophone channel (bottom). Amplitude scaling is arbitrary.

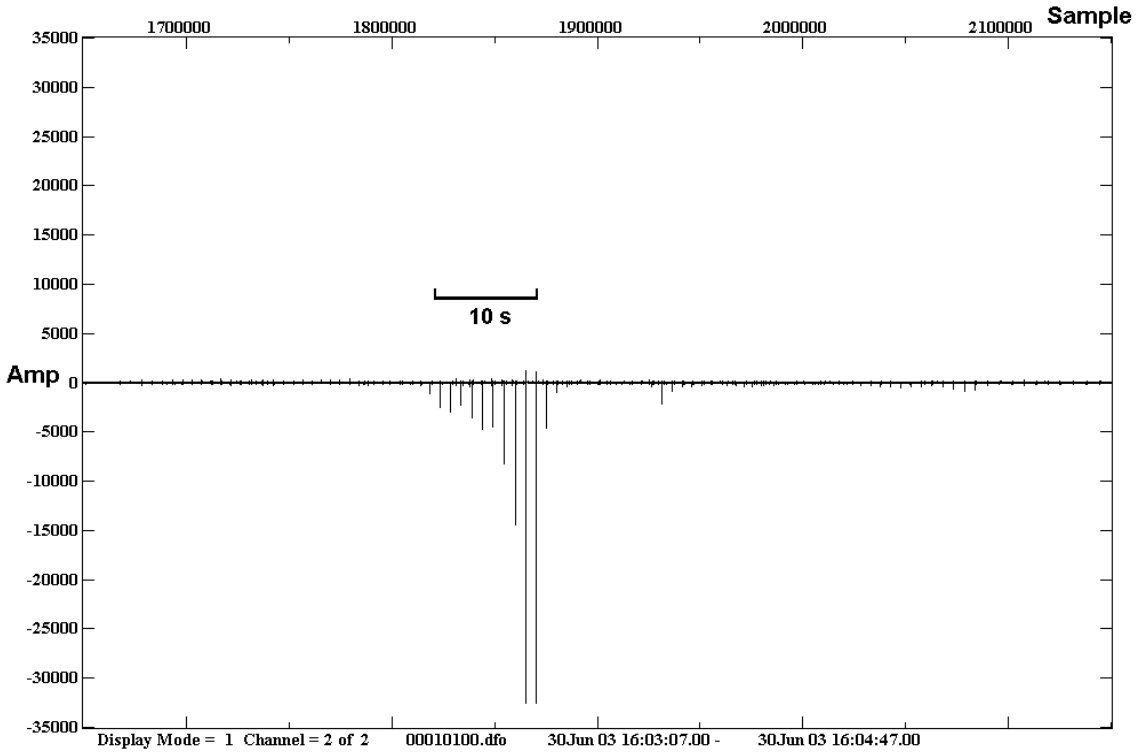

Figure 19. Output of Station #1 click detector for apparent close approach of click vocalizing whale. Detector is driven to –ve going saturation during highest amplitude clicks.

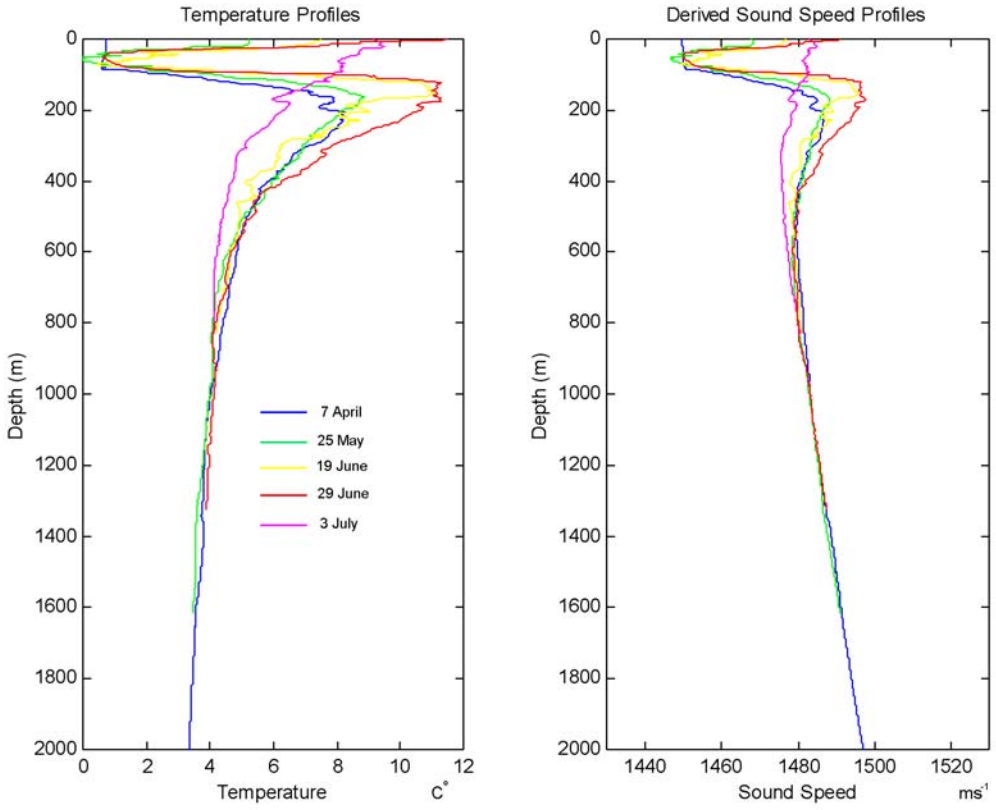

Figure 20. Temperature and sound speed profiles for the Gully Region for the spring/summer period of 2003.

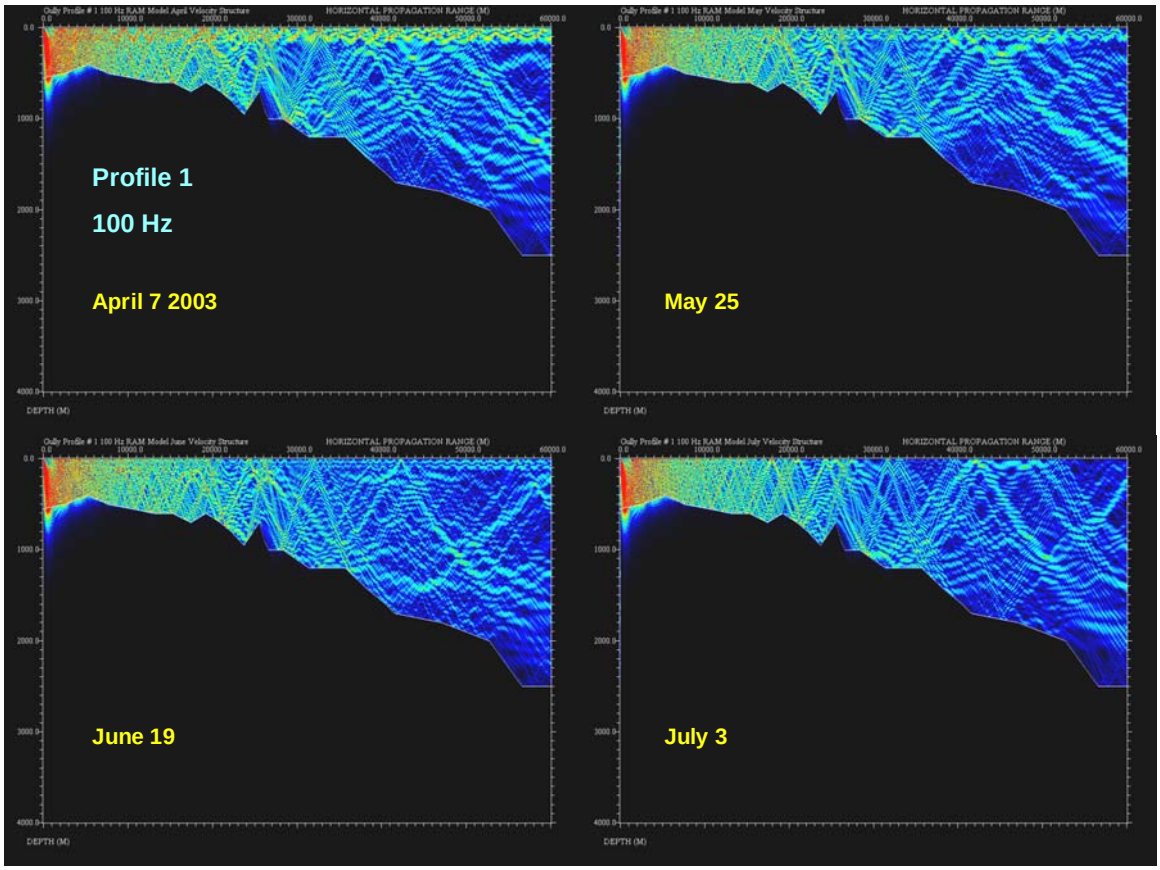

Figure 21. Sound intensities (cylindrical spreading effect removed) along Profile # 1 for source at 6 m propagating from shallow to deep water. The four component panels show the effect of varying sound speed profiles (range invariant) derived from direct measurements in April, May, June, and July of 2003.

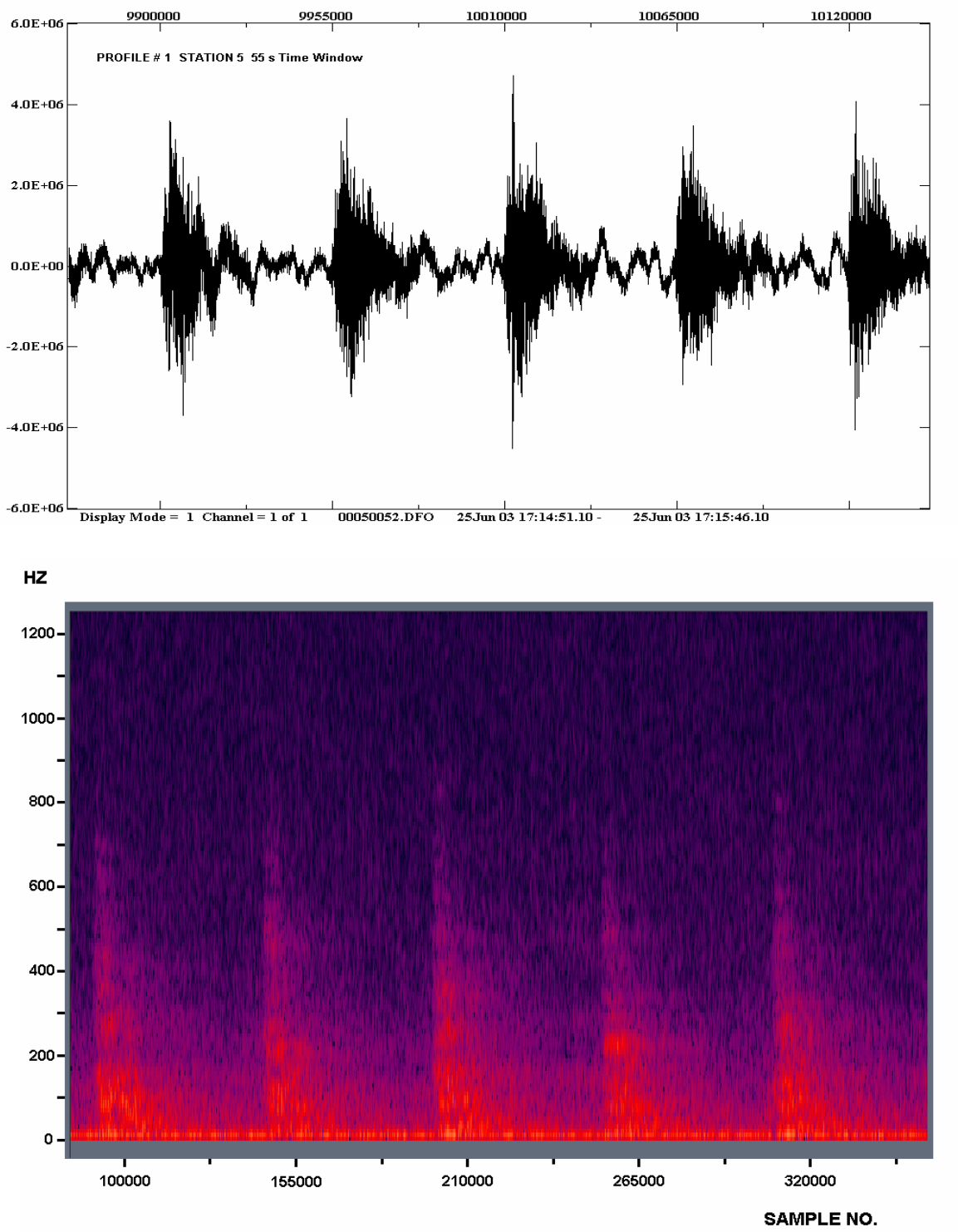

Figure 22. Profile #1 Station #5 direct hydrophone OBS signal amplitude (top) and corresponding sonogram (bottom) based on 1024 pt. FFTs. Time series duration is 55s. Signal amplitude is linear in μPa and sonogram vertical axis is linear in Hz.

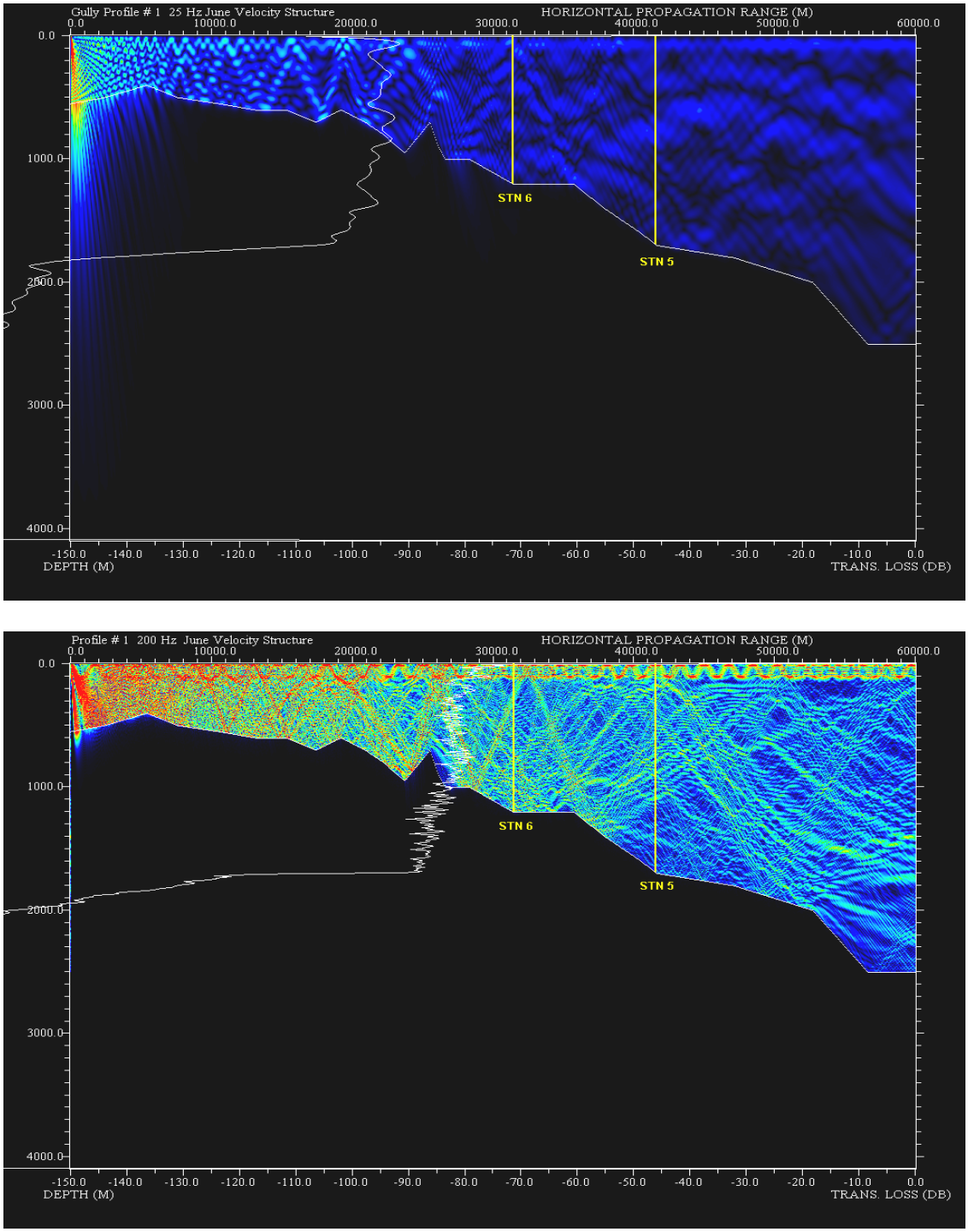

Figure 23. Profile #1 RAM model relative transmission losses at 25 Hz (top) and 200 Hz (bottom). Blue to red represent decreasing losses or higher acoustic intensities. A 10 log R range compensation has been applied to color-coded values to emphasize non-cylindrical transmission losses. Station #5 absolute transmission loss averaged over 1/3 octave bandwidth is shown in vertical profile.

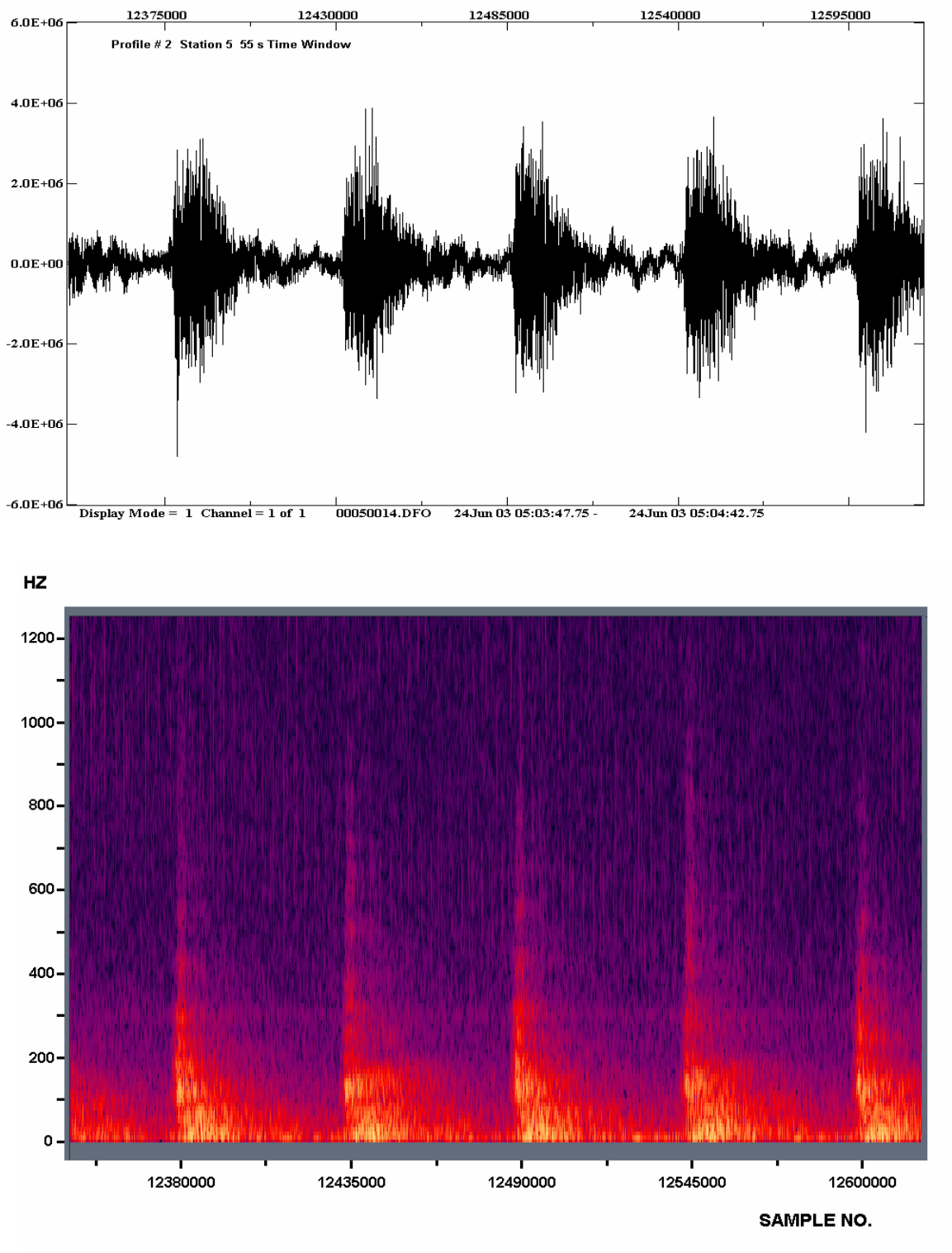

Figure 24. Profile #2 Station #5 direct hydrophone OBS signal amplitude (top) and corresponding sonogram (bottom) based on 1024 pt. FFTs. Time series duration is 55s. Signal amplitude is linear in µPa and sonogram vertical axis is linear in Hz.

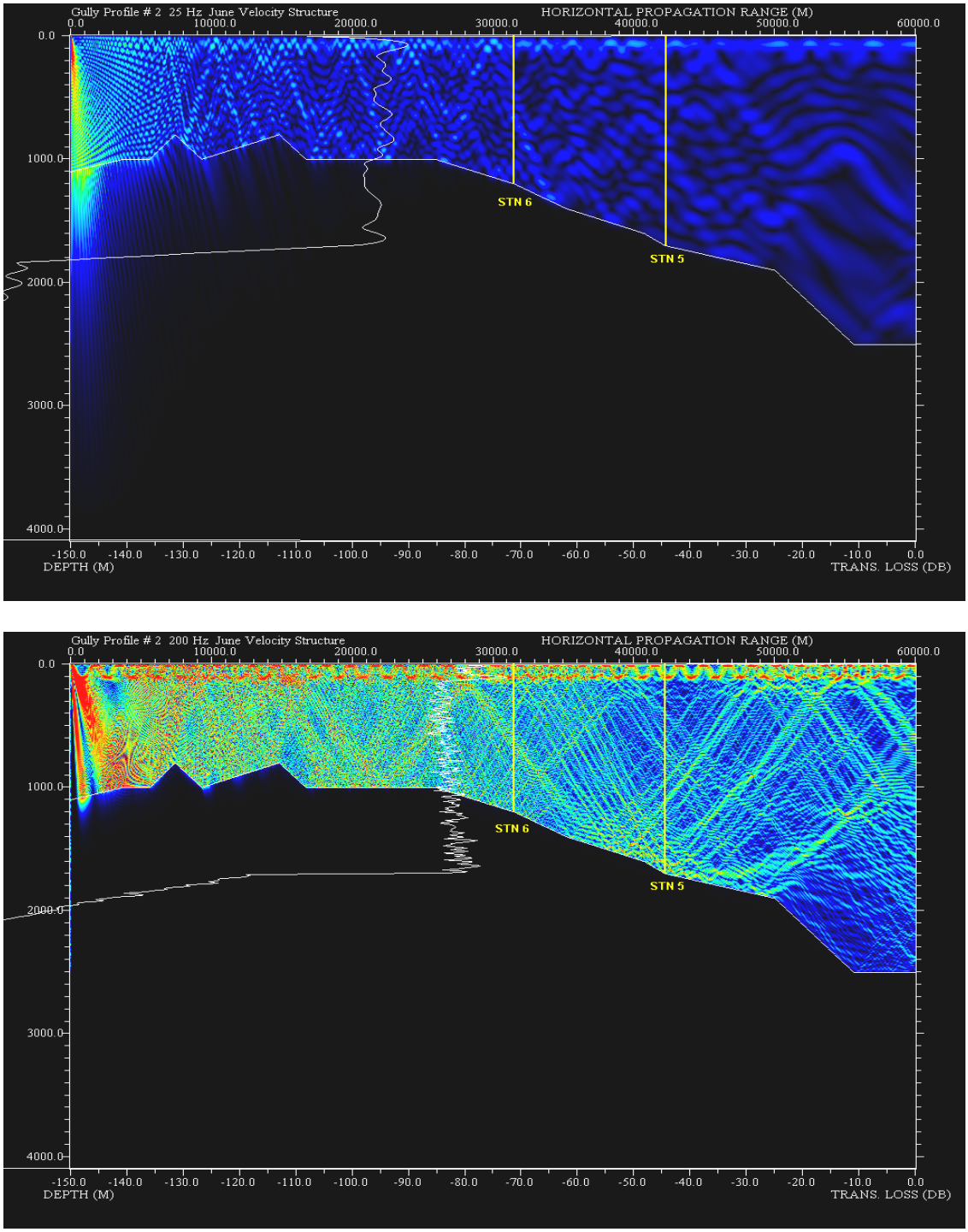

Figure 25. Profile #2 RAM model relative transmission losses at 25 Hz (top) and 200 Hz (bottom). Blue to red represent decreasing losses or higher acoustic intensities. A 10 log R range compensation has been applied to color-coded values to emphasize non-cylindrical transmission losses. Station #5 absolute transmission loss averaged over 1/3 octave bandwidth is shown in vertical profile.

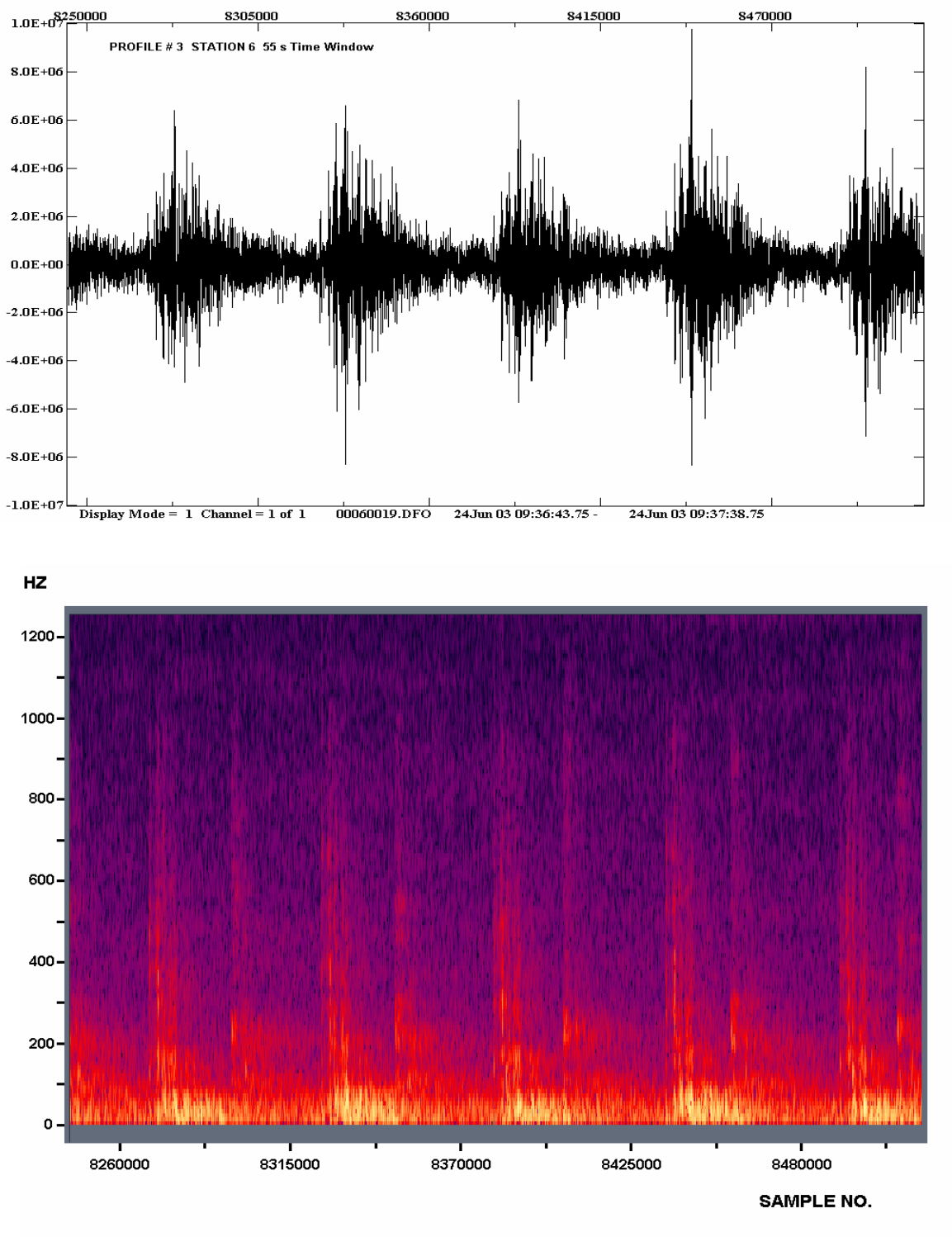

Figure 26. Profile #3 Station #6 direct hydrophone OBS signal amplitude (top) and corresponding sonogram (bottom) based on 1024 pt. FFTs. Time series duration is 55s. Signal amplitude is linear in μPa and sonogram vertical axis is linear in Hz.

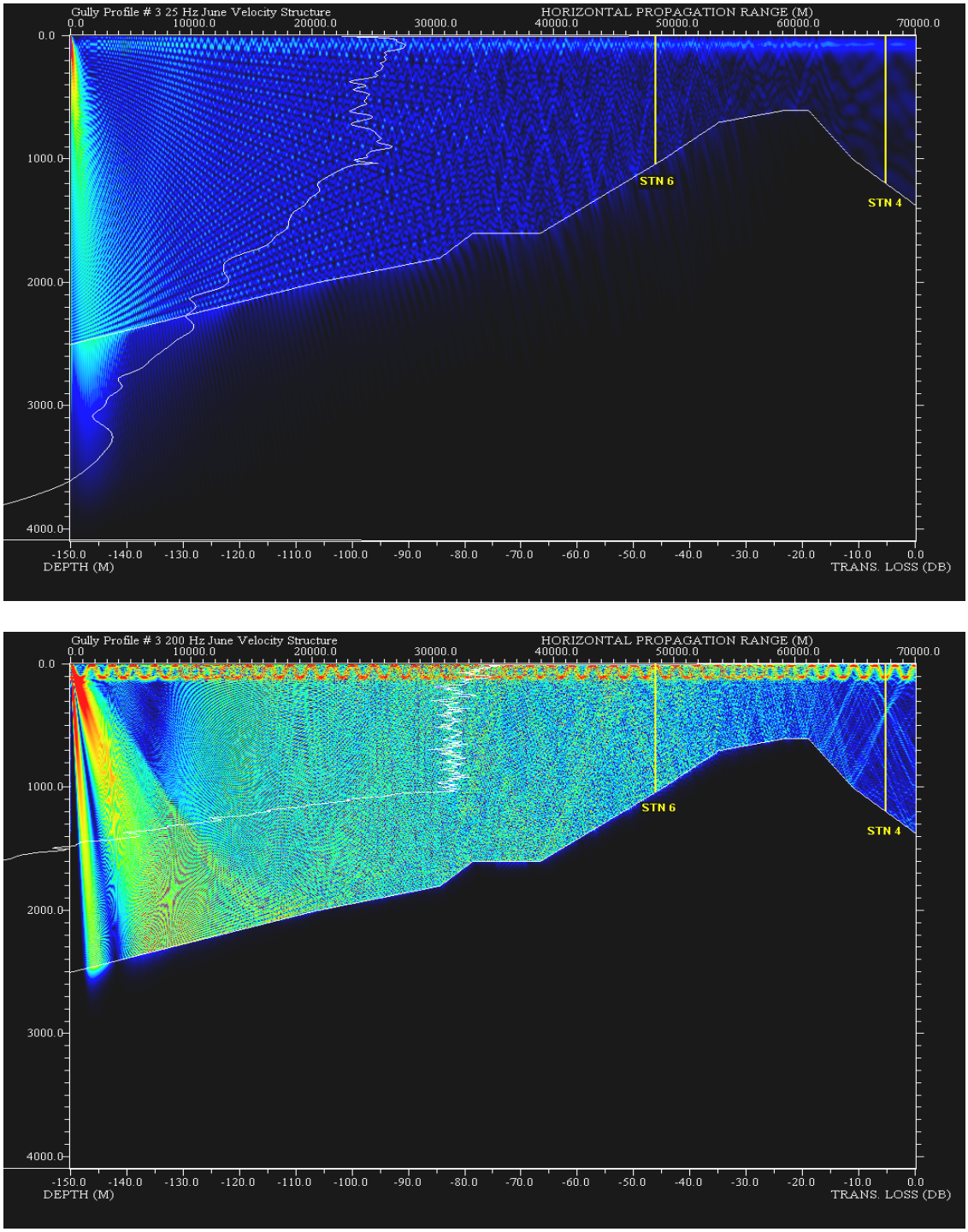

Figure 27. Profile #3 RAM model relative transmission losses at 25 Hz (top) and 200 Hz (bottom). Blue to red represent decreasing losses or higher acoustic intensities. A 10 log R range compensation has been applied to color-coded values to emphasize non-cylindrical transmission losses. Station #6 absolute transmission loss averaged over 1/3 octave bandwidth is shown in vertical profile.

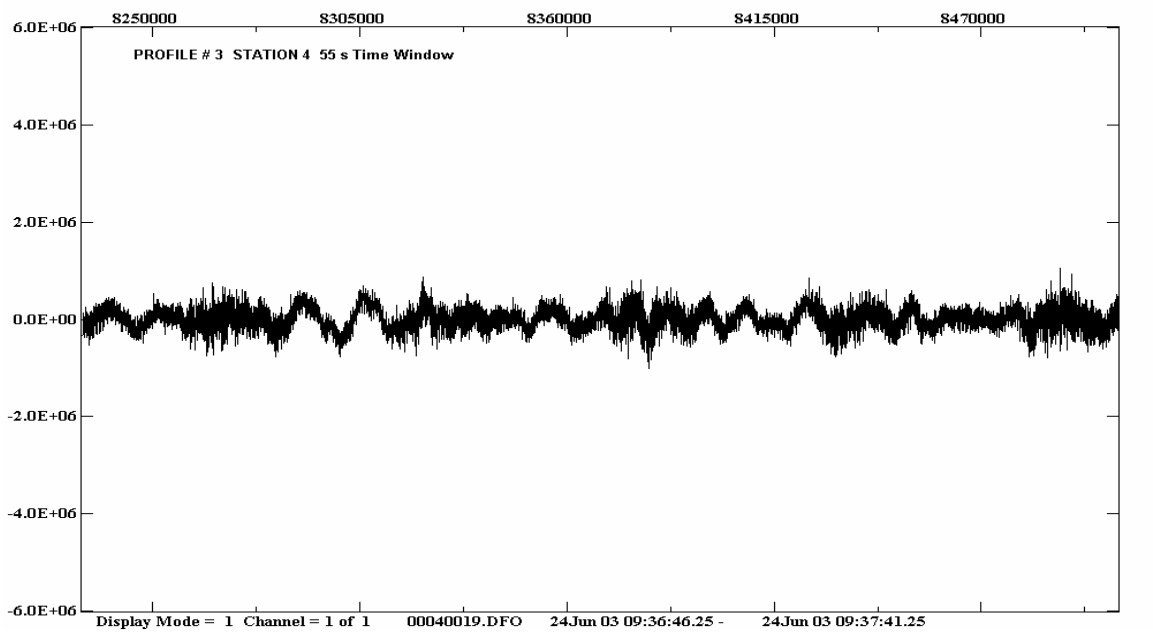

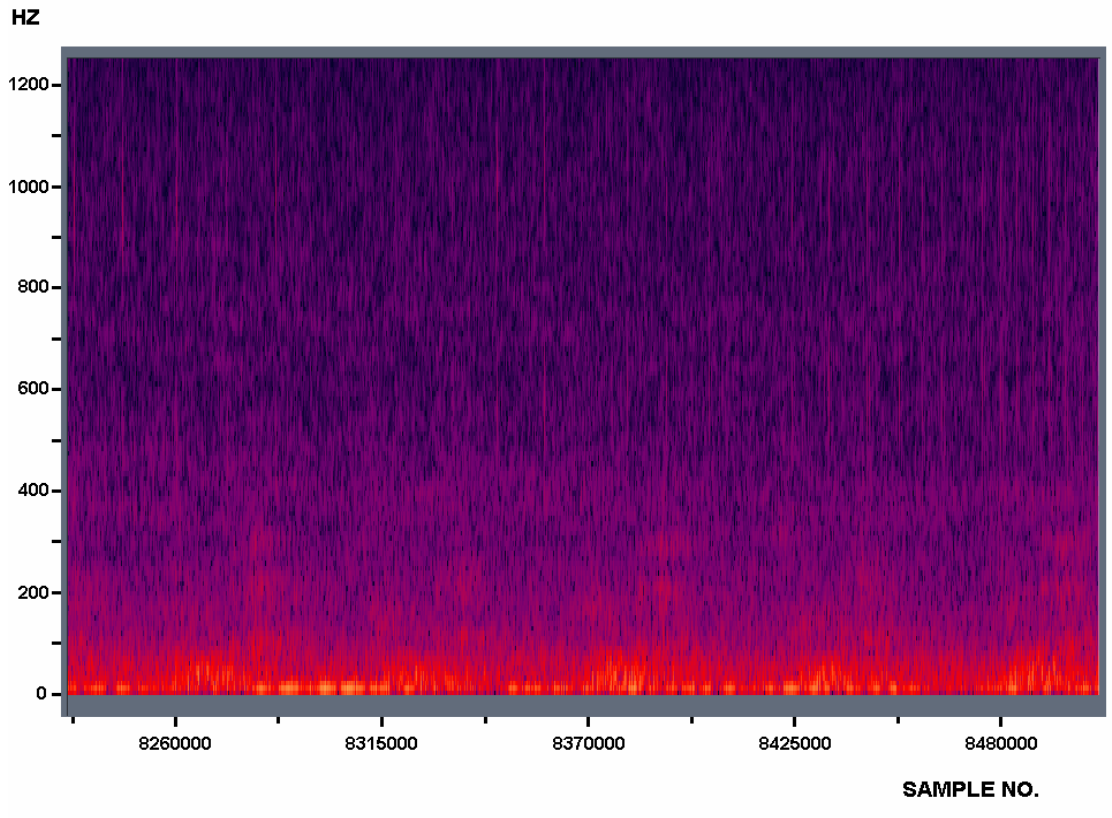

Figure 28. Profile #3 Station #4 direct hydrophone OBS signal amplitude (top) and corresponding sonogram (bottom) based on 1024 pt. FFTs. Time series duration is 55s. Signal amplitude is linear in µPa and sonogram vertical axis is linear in Hz.

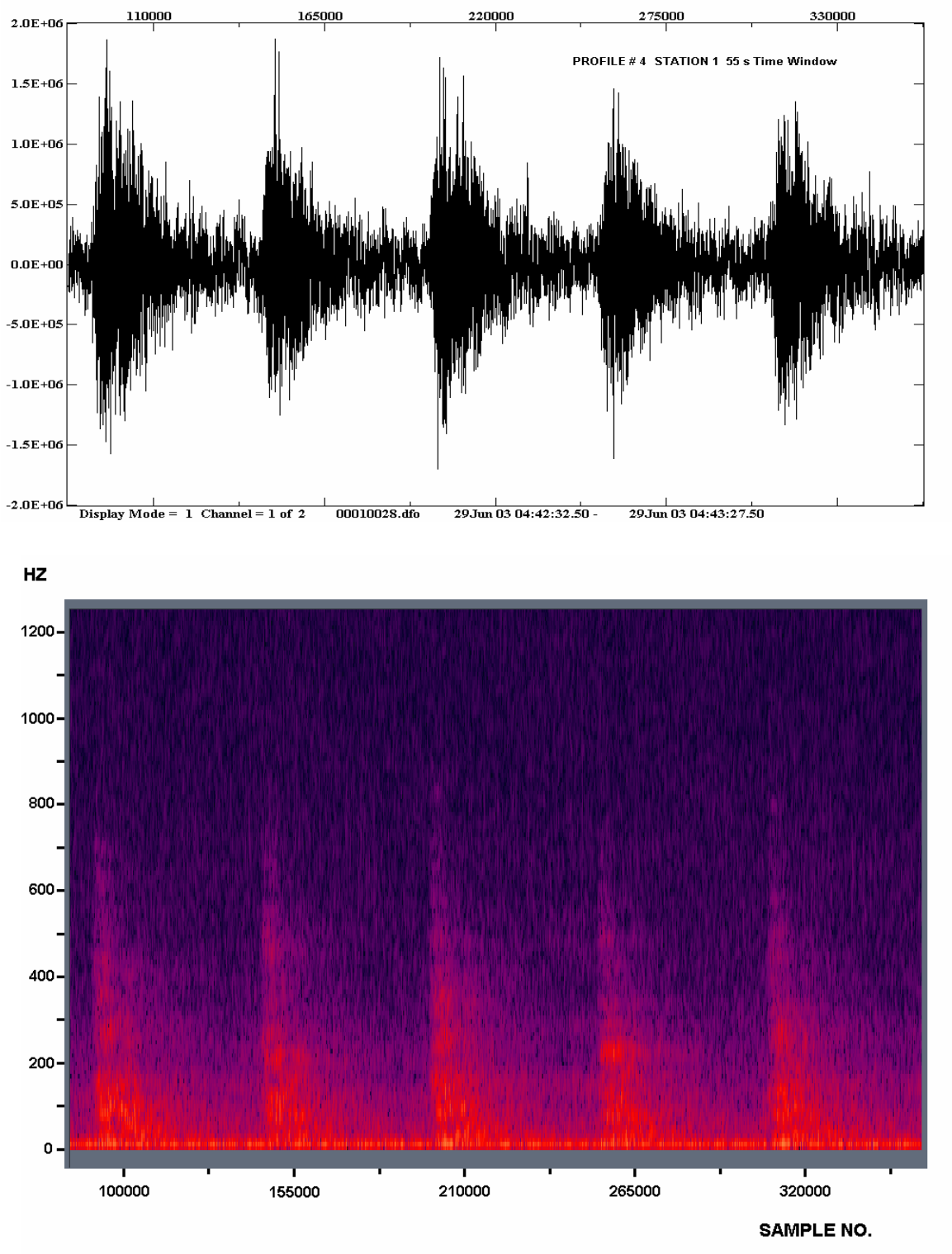

Figure 29. Profile #4 Station #1 direct hydrophone OBS signal amplitude (top) and corresponding sonogram (bottom) based on 1024 pt. FFTs. Time series duration is 55s. Signal amplitude is linear in μPa and sonogram vertical axis is linear in Hz.

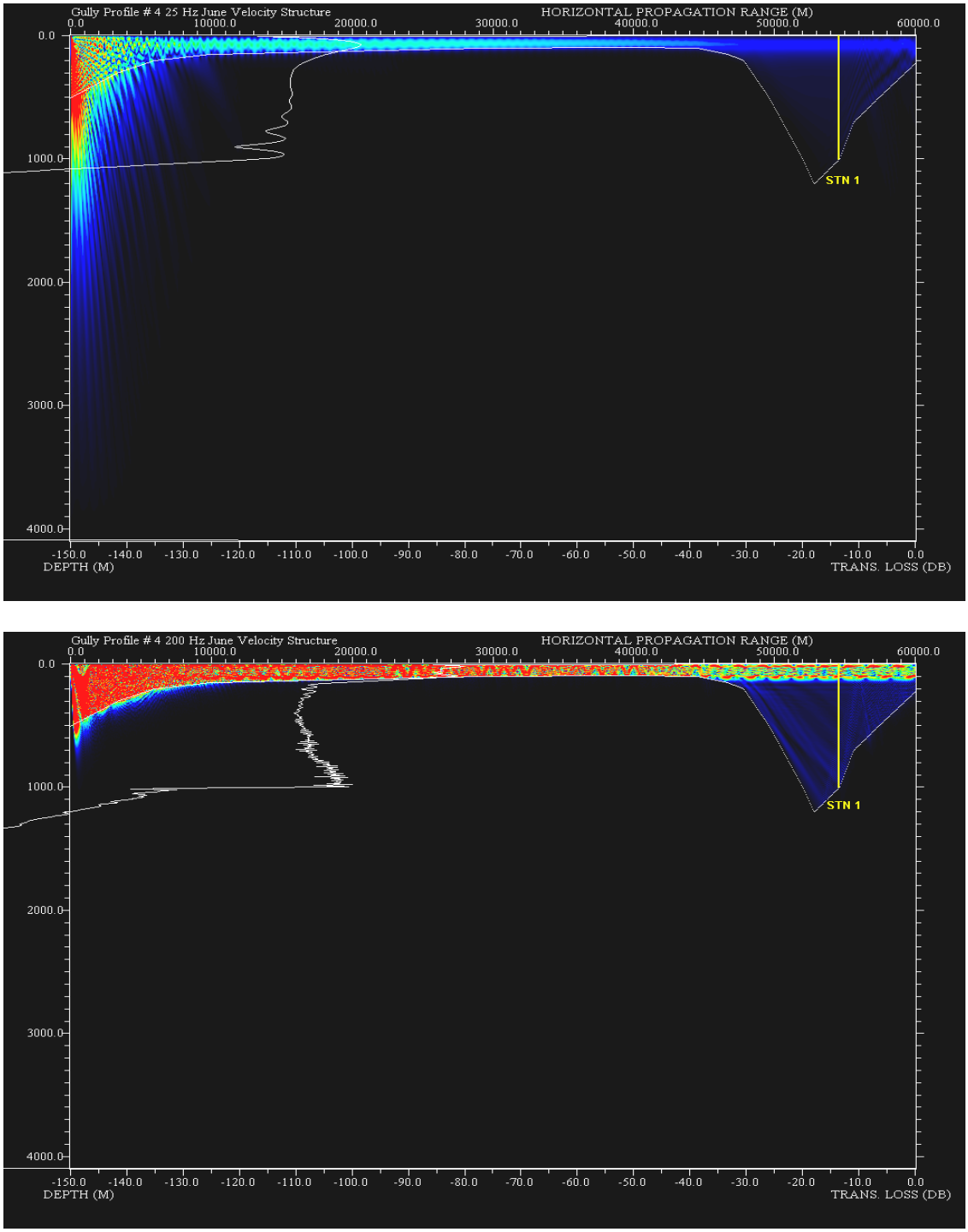

Figure 30. Profile #4 RAM model relative transmission losses at 25 Hz (top) and 200 Hz (bottom). Blue to red represent decreasing losses or higher acoustic intensities. A 10 log R range compensation has been applied to color-coded values to emphasize non-cylindrical transmission losses. Station #1 absolute transmission loss averaged over 1/3 octave bandwidth is shown in vertical profile.

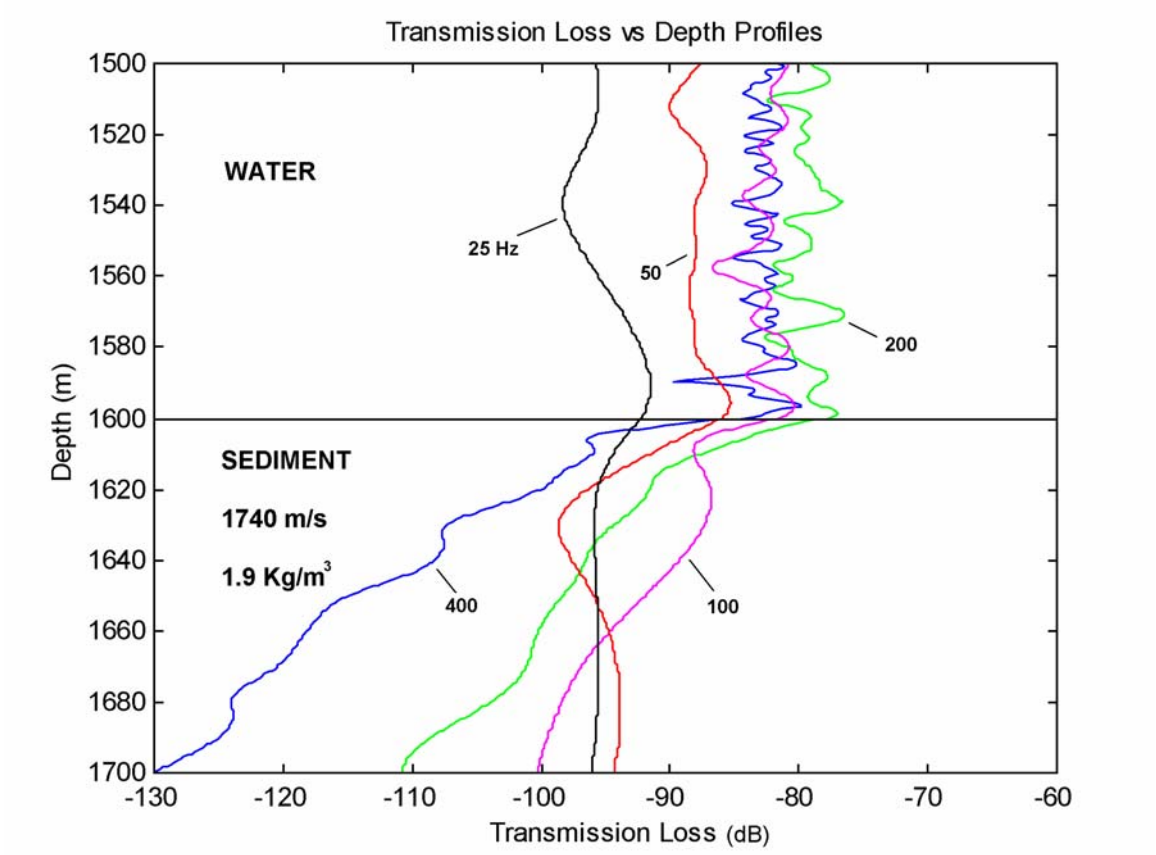

Figure 31. Plots of acoustic transmission loss vs. depth near water-sediment interface at 5 differing acoustic frequencies at a point 36 km from the origin of Profile # 3. Transmission losses have been averaged over 1/3 octave bandwidths. The June 19th sound speed profile is assumed for the water column.